An investigation into offshore groundwater and its influence on onshore coastal aquifers

by

Andrew C. Knight

Bsc. Sci. (Hons), MSc. Groundwater Hydro.

Thesis

Submitted to Flinders University

for the degree of

Doctor of Philosophy

College of Science and Engineering

July 2020

Declaration

I certify that this thesis does not incorporate without acknowledgment any material previously submitted for a degree or diploma in any other university, and that to the best of my knowledge and belief it does not contain any material previously published or written by another person except where due reference is made in the text.

.....

Andrew C. Knight

Co-authorship

This PhD thesis was produced as a series of journal publications. At the time this thesis was completed, two journal papers (Chapter 2 and Chapter 3) were published in leading international scientific journals, and another (Chapter 4) was in preparation for submission.

I am the first author on all journal publications and was responsible for leading and conducting the majority of research contained in them, including the final write up and publication of the research.

The papers in this thesis have benefited from ongoing advice and input of my supervisors, co-authors and the peer review process. I acknowledge their valuable advice and important contributions.

Additionally, I acknowledge the contribution of Gualbert Oude Essink and the anonymous reviewer who reviewed this thesis.

Acknowledgements

I would like to acknowledge my principal supervisor Professor Adrian Werner, your wisdom, passion for hydrogeology and support through-out this process has been greatly appreciated. I would also like to thank my two co-supervisors Dr Dylan Irvine and Dr Leanne Morgan, your assistance though-out my PhD candidature has been invaluable. Dylan, thank you for boundless enthusiasm and your assistance with Python. This thesis has also benefited from constructive feedback from Gualbert Oud Essink and an anonymous reviewer, thank you both for your assistance.

I would like to thank my wife Fiona for her support, and my family for their encouragement and persistent requests for progress updates. Additionally, I wish to acknowledge my Flinders University colleagues and office mates for making the process an enjoyable one.

This work would have not been possible without the financial assistance of the Australian Government though the Research Training Program Scholarship.

Summary

Fresh groundwater has been identified in the offshore extensions of numerous confined coastal aquifers globally. In recent years, several studies have proposed the use of this offshore fresh groundwater (OFG) to assist in onshore freshwater supply. As groundwater investigations in coastal regions have typically focused on the onshore portion of the aquifer, OFG remains poorly understood. This body of work examines three aspects of OFG, specifically: 1) the degree to which OFG already supports existing onshore freshwater extractions, 2) combined geophysical and analytical methods to estimate OFG extent, and 3) the behaviour of OFG in regions with alongshore head gradients in the onshore portion of the aquifer.

The first part of this study investigates the potential present-day onshore influence of OFG. This investigation tests the previous assertions that OFG by and large represents a potential (and currently under-utilised), freshwater resource for many coastal communities. Twenty-seven confined and semi-confined coastal aquifers with plausible connections to inferred or observed OFG are assessed using available salinity and hydraulic data and analytical modelling. Seven conceptual models are synthesised based on the observation data and insights gained from analytical modelling. These conceptual models demonstrate for the first time that OFG formed from paleo- or pre-development conditions can delay the onset of SWI in the onshore portion of coastal aquifers. Analytical modelling indicates that onshore pumping will lead to active-SWI at fourteen of the twenty-seven sites, while passive SWI is expected onshore in an additional ten regions. In these twenty-four regions, OFG is likely delaying the onset of SWI within the

onshore domain. The available data indicates that onshore extraction regimes are already mining OFG. As such, where OFG is connected to onshore aquifers, it should primarily be considered as an existing freshwater input rather than an untapped resource.

The second part of this study uses existing petroleum exploration data, hydraulic information and analytical modelling to provide a leading example of the use of multiple techniques to evaluate OFG. This investigation combines a large seismic data set, onshore and offshore geophysical bore-log profiles, and available onshore hydro-stratigraphic data to explore the extent of OFG in the Gambier Embayment (Australia). A novel application of Archie's law provides useful insights into the salinity profiles within four offshore wells. These profiles are compared to steady-state, sharp-interface estimates of the freshwater extent obtained from an analytical solution, using simplified conceptual models. The downhole geophysical data indicate that in the south of the study area, pore water with total dissolved solids (TDS) of 2.2 g L^{-1} is found up to 13.2 km offshore. The analytical solution produces freshwater-saltwater interface locations that are approximately consistent with the freshwater-saltwater stratification in two of the offshore wells. This investigation demonstrates both the benefits and uncertainties involved with the application of geophysical interpretations and analytical solutions to estimate OFG extent.

The final part of this study uses numerical simulations of synthetic coastal aquifers to explore the behaviour of OFG in regions that have an alongshore head gradients (AHG). Twelve numerical simulations are used to assess the response of OFG to values of hydraulic conductivity of the aquitard (K_v), the onshore head relative to sea level, and the steepness of the AHG. Each 3D simulation is compared to three 2D simulations to test the

discrepancy between 2D and 3D approaches. This investigation shows for the first time that significant volumes (up to 70%) of the freshwater discharging from the onshore aquifer to its offshore extent may in-fact return onshore through alongshore freshwater circulation (AFWC). The modelling shows that the proportion of AFWC is greater in systems with a steep AHG, low onshore heads relative to sea level, and an offshore aquitard with a low K_v. This study also identifies that 2D approaches have the tendency to overpredict the steady-state OFG extent at the location of the maximum onshore head and underpredict the OFG extent at the location of the minimum onshore head when AHGs are present. This investigation shows that the onshore movement of OFG can persist under steady-state conditions in some regions, and that the onshore movement of OFG does not exclusively represent the mining of relic OFG.

d

Table of Contents

List of Figures

List of Tables

Chapter 1

1. Introduction

Groundwater forms the largest available liquid freshwater reservoir on earth with groundwater use accounting for roughly one-third of global water withdrawals (Kundewicz and Döll, 2009). However, the availability of fresh groundwater is declining in numerous regions globally (Konikow and Kendy, 2005; Werner et al., 2013a). In coastal aquifers, fresh groundwater is threatened due to contamination and over extraction reducing the quality and quantity of available groundwater (Post et al., 2013; Michael et al., 2017). Coastal aquifers are particularly susceptible to degradation when compared to inland aquifers, as over-extraction of groundwater in coastal aquifers has the potential to generate an onshore movement of seawater, known as seawater intrusion (SWI), which is challenging to remediate (Michael et al., 2017). However, fresh groundwater has also been identified in the submarine extension of coastal aquifers in several regions globally (Cohen et al., 2010; Post et al., 2013). As the offshore extensions of coastal aquifers have traditionally received less focus than their onshore portions (Post et al., 2013), many aspects of this offshore fresh groundwater (OFG) are still poorly understood.

The potential for OFG to assist in onshore freshwater supply has been raised in several recent studies (e.g., Cohen et al., 2010; Bakken et al., 2012; Post et al., 2013). OFG has been proposed as either as a direct freshwater input, or as a low salinity water source for reverse-osmosis desalination plants (Bakken et al., 2012; Post et al., 2013). However, Post et al. (2013) proposed that OFG may already be inadvertently mined in some areas

due to onshore groundwater extractions drawing upon OFG from the offshore extensions of the onshore aquifer. Prior to the work by Post et al. (2013), OFG was dominantly framed as a potential and untapped, albeit finite, freshwater resource that may be used to supplement onshore extractions (e.g., Cohen et al. 2010, Bakken et al., 2012). The first objective of this thesis (Chapter 2) is to determine whether OFG already provides freshwater inputs to onshore extractions on a global scale, or if OFG generally represents a new freshwater resource as proposed in earlier studies.

OFG has been identified through the sampling of pore water (e.g., Krantz et al., 2004; Jiao et al., 2015) or from geophysical data such as resistivity logs. (e.g., Oteri, 1988; Groen et al., 2000; Krantz et al., 2004; Hennig and Otto, 2005). Post et al. (2013) highlight that there is a potential wealth of geophysical borehole log data relic from hydrocarbon exploration that may be applied to the identification and delimitation of new OFG bodies. While resistivity-log data has been used to constrain the salinities of groundwater in multiple studies, resistivity derived salinities can have significant uncertainty ranges attached (e.g., Pauw et al., 2017), though these uncertainties are rarely reported (e.g., Oteri, 1988; Groen et al., 2000; Hennig and Otto 2005). The second objective of this thesis (Chapter 3) is to provide a detailed example of the application of historic hydrocarbon exploration data and analytical modelling to the identification OFG, demonstrating both the benefit and uncertainty involved in the use of these data to constrain salinities in an offshore setting.

Alongshore head gradients (AHGs) have been observed onshore in coastal aquifers that have OFG identified in their submarine extensions (e.g., Nativ and Weisbrod, 1994; de Melo et al., 2001; Kalaris et al., 2002; Zulfic et al., 2008; Morgan et al., 2016). However, these AHGs are typically neglected in offshore investigations, and offshore aquifers are

commonly assessed using cross-sectional representations (e.g., Amir et al., 2013; Morgan et al., 2016, Paldor et al., 2019). Currently, the impact of AHGs on estimations of OFG extent remains unstudied both in 2D and 3D. The third objective of this thesis (Chapter 4) is to investigate the potential for onshore AHGs (such as those seen in regions of high groundwater extraction) to drive alongshore freshwater circulation through the offshore portion of the aquifer (i.e., where freshwater passes into the offshore portion of the semi-confined aquifer in places of highest onshore head before circulating within the offshore aquifer and subsequently flowing back onshore at another location).

This thesis consists of five chapters inclusive of the current chapter. Chapter 1 provides a brief overview of the driving motivation behind the three research investigations undertaken in this thesis. Chapter 2 and Chapter 3 are taken directly from international journal publications, with references for these two papers provided as at the start of the respective chapters. Chapter 4 is currently in preparation to be submitted as a journal publication. Each chapter can therefore be read independently. Chapter 5 summarises the main results and conclusions of this thesis and includes potential avenues for future investigations into OFG.

Chapter 2

2. The onshore use of offshore fresh groundwater

Accepted for publication in Hydrogeology Journal: Knight, A.C., Werner, A.D., Morgan, L.K., 2018. The onshore influence of offshore fresh groundwater. J. Hydrol. 561, 724-736. https://doi.org/10.1016/j.jhydrol.2018.03.028.

2.1 Abstract

Freshwater contained within the submarine extensions of coastal aquifers is increasingly proposed as a freshwater source for coastal communities. However, the extent to which offshore freshwater supports onshore pumping is currently unknown on a global scale. This study provides the first attempt to examine the likely prevalence of situations where offshore freshwater influences onshore salinities, considering various sites from around the world. The groundwater conditions in twenty-seven confined and semi-confined coastal aquifers with plausible connections to inferred or observed offshore freshwater are explored. The investigation uses available onshore salinities and groundwater levels, and offshore salinity knowledge, in combination with analytical modelling, to develop simplified conceptual models of the study sites. Seven different conceptual models are proposed based on the freshwater-saltwater extent and insights gained from analytical modelling. We consider both present-day and pre-development conditions in assessing potential modern contributions to offshore fresh groundwater. Conceptual models also include interpretations of whether offshore freshwater is a significant factor influencing

onshore salinities and well pumping sustainability. The results indicate that onshore water levels have declined between pre-development and present-day conditions in fourteen of the fifteen regions for which pre-development data are available. Estimates of the associated steady-state freshwater extents show the potential for considerable offshore fresh groundwater losses accompanying these declines. Both present-day and pre-development heads are insufficient to account for the observed offshore freshwater in all cases where adequate data exist. This suggests that paleo-freshwater and/or aquifer heterogeneities contribute significantly to offshore freshwater extent. Present-day heads indicate that active seawater intrusion (SWI) will eventually impact onshore pumping wells at fourteen of the twenty-seven sites, while passive SWI is expected onshore in an additional ten regions. Albeit the number of field sites is limited, there is sufficient evidence to indicate that when offshore freshwater has an onshore linkage, it is being mined either passively or actively by onshore use. Thus, offshore freshwater should be assessed in coastal water balances presuming that it serves as an existing freshwater input, rather than as a new potential freshwater resource.

2.2 Introduction

Freshwater losses occur when seawater moves landward within coastal aquifers, a process known as seawater intrusion (SWI). SWI is driven by pumping, climate change and sea-level rise, which are predicted to increasingly threaten the reliability of coastal aquifer freshwater resources, some of which are already subject to excessive rates of abstraction and display evidence of SWI impacts (Ferguson and Gleeson, 2012; Werner et al., 2013a; Werner et al., 2013b). Additionally, the salinization of onshore fresh groundwater can also occur due to the remobilisation of underlying relic seawater though vertical upconing, land subsidence and storm surge overtopping (Essink, 2001). The occurrence

of SWI is primarily evaluated in the onshore sections of coastal aquifers, despite that freshwater can exist in the submarine extensions of semi-confined and confined coastal aquifers (Kooi and Groen, 2001; Bakker, 2006). As a result, conceptual and numerical models are often truncated at or near the shoreline (Sanford and Buapeng 1996; USCoE, 1998; Delinom, 2008; Lubis et al., 2008; Bresciani et al., 2015; Knowling et al., 2015), neglecting altogether offshore processes.

Freshwater in offshore aquifers, referred to as offshore fresh groundwater (OFG), has been recognised as a potential water resource for coastal communities (Cohen et al., 2010; Bakken et al., 2012; Post et al., 2013; Jiao et al., 2015). OFG bodies are separated from seawater by a dispersive mixing zone, and are characterised by salinities that typically freshen towards the coastline (Groen, 2000; Cohen et al., 2010; Post et al., 2013). In this study, freshwater is considered to have a total dissolved solids (TDS) < 1 g L^{-1} (approximately 3% of seawater), consistent with Cohen et al. (2010) and Post et al. (2013). We also consider salinities equal to 50% of seawater concentration (i.e., TDS ≈ 17.5 g L^{-1}) for comparison to the location of sharp-interface representations of the freshwater-seawater mixing zone, obtained from analytical methods. Recent work suggests that OFG (i.e., TDS < 1 g L^{-1}) is more common than previously thought, with both Cohen et al. (2010) and Post et al. (2013) estimating that there is 3×10^5 km^3 contained globally within passive continental margins. Brackish water (TDS < 10 g L^{-1}) is estimated to total 5×10^5 km^3 (Post et al., 2013). These estimates have large uncertainties due to the scarcity of offshore data.

Two primary sources of OFG have been identified: (1) entrapped paleo-freshwater (e.g., Meisler et al., 1984; Essaid, 1990; Groen, 2000), and (2) ‘modern’ freshwater discharge (i.e., the flow from onshore aquifers to subsea aquifers under current sea-level conditions)

(Kooi and Groen, 2001; Bakker, 2006). OFG resources may be a mixture of both origins (Cohen et al., 2010; Post et al., 2013). Paleo-freshwater is thought to have been emplaced during historic glacial maxima, when lower sea levels, increased continental shelf exposure, and elevated recharge (in some regions) led to bodies of freshwater covering significant offshore distances from present-day coastlines (Groen, 2000; Cohen et al., 2010; Post et al., 2013; Siegel et al., 2014). The last glacial maximum (LGM) ended approximately 19,000 years before present (Yokoyama et al., 2000). As seas rose to their current levels, coastal migration rates exceeded the landward movement of the freshwater-seawater interface, resulting in seawater overtopping aquifers containing freshwater (Kooi and Groen, 2001; Post et al., 2013). For this to occur, an overlying aquitard is required to inhibit vertical mixing of freshwater and seawater, which is otherwise driven by buoyancy forces due to the unstable water-density configuration (Laattoe et al., 2013). This paleo-water is thought to be slowly salinizing through the diffusion of salt from adjacent strata and gradual landward movement of the freshwater-seawater interface (Groen, 2000; Post et al., 2013).

Modern contributions to OFG bodies occur within offshore confined and semi-confined aquifers that receive fresh groundwater inflow from onshore aquifers (Kooi and Groen, 2001; Bakker, 2006), referred to as OFG inflow in what follows. OFG inflow differs to submarine fresh groundwater discharge (SFGD), in that the latter is usually recognised as groundwater discharge into the sea, rather than into aquifers below the sea. This is an important distinction, because OFG inflows are inputs to offshore aquifers, whereas SFGD is an output from onshore and/or offshore aquifers. Whether or not OFG inflow occurs at the same rate as SFGD determines whether the offshore aquifer is losing or gaining freshwater. The distance that SFGD and modern OFG extend offshore is dependent on numerous factors. For example, OFG can penetrate further where the

overlying aquitard has a low hydraulic conductivity (K) and/or large thickness, the semi-confined/confined aquifer has a high K, and the groundwater head gradient driving freshwater offshore is steep (Kooi and Groen, 2001; Bakker, 2006).

Previous investigations of OFG primarily focus on the occurrence, characteristics and extent of these systems. However, where pumping lowers the onshore heads of aquifers connected to OFG bodies, drawdown may extend beyond the shoreline, potentially causing the OFG volume to reduce. In this way, OFG may partly support the total onshore extraction of fresh groundwater (Post et al., 2013; Morgan and Werner, 2015). Only a handful of localised studies have considered the interactions between OFG and onshore hydrogeological conditions. For example, regional sharp-interface modelling by McAuley et al. (2001) and Pope (2006) concluded that under current pumping regimes, the freshwater-saltwater interface will reach the New Jersey (USA) shoreline within the Atlantic City 800-foot sand aquifer in 710 years. Preliminary studies of OFG bodies offshore from Perth (Australia) (Morgan et al., 2016) and Palmahim (Israel) (Amir et al., 2013) have also been undertaken. However, it is presently unknown from a global perspective whether and for which aquifers offshore freshwater is critical for the onshore management of coastal fresh groundwater, and the degree to which onshore pumping is drawing on offshore freshwater bodies.

This study aims to develop conceptual models of coastal aquifers known to host significant OFG and where onshore pumping occurs, thereby providing initial conclusions about links between onshore and offshore conditions. We compare freshwater-saltwater distributions predicted through analytical modelling of modern hydrogeological conditions to observed onshore and offshore salinity data. From this, we can infer the level of onshore use of OFG at each study site. The rapid assessment

methods adopted in this study also allow for an initial interpretation of the likely balance between paleo- and modern OFG in select regions.

2.3 Methods

The direction of groundwater flow at the shoreline of coastal aquifers can be inferred by comparing the onshore piezometric head (h_b) to the equivalent freshwater head (h_f) imposed by the sea (Werner, 2017a). This assumes that the coastal aquifer is exposed to the sea at some location, at which point the offshore groundwater head reflects the head of the ocean. The value of h_f adopted in this study is applicable only to aquifers with onshore extents that exhibit semi-confined (rather than unconfined) conditions, because these aquifers are most likely to host significant OFG. The coastal aquifer arrangement that is adopted in this study for the purposes of applying available analytical solutions to OFG extent (arising from OFG inflow) is illustrated in Fig. 2.1.

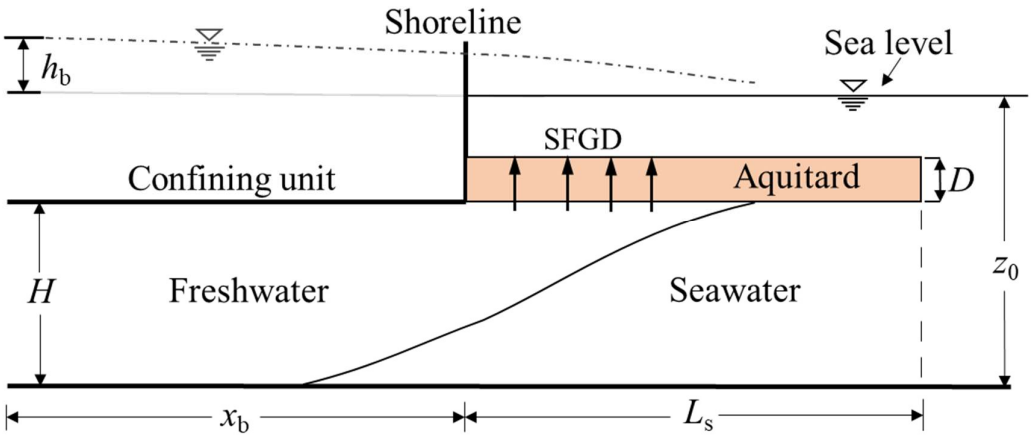

Fig. 2.1 Simplified conceptual model of an onshore-offshore coastal aquifer (adapted from Bakker, 2006). The dot-dash line represents the potentiometric surface of the confined and semi-confined components of the aquifer, the vertical dashed line indicates the offshore termination of the aquitard (coloured orange), which overlays the offshore portion of the aquifer. D is the thickness of the aquitard, H is the thickness of the

underlying aquifer, xb is the distance from the shoreline to the onshore boundary, Ls is the offshore length of the aquitard, and z0 is the depth below sea level to the aquifer base.

OFG inflows are expected to occur where $h_0 > h_f$; otherwise the onshore aquifer is likely to be drawing water from its subsea part. The value of h_f is determined by (Werner, 2017a):

$$h_f = \frac{\rho_s - \rho_f}{\rho_f}(z_0 - H) \quad (2.1)$$

Where ρ_f and ρ_s are the respective densities of freshwater and seawater [M L^{-3}]. Other variables are defined in Fig. 2.1. Hydraulic gradients indicating groundwater flow in the onshore direction (i.e., $h_b < h_f$) are associated with active SWI, whereby the landward movement of seawater is in the same direction as groundwater flow (Werner, 2017a). Active SWI is expected to eventually cause relatively rapid salinization of the near-shore aquifer (Morgan and Werner, 2015; Werner, 2017a). This contrasts to passive SWI, whereby seawater moves landwards despite freshwater flowing towards the coast, resulting in the partial salinization of the onshore aquifer. Passive SWI in offshore aquifers may occur due to a reduction in OFG inflow (without eliminating it altogether). In a sharp-interface conceptualisation, passive SWI is characterised by a landward movement of the interface toe (i.e., where the freshwater-saltwater interface intercepts the base of the aquifer) and, in some cases, the interface tip (i.e., where the freshwater-saltwater interface intercepts the top of the aquifer). The toe may eventually come to rest in the onshore or offshore regions of the aquifer, whereas the tip remains offshore due to the persistence of OFG inflow under passive SWI scenarios. In coastal aquifers with significant OFG, SWI may take place over considerable timeframes without salinization of onshore wells, because the loss of freshwater occurs in the offshore part of the aquifer.

Thus, some knowledge of offshore salinities is critical to understanding the potential for salinization of onshore aquifers from which pumping occurs.

A preliminary estimate of the steady-state extent of modern OFG is possible for coastal aquifers where $h_b > h_f$ through application of an analytical solution developed concurrently by Werner and Robinson (2018). Werner and Robinson (2018) modify the solutions of Bakker (2006) and Bakker et al. (2017), who assumed that the offshore aquitard contains seawater, to allow for alternative aquitard salinities. The modification by Werner and Robinson (2018) responds to the findings of another concurrent investigation by Solórzano-Rivas and Werner (2018), who show that where SFGD occurs, the offshore aquitard is more likely to contain freshwater, thereby changing significantly the prediction of OFG otherwise obtained from the Bakker (2006) and Bakker et al. (2017) solutions. While Bakker (2006) adopted a prescribed-flux representation of the inland boundary condition, Bakker et al. (2017) and Werner and Robinson (2018) allow for a prescribed-head condition to be implemented.

The available analytical solutions for OFG apply to idealised aquifer geometries, consistent with Fig. 2.1. They are based on a number of assumptions, including that: (1) the zone of mixing between freshwater and seawater can be represented by a line of pressure equilibrium (i.e., a sharp interface), (2) the offshore aquifer is in equilibrium with onshore heads (i.e., steady-state conditions), (3) the aquifer and the overlying aquitard (in the offshore region) are isotropic and homogeneous, and (4) freshwater flow in the aquifer is horizontal, flow in the aquitard is vertical, and seawater is stagnant. A minimal number of input parameters are required, which is commensurate with the limited available data for almost all of the aquifers considered in this study.

Coastal aquifer parameters required for the Werner and Robinson (2018) solution are obtained from existing literature, and are available at several sites around the world, as given in Table 2.1. The interface tip (x_{tip}) and toe (x_{toe}) positions were calculated for each region. The parameters required are the aquifer hydraulic conductivity (K_a) [L T^{-1}], aquitard vertical hydraulic conductivity (K_l) [LT^{-1}], H, D, z_0, h_b, x_b and L_s (see Fig. 2.1). Due to limitations in the available data, a single set of base-case aquifer properties was adopted for each site, despite that spatial variability in most parameters is likely. The distance to the edge of the continental shelf was used in areas where L_s is undefined in existing literature. The termination of the continental shelf was obtained from global bathymetry data (NCEI, 2017). In some cases, two land masses abut the offshore region, and hence it is not possible to define a distance to the edge of the continental shelf. In these instances, L_s was taken arbitrarily as the distance to the shoreline of the neighbouring land mass. The coastal aquifers of Kent (England) are an example of this, whereby the submerged continental shelf connects to France without exceeding a bathymetric depth of 55 m.

To capture some of the known spatial variability in h_b, maximum (h_{bmax}) and minimum (h_{bmin}) values were obtained, where available, from either well data or potentiometric contours. To allow for investigations of the impact of onshore development on OFG extent, pre-development heads (h_b^*) were obtained where historical head information was available. Where pre-development heads varied spatially within a single aquifer, the maximum head within the near-coastal zone was adopted. The maximum head was selected because the available measurements probably under-estimate, if anything, the true pre-development head levels given that human impacts are likely to have been occurring well before 1960 in many cases. This also allowed for the identification of

aquifers where paleo-OFG and/or aquifer heterogeneities are required to explain observed OFG extents extracted from offshore measurements.

Table 2.1. Parameters used in applying the Werner and Robinson (2018) analytical solution to estimate OFG extents.

Region	Aquifer Properties							Aquitard Properties			Sources of Data
	K_a (m/d)	z_0 (m)	H (m)	h_b* (m)	h_{bmin} (m)	h_{bmax} (m)	x_b (km)	D (m)	K_l (m/d)	L_s (km)	
Adelaide (Australia)	2.5	190	80	10	-24	6.5	5	15	0.0005	[c]80	(Zulfic et al., 2008; Ivkovic et al., 2012; DEWNR, 2013)
Albany (Australia)	5	25	20	[b]3.2	-0.6[#]	-0.6[#]	8.0	1	0.005	[d]42	(Ryder, 2004; Ivkovic et al., 2012)
Algarve (Portugal)	4	87	57	16	5	5	1	20	0.0001	[d]12	(Hugman et al., 2014; Frances et al., 2015)
Aveiro (Portugal)	1	410	200	-	5	50	1	80	[a]0.0001	[d]50	(de Melo et al., 1999; de Melo et al., 2001)
Bangkok (Thailand)	8.6	120	75	-	-20[#]	-20[#]	15	17.5	0.086	[c]740	(Lundegard et al., 1990; Buapeng and Wattayakorn, 2008; Onodera et al., 2009)
Bunbury (Australia)	20	400	300	[b]4.2	1.6[#]	1.6[#]	4.4	20	10^{-6}	125	(Schafer et al., 2008; Ivkovic et al., 2012)
Canterbury (New Zealand)	3	76	16	-	-1.5	8.5	1.9	25	0.0001	[d]50	(Fulthorpe et al., 2011; Scott and Wilson, 2012)
Carnarvon (Australia)	11	55	45	[b]1.1	1.1[#]	1.1[#]	6.1	2	0.0001	65	(Dodson, 2009; Ivkovic et al., 2012)
Eckernförde Bay (Germany)	45	200	150	-	3.5	6	5	37.5	0.0012	6	(Kalaris et al., 2002)
Gambier Embayment (Australia)	10	800	400	[b]22.2	10	20.5	5	40	0.0001	[d]30	(Ivkovic et al., 2012; Morgan et al., 2015)
Gippsland (Australia)	25	3200	2000	55	0	10	0.3	120	10^{-5}	80	(Schaeffer, 2008; Varma and Michael, 2011)
Howard Springs (Australia)	40	100	25	[b]11.9	9.7[#]	9.7[#]	8.0	15	0.0001	[c]50	(Ivkovic et al., 2012)

Jakarta (Indonesia)	0.86	140	100	-	-20[#]	-20[#]	9	20	0.0086	[c]325	(Maathuis, 2000; Lubis et al., 2008; Onodera et al., 2009)
Kent (England)	[a]5	457	53	-	26[#]	26[#]	3.3	60	[a]0.0001	[c]85	(Edmunds et al., 2001)
Nantucket Island (USA)	10	290	220	-	4[#]	4[#]	2	34	0.0095	200	(Marksamer et al., 2007; Person et al., 2012)
New Jersey (USA)	15	280	36	9	-24	-6	3	30	0.0003	[d]140	(Hathaway, 1979; Voronin et al., 1996; McAuley et al., 2001; Pope, 2006; Depaul and Rossman, 2013)
Niger Delta (Nigeria)	[a]5	325	200	-	9[#]	9[#]	25	15	[a]0.1	[b]60	(Oteri, 1988; Oteri and Atolgabe, 2003; Anomohanran, 2015)
North Holland (Netherlands)	30	55	40	-	1.5	4	1.5	3	0.02	[c]100	(Pauw et al., 2017)
Northern Florida (USA)	42.5	310	160	18	0	9	5	30	0.0003	110	(Hathaway et al., 1979; Myer, 1989; Spechler, 1994; Kinnaman and Dixon, 2009)
Palmahim (Israel)	10	190	40	-	1.5	2	2.9	30	10^{-5}	25	(Nativ and Weisbrod, 1994; Goldman et al., 2010; Amir et al., 2014)
Perth Basin (Australia)	2	3250	1500	35	-21	30	4.5	100	10^{-5}	80	(Hennig and Otto, 2005; Ivkovic et al., 2012; Morgan et al., 2016)
Ringkøbing Fjord (Denmark)	50	200	40	-	11[#]	11[#]	8	30	0.04	13	(Haider et al., 2015)
Shanghai (China)	2.6	130	50	1	-7	-1	25	80	0.0016	[d]500	(Shen and Xu, 2011)
Southern Dobruja (Bulgaria)	5	750	400	-	16[#]	16[#]	2	30	0.0001	95	(Soulet et al., 2010; Carivan et al., 2010; Chitea, 2011)
Suriname	25	185	85	3	-10	-6	5	30	0.0004	[d]130	(Hutchinson, 1990; Groen, 2000)
Uley South (Australia)	90	45	30	[b]3.5	1.8[#]	1.8[#]	2.8	5	0.0048	[d]90	(Ivkovic et al., 2012; DEWNR, 2015)
Willunga (Australia)	10	120	90	3	1.5[#]	1.5[#]	3.5	10	0.0001	[c]85	(Stewart, 2006; Lamontagne et al., 2008; Ivkovic et al., 2012, Morgan et al., 2016)

[#] Available onshore data insufficient to establish minimum and maximum h_b values.
[a] K inferred from lithological descriptions.
[b] Pre-development head inferred from linear regression of coastal observation well data.
[c] L_s taken as the distance to the shoreline of the neighbouring land mass.
[d] L_s estimated using bathymetric data.

2.4 Review of coastal aquifers with significant OFG

2.4.1 Identification of aquifers with significant OFG

We considered three conditions that are indicative of the presence of significant OFG in the selection of regions for further analysis. Firstly, we selected regions with offshore groundwater salinities below TDS 17.5 g L^{-1} (approximately 50% seawater salinity), as interpreted from offshore well observations and/or resistivity surveys. Secondly, we included semi-confined coastal aquifers where $h_b > h_f$, as this is indicative of OFG inflow. Thirdly, we identified regions where onshore freshwater is observed close to the shoreline in semi-confined aquifers despite $h_b < h_f$. These regions are thought to indicate the occurrence of OFG because active SWI conditions would otherwise be expected to have caused extensive groundwater salinization in the onshore aquifer, at least where onshore groundwater levels have been lowered for extended periods.

The identification of regions with significant OFG was initially guided by the previous investigation of Post et al. (2013). Ten of the fourteen regions identified by Post et al. (2013) that satisfied the selection criteria had sufficient data to allow for the application of the Werner and Robinson (2018) solution and were included in the analysis. In addition to the regions identified by Post et al. (2013), this study includes three regions where the presence of OFG is indicated by resistivity surveys or by freshwater measurements in offshore wells. A further fourteen regions were identified where OFG can be inferred from h_b, h_f, and/or onshore salinities. Fig. 2.2 shows the location of the twenty-seven regions analysed in this study, plus the four regions mentioned by Post et al. (2013) that were omitted from the current analysis due to data constraints. There may be other regions where OFG can be implied that were not included in this study due to either data limitations or the highly channelized nature of the recorded OFG body requiring

investigative methods beyond the scope of this study (e.g., Krantz et al., 2004; Danskin, 2012).

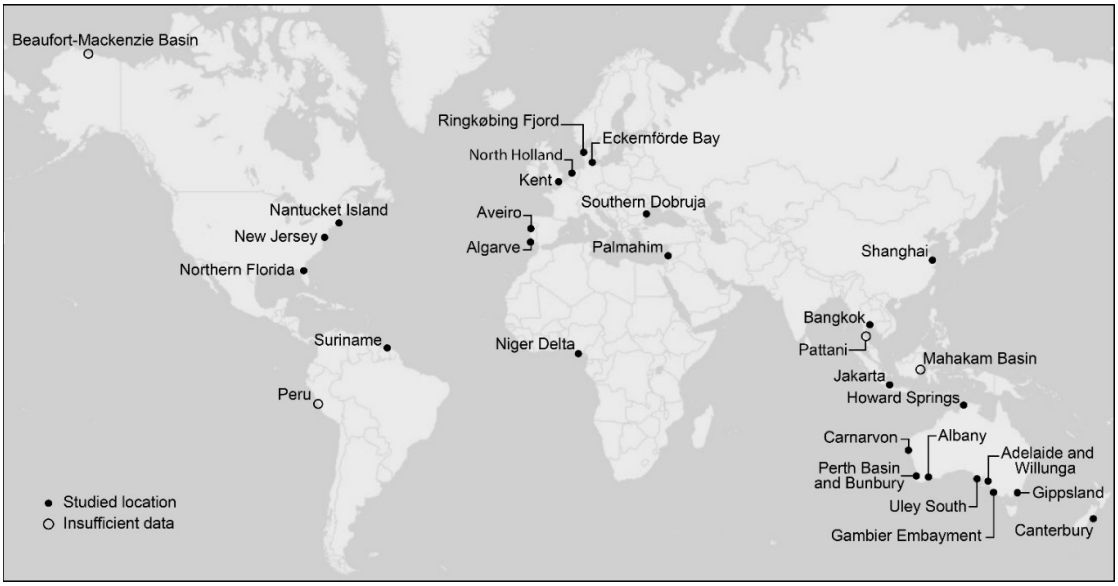

Fig. 2.2. Global distribution of regions with inferred or measured OFG analysed in this study. Willunga and Adelaide, and the Perth Basin and Bunbury share location markers due to their close proximity.

2.4.2 Identification of regions at risk of active SWI

The 'driving head' ($h_b - h_f$) (i.e., the difference between the onshore head and the equivalent freshwater head (at the top of the offshore aquifer) of the sea) was assessed for each region to identify aquifers where present-day groundwater levels are insufficient to prevent active SWI. This was undertaken by applying Eq. (2.1) to the parameters in Table 2.1, including both h_{bmin} and h_{bmax}. Negative values indicate that active SWI is likely occurring. Table 2.2 lists the driving heads for each region analysed in this study. The regions are listed in order of ascending minimum driving heads ($h_{bmin} - h_f$).

Table 2.2. Onshore saltwater observations and driving head values. References for each case are listed in Table 2.1.

Region	Saltwater observed in the onshore, semi-confined aquifer	h_{bmin} - h_f (m)	h_{bmax} - h_f (m)
Perth Basin	None observed	-64.75	-13.75
New Jersey	None observed	-30.1	-12.1
Gippsland	None observed	-30.0	-20.0
Adelaide	Relic saltwater	-26.75	3.75
Bangkok	Undefined source	-21.0[#]	-21.0[#]
Jakarta	Relic saltwater	-21.0[#]	-21.0[#]
Suriname	Relic saltwater	-12.5	-8.5
Shanghai	ND	-9.0	-3.0
Northern Florida	None observed	-3.75	5.25
Canterbury	SWI recorded	-3.0	7.0
Palmahim	ND	-2.25	-1.75
Bunbury	SWI recorded	-0.9[#]	-0.9[#]
Aveiro	None observed	-0.25	44.75
Gambier Embayment	None observed	0.0	10.5
Albany	None observed	0.48[#]	0.48[#]
Willunga	Relic saltwater	0.75[#]	0.75[#]
Carnarvon	Undefined source	0.85[#]	0.85[#]
North Holland	SWI recorded	1.13	3.63
Uley South	None observed	1.4[#]	1.4[#]
Nantucket Island	SWI recorded	2.25[#]	2.25[#]
Eckernförde Bay	ND	2.25	4.75
Algarve	None observed	4.25	4.25
Niger Delta	Relic saltwater and SWI	5.8[#]	5.8[#]
Ringkøbing Fjord	ND	7.0[#]	7.0[#]
Southern Dobruja	ND	7.25[#]	7.25[#]
Howard Springs	ND	7.8[#]	7.8[#]
Kent	None observed	15.9[#]	15.9[#]

[#] Only a single h_b measurement was obtained for this region.

ND Onshore salinity data inadequate to reasonably determine salinity status.

It is important to distinguish whether active SWI occurs at considerable distance offshore or within onshore aquifers, because this dictates the timeframe for onshore aquifer salinization and the vulnerability of wells to salinity impacts more generally. The regions

where saltwater has been observed in onshore aquifers are identified in Table 2.2, which also describes any published interpretations of the sources of saltwater. For example, 'relic' is assigned to regions where saltwater is found in the onshore aquifer and thought to have been emplaced in the aquifer prior to modern conditions, e.g., under prehistoric sea levels and climates. Relic saltwater may also include non-marine sources in onshore aquifers (e.g., mineral dissolution), although marine and non-marine salinization sources are typically not differentiated in the studies that we reviewed. In situations involving relic saltwater movement, aquifer salinization may not reflect the classic conceptualisation of SWI, where seawater movements are linked to variations in groundwater heads relative to sea levels. In Table 2.2, 'SWI recorded' is used to indicate that aquifer salinization has been observed. That is, a decline in the onshore head under modern conditions is thought to have caused the movement of the freshwater-seawater interface into, and/or landward in, the onshore aquifer. In addition, 'undefined source' is pre-scribed to sites where saltwater has been noted onshore but no information is available on its origins. Regions where there is a reasonable level of onshore investigation (i.e., at least five salinity monitoring sites in the near-shore (< 5 km) region), and yet no seawater has been identified in the onshore semi-confined aquifer, are given a 'none observed' classification in Table 2.2. Lastly, regions where the data are inadequate to reasonably ascertain the occurrence or otherwise of saltwater in the aquifer are designated 'ND'.

Fourteen of the twenty-seven regions had sufficient data to define both h_{bmin} and h_{bmax}; otherwise, only a single value for h_b has been used commensurate with the limited degree of published investigation. In nine regions, both h_{bmin} and h_{bmax} indicate active SWI within the semi-confined aquifer, based on Eq. 2.1. In five regions, significant variations between h_{bmin} and h_{bmax} result in h_{bmin} signifying active SWI, while h_{bmax} indicates OFG inflows. In three regions, both h_{bmin} and h_{bmax} indicate OFG inflow.

A comparison can be made between driving heads (and the associated implications for the freshwater-seawater relationship) and whether or not seawater is observed in the near-shore zones of coastal aquifers. Where the near-shore groundwater remains fresh despite the presence of negative driving heads (indicating landward flow; Table 2.2), the most likely explanation is that onshore salinity data are yet to identify the presence of SWI occurring seaward of pumping wells. We associate this situation to the occurrence of OFG that is delaying the onset of near-shore/onshore SWI. Conversely, significant modern OFG is less likely to be present in regions where SWI is observed and the driving head is negative, because these factors indicate that the buffering effect of OFG and the hydraulic conditions associated with OFG inflows are lacking. In four cases, the analytical solution predicts seawater within the onshore aquifer but none has been found, thereby indicating potential OFG reserves. Three regions show evidence of SWI in field measurements, and exhibit negative driving heads, and therefore, the likelihood of modern OFG in those offshore aquifers is probably low.

2.4.3 Calculated OFG extents and comparisons to offshore observations

For the regions where OFG inflows are predicted under present-day conditions, x_{tip} and x_{toe} were calculated using available present-day head data and through application of the Werner and Robinson (2018) steady-state solution. The results are presented in Table 2.3. Positive values of x_{tip} and x_{toe} indicate an offshore position, and negative values an onshore position. In addition to x_{tip} and x_{toe}, Table 2.3 also includes the cases where the driving head indicates active SWI. Where offshore salinity data are available, Table 2.3 records the distances from the shoreline to off-shore wells containing groundwater with salinities < 50% of seawater (TDS < 17.5 g L^{-1}), or OFG extents interpreted from resistivity studies. We adopt the distances presented by Post et al. (2013) for the location of the offshore wells, while the OFG extents estimated from resistivity surveys were

obtained from various references, as listed in Table 2.1. Regions in Table 2.3 are ordered by ascending x_{toe} values obtained from application of h_{bmax} to the analytical solution.

Table 2.3. Calculated x_{tip} and x_{toe} for both h_{bmin} and h_{bmax}, and distance to offshore observations with TDS < 17.5 gL^{-1}.

Region	h_{bmin}		h_{bmax}		Offshore distance (km) to measurements of TDS < 17.5 g L^{-1}
	x_{toe} (km)	x_{tip} (km)	x_{toe} (km)	x_{tip} (km)	
Perth	Active SWI		Active SWI		50
New Jersey	Active SWI		Active SWI		130
Suriname	Active SWI		Active SWI		90
Palmahim	Active SWI		Active SWI		[a]1
Gippsland	Active SWI		Active SWI		70
Shanghai	Active SWI		Active SWI		60
Bangkok	Active SWI[#]		Active SWI[#]		-
Jakarta	Active SWI[#]		Active SWI[#]		18
Bunbury	Active SWI[#]		Active SWI[#]		-
Willunga	-46.7[#]	4.5[#]	-46.7[#]	4.5[#]	-
Niger Delta	-18.5[#]	0.04[#]	-18.5[#]	0.04[#]	40
Nantucket Island	-14.4[#]	1.1[#]	-14.4[#]	1.1[#]	60
Southern Dobruja	-14.4[#]	1.1[#]	-14.4[#]	1.1[#]	95
Carnarvon	-11.4[#]	2.5[#]	-11.4[#]	2.5[#]	-
Gambier Embayment	Active SWI		-2.7	30.0	-
Eckernförde Bay	-20.6	6.0	-1.5	6.0	-
Adelaide	Active SWI		-1.1	2.7	3.5
Albany	-0.9[#]	0.1[#]	-0.9[#]	0.1[#]	-
North Holland	-1.2	0.3	0.2	0.8	2
Uley South	-0.5[#]	2.1[#]	-0.5[#]	2.1[#]	-
Ringkøbing Fjord	-0.2[#]	1.0[#]	-0.2[#]	1.0[#]	[a]12
Northern Florida	Active SWI		2.9	41.3	100
Algarve	5.9	12.0	5.9	12.0	-
Canterbury	Active SWI		6.2	8.8	-
Howard Springs	21.6[#]	34.5[#]	21.6[#]	34.5[#]	-
Kent	22.5[#]	33.0[#]	22.5[#]	33.0[#]	-
Aveiro	Active SWI		24.8	40.0	-

[#] Denotes that only a single h_b value was available for this region.
- No offshore salinity data available for this region.
[a] Extent of OFG body inferred from offshore resistivity methods.

The calculated steady-state OFG extents (Table 2.3) that correspond with present-day heads are used here in developing coastal aquifer conceptual models. These allow for the identification of regions where no onshore seawater is expected (i.e., positive x_{tip} and x_{toe}) under steady-state conditions, and regions where seawater is predicted to eventually reach the onshore aquifer (i.e., negative x_{toe}). As mentioned above, active SWI is likely occurring in nine regions, based on both h_{bmin} and h_{bmax}. In two regions, h_{bmin} indicates active SWI, while h_{bmax} indicates a positive x_{tip} and a negative x_{toe}. In three regions, h_{bmin} is consistent with the occurrence of active SWI, while h_{bmax} indicates that the interface is entirely offshore. Of the thirteen regions with only a single h_b value, the driving heads of three are commensurate with active SWI, eight with an onshore x_{toe}, and two with entirely offshore freshwater-seawater interfaces. In Algarve, the Gambier Embayment and Eckernförde Bay, x_{tip} from the analytical solution reaches L_s, indicating that present-day OFG inflows generated from h_{bmax} are sufficient to drive freshwater to the termination of the semi-confined aquifer, given sufficient time.

Where onshore salinity data are available (Table 2.2), the salinity data indicate that the observed interface does not approximate the predicted present-day steady-state interface, with the exception of Carnarvon. More specifically, in the fourteen regions with offshore salinity data, the value of x_{tip} arising from h_{bmax} is significantly landwards of known offshore groundwater with TDS < 17.5 g L^{-1}. This provides initial evidence that a component of offshore groundwater is likely sourced from either pre-development OFG inflows, paleo-freshwater, and/or the effects of aquifer heterogeneity.

2.4.4 Calculated OFG extents from pre-development conditions

To investigate the possible contribution of pre-development conditions to OFG development, the Werner and Robinson (2018) solution was applied to obtain the steady-state interface location from h_b*, which was available for fifteen of the regions included in this study. The calculated pre-development tip (x_{tip}*) and toe (x_{toe}*) are given in Table 2.4. The pre-development driving heads, and the difference in the predicted steady-state tip (Δx_{tip}) and toe (Δx_{toe}) position between pre-development (i.e., h_b*) and present-day (i.e., h_{bmax}) conditions, are also presented. Table 2.4 is ordered by the pre-development driving head (h_b* – h_f).

Table 2.4. Pre-development driving heads (h_b* - h_f), calculated pre-development freshwater extents (x_{toe}*, x_{tip}*), and the change in steady-state seawater extent from pre-development to current conditions (Δx_{toe}, Δx_{tip}).

Region	h_b* - h_f (m)	x_{toe}* (km)	x_{tip}* (km)	Δx_{toe} (km)	Δx_{tip} (km)
Perth	-8.8	Active SWI	Active SWI	[a]	[a]
Shanghai	-1.0	Active SWI	Active SWI	[a]	[a]
Suriname	0.5	-105.7	1.9	INF	INF
Carnarvon	0.9	-11.4	2.5	0.0	0.0
Bunbury	1.7	-1515.8	125.0	INF	INF
Willunga	2.0	-3.5	12.8	-43.2	-8.2
Adelaide	2.3	0.5	4.1	-1.6	-1.4
New Jersey	2.9	4.5	11.3	INF	INF
Albany	3.1	0.01	0.3	INF	INF
Uley South	3.1	0.8	3.3	-1.3	-1.2
Howard Springs	10.0	24.5	37.4	-2.9	-2.9
Gambier Embayment	12.5	3.0	30.0	-5.7	[b]0.0
Northern Florida	14.3	28.2	66.7	-25.4	-25.4
Algarve	15.3	10.7	12.0	-4.8	[b]0.0
Gippsland	25.0	-236.6	80.0	INF	INF

INF the change in interface position is infinite as active SWI is predicted for h_{bmax}.

[a] no change calculable as active SWI is predicted for both h_{bmax} and h_b*.
[b] x_{tip} is calculated to reach L_s for both h_{bmax} and h_b*.

In eight of the fifteen regions listed in Table 2.4, the extents calculated from h_b* place the entire interface offshore. Active SWI is predicted in two regions, while an onshore interface toe is predicted in five regions. In three regions, there is no change in xtip from pre-development to present-day conditions, as both h_b* and h_{bmax} are sufficient to drive freshwater to the offshore termination of the aquitard. Except for Carnarvon, present-day water levels are lower than their pre-development counterparts, causing a potential loss in stored freshwater due to human activities. Large seasonal water level fluctuations at Carnarvon mask any longer-term trends, and therefore, the head drop from 1960 to 2016 (extrapolated from metered records covering the period 1974 – 2009) is presumed negligible. In five regions, head declines (predevelopment to present-day) result in a reversal of flow at the coastline, whereby OFG inflows are calculated from the estimated value of h_b* and active SWI arises from the value of h_{bmax}. In three regions, the decline in h_b causes the steady-state interface toe to move onshore, resulting in a prediction of onshore passive SWI. In regions where h_{bmax} predicts either active SWI or an onshore interface toe, yet pre-development heads indicate an entirely offshore interface, it is likely that onshore freshwater extractions have historically relied at least partly on OFG emplaced under pre-development conditions. Some reliance on OFG is also expected, albeit to a lesser degree, in semi-confined coastal aquifers where the toe is predicted to have moved landward between pre-development and present-day conditions.

In all regions listed in Table 2.4, x_{tip}* is significantly landwards of where offshore groundwater with TDS < 17.5 g L^{-1} is observed (Table 2.3). This suggests that for the regions included in this study, paleo-freshwater and/or aquifer heterogeneity likely

contribute to the observed offshore salinities. The contribution of paleo-freshwater proposed in this study is in agreeance with previous regional studies that also propose paleo-freshwater contributions to OFG (e.g., in Suriname (Groen et al., 2000), Nantucket Island (Marksamer et al., 2007), South Florida (Morrissey et al., 2010), and Southern Dobruja (Soulet et al., 2010)). In both Perth and Shanghai, h_b* is not sufficient to generate OFG inflows, thereby indicating the occurrence of active SWI, even under predevelopment conditions. This suggests that the onshore aquifer may have been drawing on OFG prior to 1960 (e.g., due to pre-1960 groundwater development and/or disequilibrium over geological timescales), and that in these regions, onshore reliance on OFG may have been occurring for considerable periods.

2.4.5 Known limitations of analytical methods for calculating OFG extents

The simplifications of real-world aquifers required to resolve the Werner and Robinson (2018) analytical solution impart significant uncertainties in the resulting estimates of OFG extent. For example, most coastal aquifers considered in the current study slope downwards in the offshore direction, whereas Werner and Robinson (2018) assume that the aquifer is horizontal, consistent with earlier conceptual models by Bakker (2006) and others. The extent of freshwater in sloping aquifers is likely to be less than that predicted by the Werner and Robinson (2018) solution, because downward-sloping aquifers are subjected to increasingly higher heads (imposed by the sea) in the offshore direction (due to the higher equivalent freshwater heads of the sea with increasing depth). Also, seaward slopes tend to restrict landward seawater movement because the heavier seawater must overcome the gravity forces that accompany the aquifer slope (e.g., Koussis et al., 2012).

Our analysis also suffers from the usual challenges of finding reliable aquifer properties. The offshore environment is often poorly characterised (Post et al., 2013). Some aquifers do not have clearly defined locations offshore where they connect to the sea, due to highly heterogeneous overlying aquitards, complex geologies, and/or the paucity of offshore geological information. For example, in the northern portion of the Upper Floridian aquifer, Foyle et al. (2002) identify several discrete zones where either aquitard thinning or incision by paleo-channels results in locally increased fluid exchange between the semi-confined aquifer and the overlying seawater column. Despite this, prior analytical modelling of this system by Bakker (2006) adopted the edge of the continental shelf as the aquifer-ocean connection. In general, where aquitards are heterogeneous and/or discontinuous, analytical solutions that presume uniform aquitard properties likely over-predict the steady-state OFG extent. Thus, it is noteworthy that our analytical results underestimate the known offshore freshwater extents.

While the Werner and Robinson (2018) solution treats the coastal aquifer as homogenous, offshore aquifers often contain significant heterogeneities (e.g., Michael et al., 2016). Using numerical modelling, Michael et al. (2016) show that where heterogeneity results in well-connected preferential flow pathways, freshwater can penetrate further offshore than in equivalent homogeneous K models. They conclude that the assumption of homogeneity could result in an under-estimation of the extent of OFG generated by OFG inflows. However, the coastal aquifer arrangement adopted by Werner and Robinson (2018) differs to that used by Michael et al. (2016) in their homogenous K models. Werner and Robinson (2018) separate the offshore extent vertically into an aquifer and an aquitard, hence deviating from the single hydro-stratigraphic unit used by Michael et al. (2016) to compare homogeneous and heterogeneous realisations. It is unknown if the

impacts of heterogeneity obtained by Michael et al. (2016) are of the same magnitude as would be obtained for the layered aquifer-aquitard arrangement adopted by Werner and Robinson (2018).

Another limitation of the current approach is the reliance on predicted interface locations that are in steady state. Coastal aquifers are slow to respond to changes in hydraulic conditions (Post et al., 2013), and therefore, the long periods required to approach steady-state salinity distributions may exceed the timescales of marine regression-transgression sequences. Thus, steady-state conditions may not be realistic, and only representative of the potential for the interface to move to a new alignment. That is, the predicted interface positions may only inform the potential for interface movement, thereby reflecting the current knowledge of coastal aquifer conditions and the associated human-induced head changes over time.

The limitations mentioned above result in varying, albeit unknown, uncertainties associated with the calculated steady-state tip and toe positions. The inferred uncertainty likely increases with distance offshore, given that aquifer parameters obtained from nearshore measurements are increasingly less likely to be representative of subsea aquifer properties in the offshore direction.

2.4.6 Conceptual models for coastal aquifers with OFG

We propose several alternative conceptual models of onshore-offshore groundwater systems, founded on available case studies and on the interpretations of interface conditions derived from Tables 2.2 and 2.3. The conceptual models shown in Fig. 2.3, while not exhaustive, present important relationships between onshore extractions and

OFG (and its sources) observed in the regions included in this study, along with other critical elements of the offshore hydrogeology that are fundamental to management decision-making regarding coastal fresh groundwater.

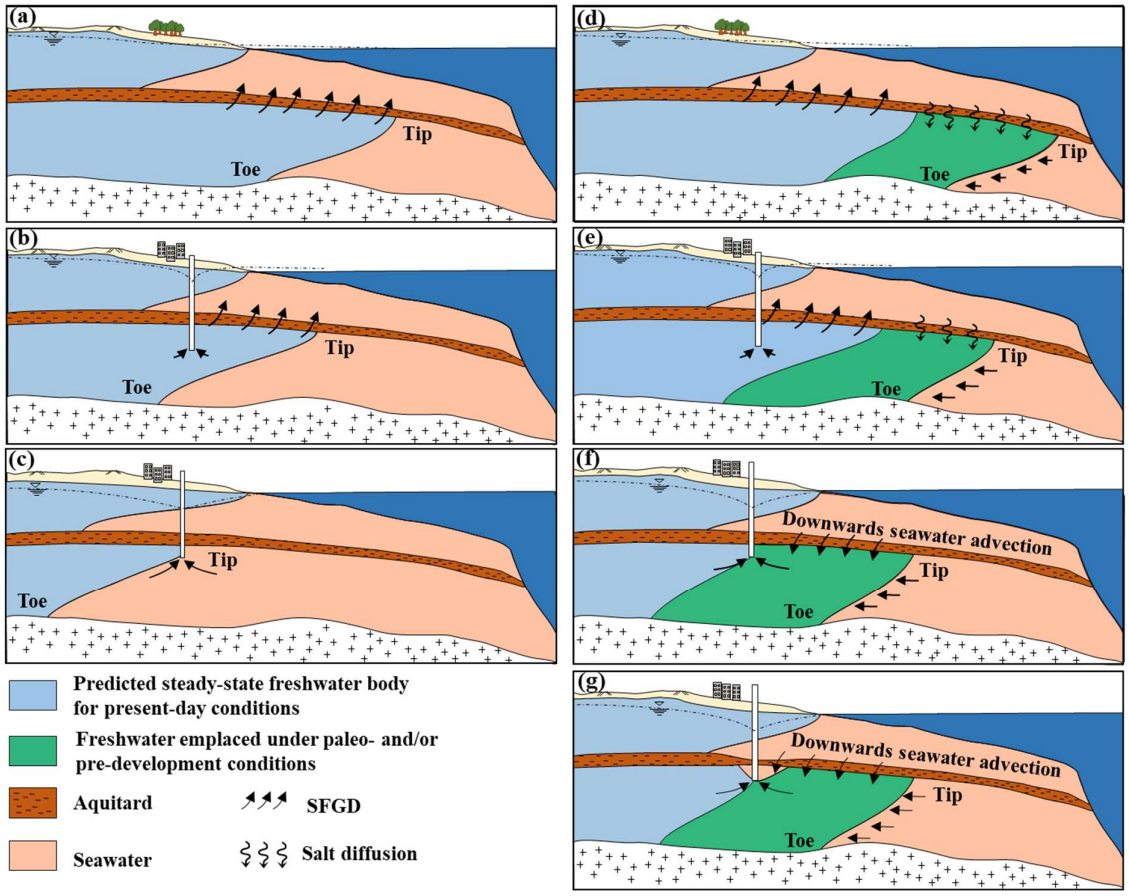

Fig. 2.3. Conceptual models of OFG, its origins, and its association with onshore pumping: (a) OFG generated by OFG inflows; minimal human development, (b) Pumping has resulted in a reduction in the OFG, without well salinization, (c) Pumping has caused aquifer salinization through active SWI. In (a), (b) and (c), any OFG is the result of present-day groundwater discharge, and salinity distributions reflect steady-state conditions, thereby representing predicted future/long-term situations arising from present-day configurations. (d) OFG includes both modern and paleo-sources, with

minimal human development, (e) Pumping reduces the extent of present-day OFG, without accessing pre-development and/or paleo-freshwater or seawater, (f) Pumping draws at least partly on pre-development and/or paleo-freshwater, and (g) Other, more complex situations, such as top-down seawater leakage through aquitards. In (d), (e), (f) and (g), the transient condition is shown, whereas the steady-state condition is expected to eventually result in loss of freshwater from paleo- and/or pre-development sources through dispersive processes, and in well salinization in (f) and (g).

The first three conceptual models (Fig. 2.3a-c) represent steady-state interface situations whereby any OFG is attributable only to stable, long-term continental discharge (i.e., the assumption of Bakker (2006) and others). In the first conceptual model (Fig. 2.3a), the interface is entirely offshore. In Fig. 2.3b, the toe is onshore and the tip is offshore. The well shown in Fig. 2.3b may or may not have caused the onshore (i.e., rather than offshore) position of the toe. Fig. 2.3c shows the final, anticipated situation arising from active SWI, causing salinization of onshore wells.

The four models shown in Fig. 2.3d-g incorporate paleo-freshwater and/or freshwater emplaced by pre-development inflows, whereby present-day OFG inflows are only responsible for a portion of OFG. The presence of paleo-freshwater and/or freshwater emplaced by pre-development OFG inflows results in freshwater occurring seaward of the steady-state interface location that corresponds with present-day water levels. Bodies of offshore paleo-freshwater can be considered as unstable, because they are likely being reduced by the diffusion of seawater, vertical leakage, and/or from hydraulic conditions that tend to draw the interface onshore, at least in aquifers where groundwater is flowing. This assumes that paleo-freshwater no longer has a modern-day source.

We consider the conceptual models shown in Fig. 2.3a-c to be the steady-state equivalents of Fig. 2.3d-f, whereby freshwater from paleo- and/or pre-development sources are eventually exhausted leading to the realisation of interface locations that correspond with present-day hydraulic conditions. Fig. 2.3d-f represent aquifers with decreasing OFG inflows, such that Fig. 2.3d is the result of the highest OFG inflows. In Fig. 2.3d, the predicted present-day steady-state interface is entirely offshore. However, due to the presence of pre-development and/or paleo-freshwater, the actual freshwater-saltwater interface occurs seaward of the steady-state interface predicted for present-day conditions. In Fig. 2.3e, seawater is entirely offshore, although under steady-state conditions, seawater is expected to cross the shoreline due to passive SWI (see Fig. 2.3b). The persistence of OFG inflows ensures that part of the onshore aquifer remains fresh despite passive SWI predicted onshore. In Fig. 2.3f, h_b is lower than h_f. This causes both the downwards advection of seawater through the offshore aquitard and landward movement of the interface in the form of active SWI. In this conceptual model, the persistence of freshwater between the pumping well and the shoreline is completely reliant on the presence of OFG, and in particular, paleo-freshwater.

Fig. 2.3g represents one of many possibilities for deviations from the idealised conceptual model adopted in the analytical solutions applied in this investigation. Here, we show an aquitard that contains a zone of thinning, which causes localised salinization of the underlying aquifer. While Fig. 2.3g displays a conceptualisation of downward leakage, we acknowledge numerous other conceptual models involving a wide range of aquifer salinization mechanisms, including the influence of aquifer and aquitard heterogeneity, the upward leakage of saltwater through underlying aquitards, the movement of paleo-

saltwater, and salinization from other (e.g., non-marine) sources. Other situations may include temporary or three-dimensional processes that are difficult to illustrate in cross-section, such as up-coning and variability in the long-shore direction causing seawater to move firstly landward and then towards wells from directions not necessarily perpendicular to the shoreline. The naming of conceptual models in the remainder is consistent with the sub-figure labelling in Fig. 2.3 (e.g., Fig. 2.3a shows "model A").

The likelihood that OFG has an influence on onshore salinities can be inferred for models D-F. In model D, the predicted steady-state interface is entirely offshore, meaning that it is unlikely that OFG contributes to present-day onshore salinities. In model E, OFG serves to delay the appearance of seawater in the onshore aquifer, although well salinization is not anticipated. Pre-development and/or paleo-freshwater stored in the aquifer may be removed through pumping, leakage through the overlying aquitard, and/or diffusion-driven salinization. For model F, pumping is at least partly maintained by the landward movement of OFG from offshore, and the future availability of fresh groundwater is closely related to the pre-development and/or paleo-OFG extent. As model G represents many alternative complex situations, there is a wide variety of possible levels of onshore use of OFG arising from this model.

2.4.7 Global assessment of the potential onshore influence of OFG

Using the available data (i.e., related to onshore and offshore salinity) and the predicted present-day steady-state interface position, each of the twenty-seven regions considered in this study are assigned one or more of the conceptual models developed in Section 2.4.6. The results are given in Table 2.5, which also includes the estimated likelihood that

onshore salinities are influenced significantly by OFG. The assigned likelihoods shown in Table 2.5 are largely subjective, being based on the available data and analytical solution results presented above. For example, regions consistent with model D are assumed to have only a low likelihood of OFG influencing the onshore salinity. In regions similar to model E, OFG is assumed to have a moderate influence on the onshore salinity. In regions consistent with model F, there is a high inferred likelihood that OFG significantly influences the onshore salinity. In several regions, variations in h_{bmin} and h_{bmax} require the assignment of one or more conceptual models to encompass the observed and predicted conditions. Where multiple conceptual models are assigned, a range of inferred levels of OFG influence is also given.

Table 2.5. Conceptual models representative of present-day conditions in each region, and the inferred likelihood that OFG influences onshore salinities (ordered by inferred likelihood of OFG influence).

Region	Assigned conceptual model	Inferred likelihood that OFG influences onshore salinities
Bangkok	^{s}G	High
Suriname	F	High
Bunbury	^{s}F	High
Gippsland	F	High
Jakarta	F	High
New Jersey	^{s}F	High
Palmahim	F	High
Perth Basin	F	High
Shanghai	F	High
Adelaide	E, F	Moderate - High
Gambier Embayment	E, F	Moderate - High
Albany	F	Moderate
Nantucket Island	^{s}E	Moderate
Niger Delta	^{s}E	Moderate
Southern Dobruja	E	Moderate
Uley South	E	Moderate

Willunga	E	Moderate
Ringkøbing Fjord	E	Moderate
Aveiro	D, F	Low - High
Canterbury	[s]D, F, G	Low - High
Northern Florida	D, F	Low - High
Eckernförde Bay	D, E	Low - Moderate
North Holland	[s]D, E	Low - Moderate
Kent	A or D	Low
Algarve	A or D	Low
Howard Springs	A or D	Low
Carnarvon	[s]B or E	Unknown

[s] Saltwater attributed to either SWI or from undefined origins in the onshore aquifer.

Sixteen of the regions shown in Table 2.5 could be described using a single conceptual model and were assigned a single likelihood of OFG influencing their onshore salinities. In nine and seven regions, it is inferred that there are high and moderate likelihoods, respectively, that onshore salinities are influenced by OFG. In four regions (Carnarvon, Kent, Algarve, and Howard Springs), the available salinity data are insufficient to allow for comparison with the steady-state estimates of the interface position. In these four regions, it was not possible to differentiate between the steady-state models (A-C) and their transient equivalents (D-F). In Kent, Algarve, and Howard Springs, the steady-state interface predicted for present-day conditions is entirely offshore. As a result, it is inferred that there is a low likelihood that OFG influences onshore salinities in these three regions. While SWI is recorded onshore in Carnarvon, the available onshore salinity data are insufficient to determine the position of the interface. In addition, no offshore salinity data are available for comparison to the predicted OFG extent. As a result, no inference can be made as to whether the approximate steady-state salinity distribution has been achieved, and hence the possible onshore influence of OFG remains unknown.

In seven regions, spatial variations in h_b result in multiple conceptual models being required to encompass the predicted and observed conditions. Accordingly, there is spatially variability in the likelihood that onshore salinities are influenced by OFG. Large differences between h_{bmin} and h_{bmax} in Northern Florida, Canterbury, and Aveiro create conditions whereby model D best represents the conditions associated with h_{bmax}, whereas models F and/or G are consistent with the conditions predicted for h_{bmin}. The occurrence of conceptual models involving OFG inflows (models D and E) and active SWI (model F), in a single region, indicates that freshwater recirculation may be occurring within the offshore aquifer. That is, freshwater may discharge to the submarine aquifer in one area, and then flow alongshore within the offshore aquifer, before being drawn back onshore by pumping. However, significant offshore groundwater flow parallel to the coastline has not been identified in previous publications. Rather, OFG distributions are typically studied using transects perpendicular to the shoreline, and thus, the effect of this transverse movement in the offshore aquifer on OFG distributions is presently unknown. The importance of alongshore flow, particular in relation to the use of cross-sectional analysis, requires further investigation.

Previous work in Canterbury and Bangkok identify that the vertical movement of seawater from overlying strata is at least partly responsible for the SWI observed in the onshore aquifer. As a result, conceptual model G was used to describe the coastal aquifer in these two regions. In Canterbury, historical SWI was linked to the downwards migration of seawater from an overlying estuary, resulting in localised SWI (Scott and Wilson, 2012). In Bangkok, regional salinization of the semi-confined aquifer is thought to be at least partially driven by downwards leakance of saltwater from overlying salinized aquifers (Buapeng and Wattayakorn, 2008; Onodera et al., 2009). In Table 2.5,

SWI or saltwater from an undefined source is noted in eight regions (including Canterbury and Bangkok). With the exception of Canterbury and Bangkok, previous studies propose that SWI is primarily a result of the interface moving horizontally landward in these regions.

The inferred likelihoods given in Table 2.5 are shown in Fig. 2.4. The propensity of a region to be classified as having a high, moderate, or low likelihood of OFG influencing the onshore salinity appears to be largely independent of its spatial location. Perhaps regions in Europe have a slightly lower tendency to be classed as having a high likelihood that OFG influences onshore salinities, than elsewhere. However, anthropogenic factors such as population density, and the high variability and scantness of OFG data, make it difficult to detect the influence of climate, recharge and geology, thereby obscuring any spatially controlled, global-scale relationships.

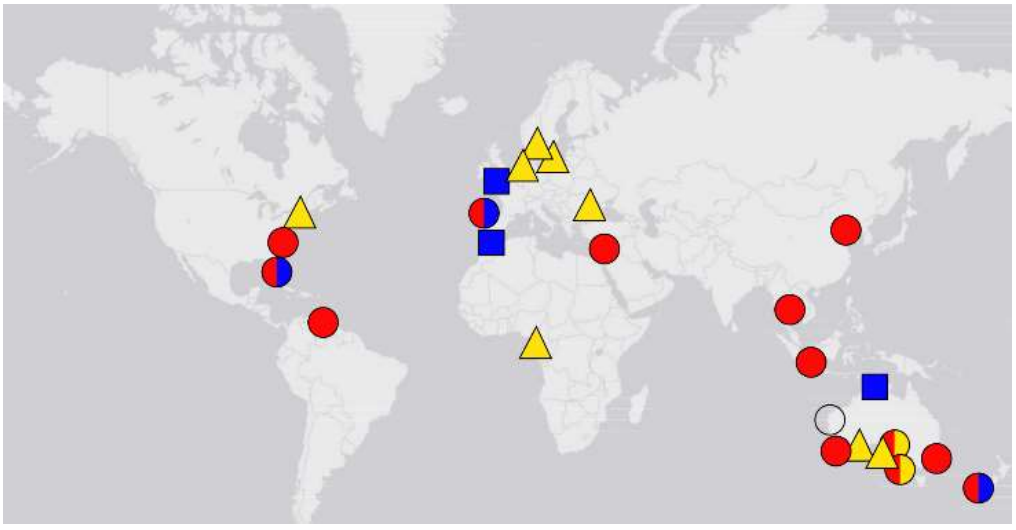

Fig. 2.4. Global distribution of the studied regions showing the inferred likelihood that OFG influences the onshore salinity. Red circles indicate regions with a high inferred likelihood, yellow triangles a moderate inferred likelihood, and blue squares a low

inferred likelihood. Duel coloured circles indicate that multiple inferred likelihoods were assigned to the region, with red, yellow, and blue shading indicating high, moderate, and low likelihoods, respectively.

OFG is possibly assisting in the maintenance of coastal water qualities in 70% of the regions included in this study. However, only three of these regions have investigations into their onshore-offshore freshwater interactions (Pope, 2006; DePaul and Rosman, 2015; Amir et al., 2013; Morgan et al., 2016). The scarcity of studies into the onshore use of OFG suggests that much of this use is either inadvertent, or at least is not informed by knowledge of the contributions to freshwater availability of OFG emplaced under paleo- and/or pre-development conditions. In regions where it is highly or moderately likely that OFG influences the onshore salinities, regional investigations that incorporate OFG into water management decision-making are vital for understanding the long-term viability of groundwater pumping from the onshore aquifer.

2.4 Conclusions

In this study, we present seven simplified conceptual models that characterise onshore-offshore freshwater interactions. The proposed models describe, for the first time, the main predicted and observed onshore-offshore freshwater interactions in semi-confined coastal aquifers that extend offshore. They show how OFG generated from paleo- or pre-development conditions can delay the onset of SWI in the onshore portion of coastal aquifers, assisting in the persistence of freshwater supply from onshore coastal wells.

A first-pass evaluation of the likely onshore influence of OFG was undertaken in twenty-seven coastal aquifers through the application of a recently developed analytical solution, in conjunction with available onshore and offshore salinity data. The findings of this

investigation suggest that OFG has a moderate-to-high influence on onshore salinities in twenty-three of the studied regions. Included in these twenty-three regions are fourteen regions where water of TDS < 17.5 g L^{-1} has been found offshore. These findings indicate that all the known OFG bodies with onshore linkages are likely already being mined either passively or actively through onshore extractions, and as such, should be assessed in regional water balances so that future freshwater availability is well understood.

Estimates of the onshore groundwater conditions prior to contemporary groundwater development indicate that OFG was being generated through discharge to offshore aquifers in thirteen of the fifteen regions for which pre-development data are available. Onshore heads were found to decline between pre-development and present-day conditions in fourteen of the fifteen regions with pre-development data. This decline results in a landward movement of the predicted steady-state freshwater-saltwater interface and a reduction of OFG. The steady-state freshwater-saltwater interface positions obtained through the application of the analytical solution for both present-day and pre-development conditions were unable to explain the available offshore salinity data in all regions investigated. As a result, either aquifer heterogeneity or paleo-OFG are required to explain observed offshore salinity data for the regions considered in this study. While analytical methods provide a useful tool in screening sites for further investigation, transient numerical approaches that include paleo-freshwater are likely required for the realistic estimation of OFG volume and extent.

At present, the contribution of OFG to onshore water supply is poorly recognised in the existing literature. The potentially widespread influence of OFG on onshore groundwater identified in this paper suggests that there is a need for further work investigating both the vulnerability of OFG to onshore drawdowns, and the transient behaviour of OFG under both passive and active SWI conditions, if coastal freshwater resources are to be managed responsibly.

2.5 Acknowledgments

The author Andrew Knight is supported by a Research Training Program scholarship. Adrian Werner is the recipient of a Future Fellowship (project number FT150100403). Leanne Morgan is partly funded by Environment Canterbury, New Zealand. We thank Wes Danskin and an anonymous reviewer for their suggestions for improvements to this article

Chapter 3

3. Combined geophysical and analytical methods to estimate offshore freshwater extent

Accepted for publication in Journal of Hydrology: Knight, A.C., Werner, A.D., Irvine, D.J., 2019. Combined geophysical and analytical methods to estimate offshore freshwater extent. J. Hydrol. 576, 529-540. https://doi.org/ 10.1016/j.jhydrol.2019.06.059.

3.1. Abstract

Offshore fresh groundwater is increasingly suggested as a potential water resource for onshore human demands. In many cases, onshore pumping already draws significant fresh groundwater from offshore. However, offshore aquifers and the extent of offshore freshwater are usually poorly characterised due to data scarcity. This study combines geophysical data, hydraulic information and a first-order mathematical analysis to investigate offshore freshwater extent in the Gambier Embayment (Australia). A large seismic data set, combined with onshore and offshore bore-log geological profiles, are used to explore the regional offshore hydro-stratigraphy. Aquifer hydraulic parameters and onshore heads are obtained from onshore investigations. A novel application of Archie's law, geophysical data and onshore hydrochemical data provide useful insights into the salinity profiles within four offshore wells. These are compared to steady-state, sharp-interface estimates of the freshwater extent obtained from a recently developed analytical solution, albeit using simplified conceptual models. Salinities derived from resistivity measurements indicate that in the south of the study area, pore water with total dissolved solids (TDS) of 2.2 g L^{-1} is found up to 13.2 km offshore. Offshore pore-water

salinities are more saline in the northern areas, most likely due to thinning of the offshore confining unit. The analytical solution produced freshwater-saltwater interface locations that were approximately consistent with the freshwater-saltwater stratification in two of the offshore wells, although analytical uncertainty is high. This investigation provides a leading example of offshore freshwater evaluation applying multiple techniques, demonstrating both the benefit and uncertainty of geophysical interpretation and analytical solutions of freshwater extent.

3.2 Introduction

Increasing coastal populations and the impacts of a changing climate are predicted to threaten the freshwater resources of many coastal communities (Post et al., 2013; Michael et al., 2017). Several studies have suggested the use of fresh and brackish water contained within confined and semi-confined submarine aquifers to assist in meeting the freshwater demands of coastal communities (Cohen et al., 2010; Bakken et al., 2012; Post et al., 2013; Jiao et al., 2015). Here, we consider freshwater salinities as total dissolved solids (TDS) < 1 g L^{-1}, while brackish water salinities are 1 g L^{-1} < TDS < 10 g L^{-1}. The landward movement of fresh and/or brackish groundwater stored in subsea aquifers likely delays onshore seawater intrusion (SWI) in several regions globally (Knight et al., 2018). However, as coastal groundwater investigations frequently focus on the onshore resources and coastal fringe processes more generally, the behaviour of fresh groundwater within submarine aquifers remains understudied (Bratton, 2010; Post et al., 2013; Werner et al., 2013).

The occurrence of subsea freshwater and brackish water (referred to collectively as offshore fresh groundwater (OFG) in what follows) is thought to form through two main mechanisms. Firstly, OFG can form where fresh groundwater discharges from an onshore confined or semi-confined aquifer (hereafter termed "semi-confined") into the offshore continuation of the aquifer (Kooi and Groen, 2001; Bakker, 2006). Secondly, increased continental shelf exposure due to vastly different hydraulic conditions during glacial maxima, in some cases leading to increased groundwater hydraulic gradients, are thought to have facilitated the emplacement of freshwater in present-day submarine aquifers (Cohen et al., 2010; Post et al., 2013; Morgan et al., 2018). Both mechanisms require an

overlying aquitard to inhibit the rapid vertical mixing of fresh and saline waters that would otherwise occur due to the buoyancy forces induced from seawater overlying freshwater.

Various methods have been applied to assess OFG reserves, although there are few studies that adopt multiple techniques to characterise offshore aquifers for the purposes of freshwater exploration, i.e., to estimate OFG extents. Direct observations of OFG include the sampling of pore-water salinities from offshore core samples (e.g., Jiao et al., 2015), and the sampling of pumped fluids from short-screened intervals offshore (e.g., Krantz et al., 2004). Geophysical methods for characterising OFG include downhole deep-induction resistivity logs and resistivity transect surveys (e.g., Oteri, 1988; Groen et al., 2000; Krantz et al., 2004; Hennig and Otto, 2005). The inverse relationship between resistivity and fluid salinity, contained in Archie's Law (Archie, 1942), can allow for freshwater to be inferred from both transect and downhole resistivity data. However, the method requires knowledge of porous medium resistivities, leading to seldom reported uncertainties in the pore-water resistivities calculated using Archie's law.

There are limited documented studies investigating how regional variations in the hydro-stratigraphy impact offshore salinities. Krantz et al. (2004) used a combination of seismic, resistivity and drill-hole data from aquifers below Indian River Bay (Delaware, USA) to conclude that OFG can preferentially form within sand-filled incised valleys that are silt-capped, with OFG within such channels able to reach several kilometres offshore. Mulligan et al. (2007) identified that when the overlying confining unit is incised by paleo-channels, enhanced vertical flows resulting in increased freshwater-saltwater mixing are likely. Pauw et al. (2017) used onshore data and analytical modelling to

demonstrate how shore-parallel variability in the onshore hydro-stratigraphy can alter the OFG extent. Michael et al. (2016) used cross-sectional numerical modelling to show that, in comparison to a homogeneous aquifer, freshwater can extend further offshore in aquifers that have strong vertical heterogeneity but well-connected horizontal flow paths. To date, there is no study supported by offshore data that investigates the potential alongshore variability of OFG extent on a regional scale.

Despite the fact that OFG is considered to be widespread (Post et al., 2013), only three OFG bodies are evidenced by offshore data from the Australian continental shelf, i.e., Perth basin (Hennig and Otto, 2005; Morgan et al., 2018), Adelaide Plains sub-basin (Knight et al., 2018), and Gippsland basin (Varma and Michael, 2012). In all cases, OFG has been found adjacent to significant onshore pumping, which is thought to be mining offshore freshwater to supplement onshore demands (Knight et al., 2018). In the Gambier Embayment (GE), located in the southeast of South Australia (Fig. 2.1), groundwater supports extensive irrigation schemes and provides water supplies for three coastal towns. Previous studies of the GE suggest that local head conditions in the regional semi-confined aquifer may be conducive to the formation of an extensive OFG body (e.g., Pollock, 2003; Bush, 2009; Morgan et al., 2015), although the occurrence and magnitude of this resource are currently unsubstantiated.

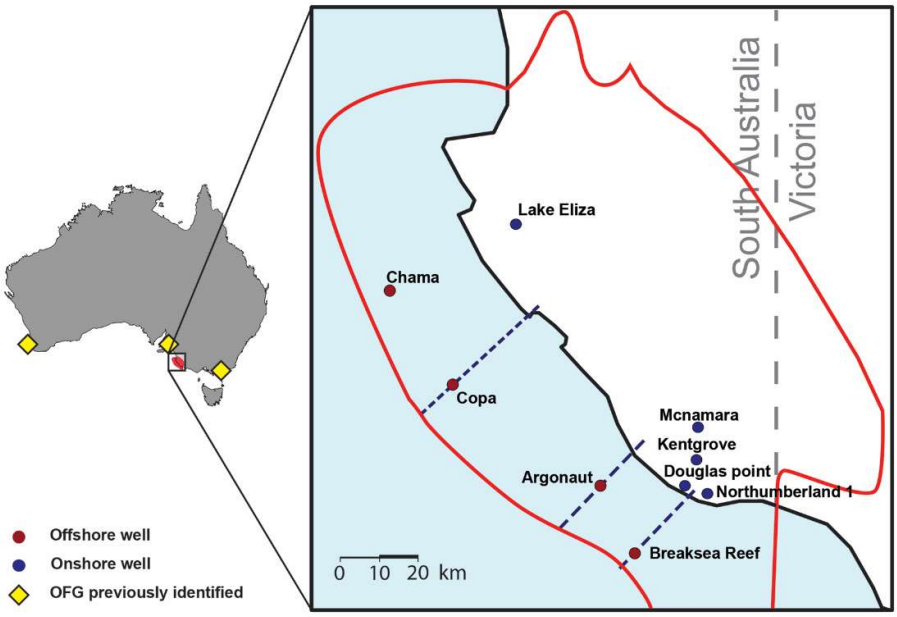

Fig. 3.1. Regional map showing the location and extent of the GE, delineated by the red line. Current accounts of Australian OFG, identified in existing literature, are marked by yellow diamonds on the national map. Blue and red dots mark onshore and offshore petroleum exploration wells, respectively. Blue dashed lines show the transects used in the current study to apply analytical modelling, herein referred to by the respective wells though which they pass.

Previous studies of the GE by Pollock (2003) and Bush (2009) include offshore interpretations of the main regional semi-confined aquifer (i.e., the Lower Tertiary Confined Aquifer (LTCA)). However, digital copies of the lithological surfaces presented by Pollock (2003) are no longer available and do not separate the LTCA from the overlying confining unit. The hydro-stratigraphic surfaces presented by Bush (2009) terminate at the offshore petroleum exploration well (herein referred to as offshore wells) locations despite the system extending tens of kilometres past the well locations. Neither of these previous seismic studies have generated the hydro-stratigraphic surfaces required to assess the extent of OFG in the GE.

This study aims to provide a best estimate of offshore pore-water salinities in the regional semi-confined aquifer of the GE using available data and through application of the analytical solution of Werner and Robinson (2018). The study also aims to identify the offshore distribution of the upper semi-confined aquifer in the GE, at least at a resolution reasonable for the large scale of the study area, using seismic-line survey data. Knowledge of the offshore hydro-stratigraphy is vital for understanding potential offshore groundwater fluxes, for the interpretation of calculated offshore salinities, and to inform the application of analytical approaches. We aim to establish offshore salinities in the regional semi-confined aquifer of the GE using legacy downhole geophysical data from both onshore and offshore petroleum exploration wells. This study represents the first attempt at using onshore salinity-resistivity relationships to inform the offshore application (and uncertainties) of Archie's law, with the aim of inferring groundwater salinities and the extent of OFG. We compare the salinities calculated from geophysical data against those predicted by analytical modelling to explore the potential influence of present-day hydrological forcing. The Werner and Robinson (2018) analytical solution is applied to a range of conceptual models, each representing simplified versions of the offshore conditions of the GE as determined from available field data.

3.3 Study area

The GE is the western sub-basin of the Otway Basin, an extensive passive rift-sag-rift basin (Boult and Hibburt, 2002) that reaches the city of Melbourne, some 500 km east of the South Australian-Victorian border (Fig. 3.1). The GE is bounded in the northwest by the Tartwaup Hinge Zone and in the southeast by the Portland Trough (Freeman et al., 2010). The offshore regions of the basin are heavily faulted. Offshore fault lines are

generally steeply dipping towards the southwest and have a northwest-southeast strike (Freeman et al., 2010; Holford et al., 2014; Clarke et al., 2015). Previous studies of the GE have identified three hydro-stratigraphic units of importance to anthropogenic activities (Love et al., 1993; Smith et al., 2012; Morgan et al., 2015; Clarke et al., 2015). These are: (1) an Upper Unconfined Aquifer (UUA) comprised primarily of the Gambier Limestone; (2) an Upper Tertiary Aquitard (UTA), consisting of marl intervals and the upper clay layer of the Dilwyn Formation; (3) a Lower Tertiary Confined Aquifer (LTCA), which encompasses several interbedded, and generally unconsolidated, sand and carbonaceous clay layers of the Dilwyn Formation (Clarke et al., 2015). The UUA, UTA and LTCA are primarily offshore dipping. These units reach a maximum combined thickness of ~1 km in the south of the study area, and thin towards the north (Love et al., 1993). Previous onshore investigations of the GE assume a lower hydro-stratigraphic boundary consisting of the lower clay unit of the Dilwyn Formation in the south, and the Sherbrook Formation (comprising interbedded sands and clays) in the north (Morgan et al., 2015). This lower boundary is based on the assumption that current anthropogenic activities are unlikely to interact with water contained in the Sherbrook Formation (Morgan et al., 2015). We adopt the same assumption in our study.

3.4 Methods

3.4.1 Offshore stratigraphy from seismic-line surveys

In the offshore region of the GE, 32 shore-perpendicular seismic lines and 19 shore-parallel seismic lines were selected for the interpretation of the offshore stratigraphy. Seismic and geophysical well data were obtained from the South Australian Government, Department of the Premier and Cabinet, Energy Resources Division (J. Davies, 2017, pers. comm., 14 December 2017). To generate a regional-scale model of the offshore distributions of the UUA, UTA and LTCA, seismic-line surveys were selected at 3 km spacings in both the shore-parallel and shore-perpendicular directions. Where possible, seismic lines that include multiple well ties (i.e., passing through one or more wells from which downhole lithology has been recorded) were chosen. Seismic data are of varying quality and were acquired at different times. Consequently, it was not possible to determine a minimum resolvable vertical resolution that could be applied to the entire data set. However, previous work using the same data found that seismic reflectors are clearly imaged for units with a two-way travel-time (TWT) under 2000 ms (Freeman et al., 2010). The seismic-line survey data contain no information within 5 km of the shoreline due to a regulatory exclusion zone.

We adopt the methodology used by Pollock (2003) for the interpretation of the hydro-stratigraphic horizons. The top of the UUA, UTA, LTCA, and the Sherbrook Formation were selected to characterise the regional hydro-stratigraphy. As seismic-line surveys have a vertical axis measured in the time domain, a conversion between the measured TWT and depth is required to identify the target horizons on downhole lithology logs. A

regional depth-to-TWT relationship of $z = -1132 \times TWT^{1.2678}$ (R^2 of 0.99) was obtained from regression of the available synthetic-seismogram data (i.e., measured TWT values at set depths) from the Breaksea Reef, Chama, and Copa wells (see Fig. 3.1 for well locations). We use the elevation datum "m AHD" (metres Australian Height Datum), where 0 m AHD is approximately mean sea level. The interpreted seismic horizons for the LTCA were compared against the available hard-copy data presented by Pollock (2003) to ensure that the interpreted seismic sections were equivalent.

Natural-neighbour interpolation was used to generate continuous surfaces for each hydro-stratigraphic unit. Natural-neighbour interpolation was selected due to the linear and clustered characteristics of the seismic-line survey data. The input data consisted of both offshore data points obtained from the tracing of the seismic-line surveys and onshore data points acquired from Morgan et al. (2015). A cell size of 500 m was selected due to the large scale of the study area. The surfaces representing the top of the UTA and LTCA were clipped to honour the extents of these units interpreted from the seismic-line surveys. As this study focuses on the LTCA, the extents of the UUA and pseudo-basement surfaces were restricted to an arbitrarily chosen 10 km from the spatial limits of the available data, as beyond this distance, the surfaces are unlikely to be realistic.

3.3.2 Calculating offshore groundwater salinities from geophysical borehole logs

3.3.2.1 Obtaining regional parameters for application of Archie's law

Archie's law (Archie, 1942) is an empirically derived relationship that allows for the calculation of fluid resistivity (r_f) (Ω-m) from a measured bulk resistivity (r_o) (Ω-m) in

formations with a relatively non-conductive matrix (e.g., sand, free from clay minerals). Archie (1942) proposed that r_f, r_o, porosity (i.e., total porosity; φ), and a cementation exponent (m) can be related using:

$$r_o = r_f \varphi^{-m} \quad (3.1)$$

In Archie's law, m is related to the degree of connectedness of the pore network (Glover, 2009). A value of $m = 1$ represents a bundle of capillary tubes with all pore spaces connected, while higher values (e.g., 2.5 to 5) represent carbonates with poorly connected pore spaces (Glover, 2009). Typical values of m for sandstone range from 1.3 to 2.6 (Archie, 1942). Values of m are usually established by taking the best-fit slope through a plot of $\log(r_o/r_f)$ versus $\log(\varphi)$ or through re-arranging Eq. 3.1 to solve for m directly (Glover, 2016).

Despite extensive petroleum exploration within the GE, no pre-existing values of m have been reported within the available literature. Values of m were obtained by applying Eq. 3.1 to five onshore petroleum exploration wells (Fig. 3.1) where r_o and lithological data were available. However, values of r_f in the LTCA were unavailable in all the petroleum exploration wells (both onshore and offshore). In addition, no onshore monitoring wells had both φ and r_o data recorded in the LTCA. To apply Eq. 3.1 to the onshore petroleum exploration wells, values of r_f corrected to 25°C were adopted from the nearest short-screened onshore monitoring well in the LTCA with hydrochemical data available (DEW, 2019). Groundwater salinity measurements elsewhere within the onshore region of the LTCA have low variability over distances similar to the distances between the groundwater monitoring wells where r_f values were obtained and the onshore petroleum exploration wells. For example, the recorded TDS changed by 25 mg L^{-1} between two

onshore monitoring wells (well 7022-7871 and well 7021-3339) that were ~10 km apart. The distances between the petroleum exploration wells and the onshore monitoring wells were under 10 km. As r_f data were only available for the upper sand interval of the LTCA, r_o data were also restricted to this interval. The upper sand intervals of the onshore petroleum wells were at similar depths to the screened interval depths in the onshore monitoring wells from which r_f data were obtained. Upper clean sand horizons in each well were identified from downhole lithological descriptions, with gamma ray logs used to discern clean sands from those with significant clay. Using this approach, the GE was found to have clean sand horizons with a gamma ray signature of < 25 API. Lithological descriptions for LTCA sand horizons and the data available for each of the wells used in this study are presented in Appendix 1 (Table A1.1). As a variable number of geophysical data points were available within the upper sand horizon in each well, the mean m value for each onshore petroleum exploration well (m_w) was obtained. The regional value for the LTCA of m (m_r) was obtained by taking the mean of the m_w values. The standard deviation of m_r (σ_m) was also obtained.

Porosity can be estimated from both bulk density and sonic logs. Of the wells included in this study, only Argonaut and Chama have both bulk density and sonic logs in the targeted hydro-stratigraphic units. Except for the Copa well, all wells (both onshore and offshore) have sonic log data. A regional value of porosity was used in the application of Eq. 3.1 to the Copa data because both sonic and bulk density logs were absent at the depths of interest to this study. In the Argonaut and Chama wells where both sonic and density data were available, porosity was preferentially determined for each data point from bulk density logs, according to:

$$\varphi_b = \frac{\rho_m - \rho_b}{\rho_m - \rho_w} \tag{3.2}$$

Where φ_b is the bulk-density-derived porosity, ρ_m is the density of the solid matrix (~2650 kg m^{-3}; e.g., Groen et al., 2000), ρ_b is the measured bulk density of the saturated porous media (kg m^{-3}), and ρ_w is the density of water (~1000 kg m^{-3}). Excluding the Argonaut, Chama and Copa wells, porosity was determined for each LTCA data point (representing clean sand) from sonic-log data using the Wyllie time-average equation (Wyllie et al., 1958):

$$\varphi_s = \frac{\Delta t_z - \Delta t_{ma}}{\Delta t_f - \Delta t_{ma}} \quad (3.3)$$

Where φ_s is the sonic-derived porosity, Δt_z is the measured acoustic transit time (i.e., the time taken for the seismic wave to travel a unit distance) (μs m^{-1}), Δt_{ma} is the acoustic transit time of the rock matrix (192.9 μs m^{-1}) taken from well completion reports, and Δt_f is the acoustic transit time of interstitial fluids (a value of 616 μs m^{-1} was adopted from the well completion reports). As sonic porosities in unconsolidated sediments tend to overestimate the total porosity, the sonic porosity was divided by a correction factor (c_p), calculated using (Raymer et al., 1980):

$$c_p = \frac{\varphi_s}{\varphi} \quad (3.4)$$

The regional value of c_p for the GE was taken as the mean c_p from the Argonaut and Chama wells, for which φ_s were available and φ could be approximated as φ_b values.

In Copa, neither sonic nor bulk-density logs were available in the LTCA. To enable the application of Eq. 3.1 to the Copa well data, a single regional LTCA φ value was established by taking the mean of the calculated φ values of all data points in the LTCA

sand layers (using data from the other eight wells (both onshore and offshore) included in this study).

As electrical resistivity is dependent on temperature, r_o was converted to equivalent values at a standard temperature of 25°C, using (Jorgensen, 1996):

$$r_{25,z} = \frac{1.8(T_z+3\ )}{84} r_{o,z} \tag{3.5}$$

Where $r_{25,z}$ is the bulk resistivity (Ω-m) adjusted to 25°C at depth z, $r_{o,z}$ is the bulk resistivity (Ω-m) measured at depth z, and T_z is the temperature (°C) at depth z (m). T_z is calculated from the local geothermal profile obtained from drilling completion reports, of:

$$T_z = 0.2759z + 19 \tag{3.6}$$

3.3.2.2 Calculating offshore salinity profiles

The downhole r_f profiles of four offshore wells in the GE were calculated by applying a re-arranged form of Eq. 3.1 to temperature-corrected resistivity data from each well. Temperature corrections were undertaken using Eq. 3.5. To identify the possible r_f values due to uncertainty surrounding the estimation of m_r, pore-water resistivities were calculated from Eq. 3.1 using m values of m_r, $m_r \pm 1\sigma_m$, and $m_r \pm 2\sigma_m$. The calculated fluid resistivities were converted to an approximate TDS (mg L^{-1}) at depth z using an empirically derived relationship of:

$$TDS_z = \frac{10{,}000 \times 0.55}{r_f} \tag{3.7}$$

A mean TDS value for each sand interval ($\overline{TDS}$) was established by averaging the calculated pore-water salinities of all the data points contained within each respective sand interval. This was repeated to obtain $\overline{TDS}$ values for all sand intervals, and using alternative values of m (i.e., m_r, $m_r \pm 1\sigma_m$ and $m_r \pm 2\sigma_m$).

3.3.3 Sharp-interface analytical modelling of present-day steady-state conditions

To explore the possible OFG extent attributable to present-day OFG inflows in the LTCA, the analytical solution of Werner and Robinson (2018) was applied to three simplified shore-normal transects. The Werner and Robinson (2018) solution assumes that the aquifer is flat lying, isotropic, homogeneous, of constant thickness, and is confined onshore and semi-confined offshore. The solution also assumes that: (1) the system is at steady state with respect to onshore heads, (2) the freshwater-saltwater interface can be represented by a line of pressure equilibrium (i.e., a sharp interface), (3) shore-parallel flow is negligible, and (4) vertical freshwater flow in the aquifer can be neglected, while horizontal flow in the semi-confining unit is ignored.

The modelled transects pass through the Breaksea Reef, Argonaut, and Copa wells (Fig. 3.1). As the interpreted seismic-line survey data indicated that the LTCA and UTA are not continuous between the onshore environment and Chama, the analytical solution of Werner and Robinson (2018) cannot be applied to investigate the potential salinity at Chama from current onshore conditions. Also, the top of the LTCA has an offshore slope of around 1% on average, whereas the analytical solution assumes that the aquifer is horizontal. To account for this, two different sets of geometric conditions (aquifer depth and thickness) were used in applying the analytical solution to each transect, namely: (1)

reflecting the conditions at the shoreline, and (2) reflecting the conditions at the offshore wells.

The Werner and Robinson (2018) solution requires the hydraulic conductivity (K) of the aquifer (K_a, m d^{-1}), the thickness of the aquifer (H), the thickness of the semi-confining unit (D), a specified head (h_b) at a distance onshore (x_b), the vertical K of the semi-confining unit (K_l, m d^{-1}), the length of the offshore semi-confining unit (L_s), the depth to the base of the semi-confined aquifer below sea level (z_0), and the densities of fresh (ρ_f, kg m^{-3}) and saline water (ρ_s, kg m^{-3}). The Werner and Robinson (2018) solution allows for the designation of the pore-water salinity of the semi-confining unit, which in this case was set to freshwater, following the recommendation of Solórzano-Rivas and Werner (2018). The parameter sets applied to the Werner and Robinson (2018) solution are listed in Table 3.1. Parameters obtained from the offshore wells are denoted by an asterisk. Otherwise, parameters reflect onshore data. The analytical solution was applied to both present-day and pre-development heads (h_b and h_b^p, respectively) in the onshore aquifer. Values for h_b^p are approximate only, and were estimated by extrapolation based on temporal head slopes from earliest recordings (typically in the 1970s). The tip and the toe (where the freshwater-saltwater interface coincides with the aquifer top and bottom, respectively) were obtained by applying the parameters in Table 3.1 to the analytical solution. Resistivity-derived salinities of TDS ≈ 17.5 g L^{-1} (50% of seawater) were used to compare to the tip and toe positions calculated using the sharp-interface analytical solution in the same manner as previous publications (e.g., Werner, 2017b).

Table 3.1. Parameters used in applying the Werner and Robinson (2018) solution.

Well	General properties						Onshore properties			Offshore properties		
	K_a (m d^{-1})	h_b (m)	h_b^p (m)	x_b (km)	K_l (m d^{-1})	L_s (km)	H (m)	z_0 (m)	D (m)	H^* (m)	z_0^* (m)	D^* (m)
Breaksea Reef	[a]3.1	[b]17.1	22	0.5	[a]0.0001	33.9	358	694	42	290	905	106
Argonaut	[a]3.1	18.9	22	11.0	[a]0.0001	32.4	415	780	125	356	710	43
Copa	[a]3.1	16.8	23	1.1	[a]0.0001	40.0	73	403	55	46	500	44

[a] Value adopted from Morgan et al. (2015).

[b] Head value averaged from past two years due to a strong seasonal fluctuation.

3.5 Results

3.5.1 Offshore hydro-stratigraphy

The horizons traced in the seismic-line surveys show evidence of extensive shore-parallel faulting within the offshore hydro-stratigraphic units. Fault-induced displacement appears to have led to localised thinning of the UTA in several survey lines. The interpreted seismic horizons corresponding to the hydro-stratigraphic units for the UTA and the LTCA indicate that the respective units either pinch out underneath the UUA at the continental slope; or remain covered by the UUA rather than terminating at the seafloor. An example of this is visible in Fig. 3.2a. The northern offshore extent of the UTA and

LTCA was determined by considering that these two units appear to onlap (i.e., pinch out) against a local high in the underlying Sherbrook Formation (Fig. 3.2b), causing the interpreted units to become discontinuous. An example of this onlap is highlighted in Fig. 3.2b. Other seismic-line surveys that pass through Chama appear to show similar onlap against the Sherbrook Formation in other directions outwards from the Chama well (see Fig. 3.3a). This suggests that the UTA and LTCA recorded in the downhole-lithological log at Chama are disconnected from their onshore counterparts. Fig. 3.2a also provides an interpreted cross section of the aquifers of interest to this investigation. Two additional interpreted cross sections are provided in Appendix 1 (Fig. A1).

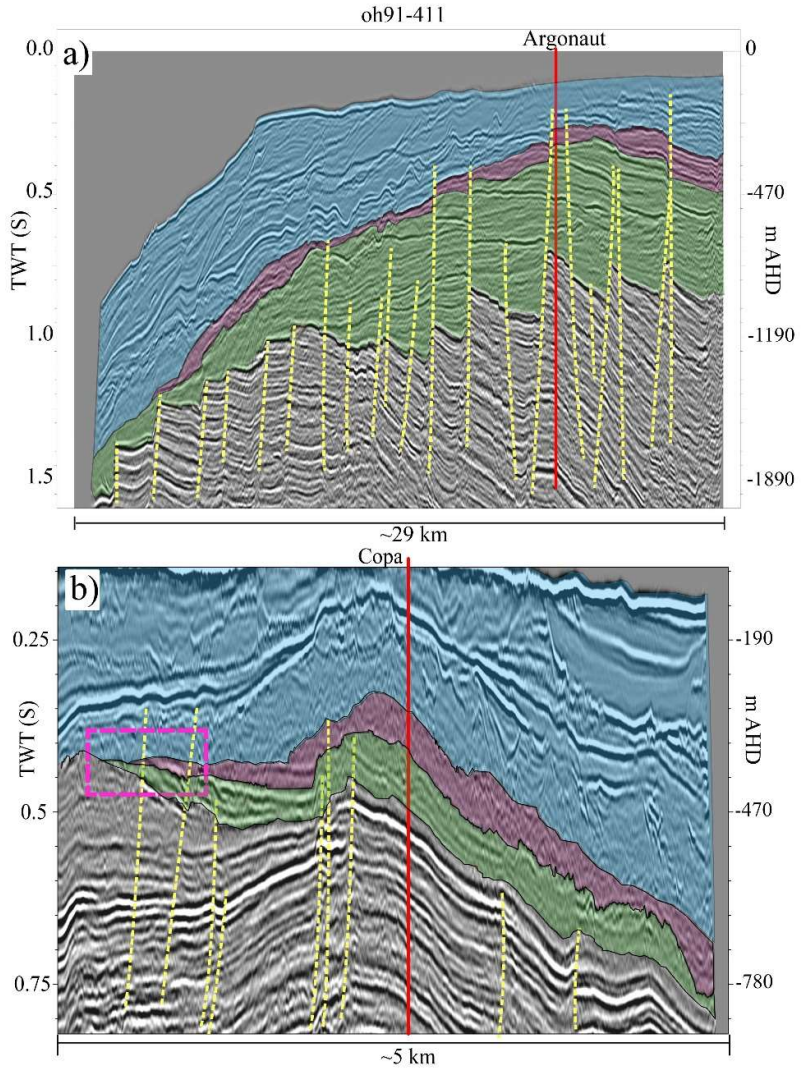

Fig. 3.2. Seismic-survey lines passing through Argonaut and Copa (upper (a) and lower (b) panels, respectively). Well locations are marked by the solid red lines, while major interpreted faults are shown by the dashed yellow lines. Blue, pink, and green shading indicate the UUA, UTA, and LTCA units, respectively. Pink dashed box in (b) highlights the area where the UUA and LTCA appear to onlap against the Sherbrook Formation. The locations of seismic-lines are marked in Fig. 3.3b. The seismic line shown in (a) runs perpendicular to the shoreline from A to A' as marked on Fig. 3.3. The shoreline is located ~5 km to the right of (a). The seismic line shown in (b) runs parallel to the shoreline from B (northwest) to B' (southeast), also marked on Fig. 3.3.

The isopach distribution for the UTA and LTCA are shown in Fig. 3.3. While both the interpolation process and the large cell size chosen acted to dampen high frequency features (e.g., sharp fault-driven elevation changes) in the interpolated offshore hydro-stratigraphic surfaces, there is still noticeable variability regionally in the offshore thickness of the UTA and LTCA. South of Argonaut, the calculated thickness of the UTA (Fig. 3.3a) varies predominantly between 50 m and 150 m. North of Argonaut, the UTA is mainly 25 m to 100 m thick. The LTCA also displays increased thickness south of Argonaut (Fig. 3.3b), with thicknesses predominantly between 450 m to 1145 m thick. North of Argonaut, the LTCA thins to between 100 m and 550 m. This northward thinning is also visible in the three interpreted cross sections presented in the Appendix 1 (Fig. A1.1). Three paleo-channel features described by Pollock (2003) were interpreted to incise through the UTA and into the LTCA close to the continental slope (Fig. 3.3a), with the largest of these paleo-channels occurring midway between Copa and Argonaut. As these paleo-channels incise through the UTA, they may reduce the semi-confined offshore extent of the LTCA, and lead to saltwater entering the aquifer preferentially from above. Two maps that display the top of the UTA and LTCA are presented in the Appendix 1 (Fig. A1.2 and Fig. A1.3).

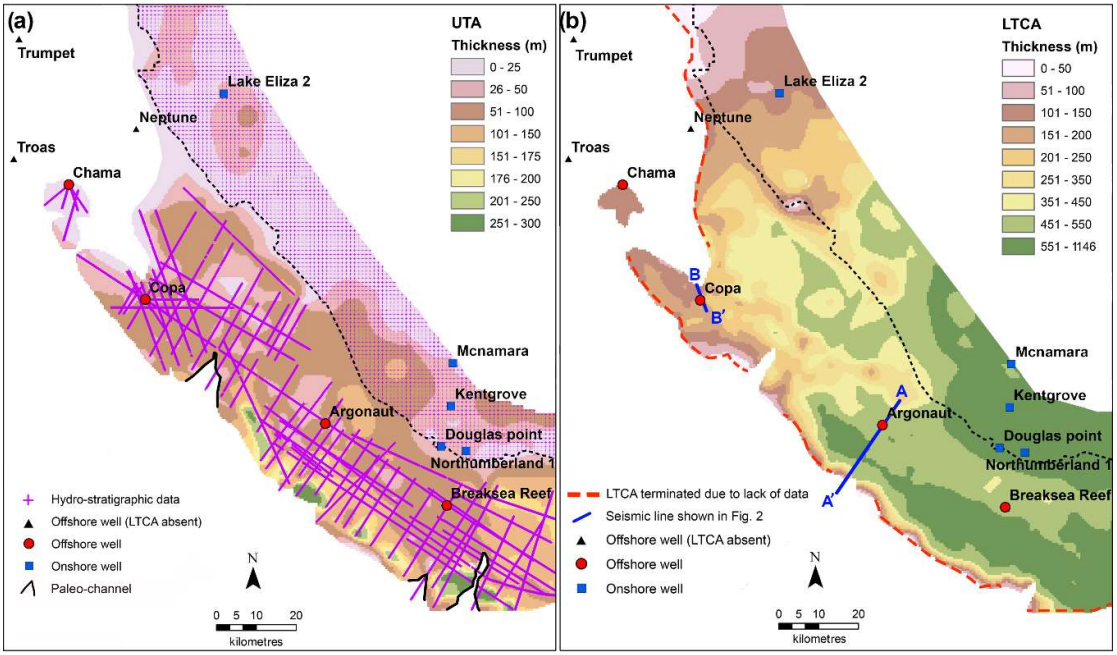

Fig. 3.3. Isopach maps of (a) the UTA and (b) the LTCA. The blue squares and red dots indicate onshore and offshore wells, respectively. Black triangles indicate offshore wells where the UTA and LTCA are absent in lithological logs. The black-dashed line marks the coastline. In (a), the purple crosses, which appear as purple lines due to their high density, show the data points used in the interpolation of hydro-stratigraphic surfaces. Interpreted paleo-channel extents are marked by solid black lines. In (b), the two seismic-line segments shown in Fig. 3.2 are marked by blue lines (AA' and BB'), while the red dashed lines indicate where the LTCA and the UTA are terminated due to distance from data points.

3.5.2 Establishing regional parameters for Archie's Law

Using the onshore petroleum exploration well data, an m_r value of 1.40 and a σ_m of 0.14 were obtained. The regional value of c_p established from paired sonic and density logs was 1.74. The available density and corrected sonic data produced an average φ of 0.37,

along with σ_φ (standard deviation of the calculated porosities for LTCA clean sand intervals, extracted from the other eight wells included in this study) of 0.068. There was no clear relationship between φ and depth, or between m and depth. These data are presented in the Appendix 1 (Fig. A1.4 and Fig. A1.5).

3.5.3 Offshore salinity profiles from geophysical data

Fig. 3.4a shows the TDS values for each r_o measurement (limited to sand intervals) in the Argonaut well. Despite substantial TDS variability, the two shallower sand intervals show distinctly lower TDS values than the two deeper sand intervals. There is significant scattering of TDS values within each sand layer. This scattering is greater in the two lower sand intervals where calculated TDS values are higher. The observed scattering of the calculated TDS values in an individual sand layer was due to fluctuations in both φ and r_o with depth. This suggests that a single calculated TDS value is unlikely to be representative of the pore-water salinities that would be encountered across the entire

sand interval.

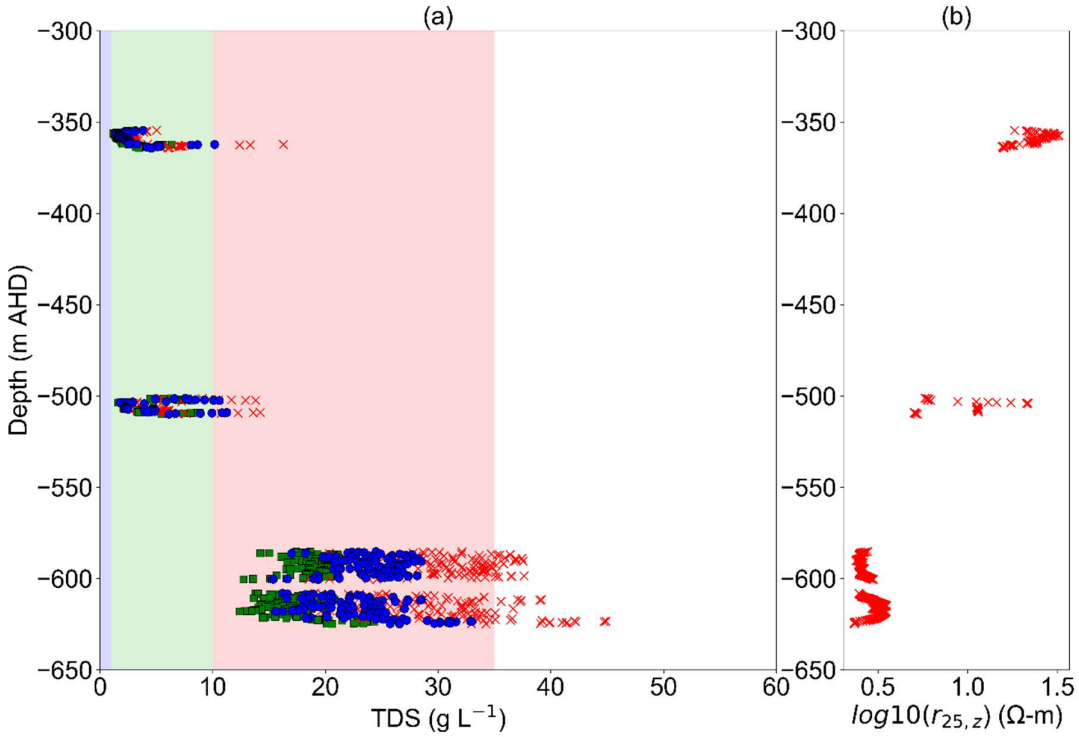

Fig. 3.4. (a) Calculated TDS values for each r_o measurement of the Argonaut well with depth. Cyan circles, red crosses and green squares show TDS values obtained using m values of m_r, $m_r + 2\sigma_m$ and $m_r - 2\sigma_m$, respectively. Blue, green, and red background shading indicates fresh, brackish, and saline pore water, respectively. White shading indicates a TDS above that of typical seawater. In (b), the temperature corrected r_o values versus depth for Argonaut are displayed. Temperature corrections were undertaken using Eq. 3.5.

The mean values of TDS ($\overline{TDS}$) for each sand layer in the four offshore wells of interest (Argonaut, Breaksea Reef, Chama and Copa) are presented in Fig. 3.5. $\overline{TDS}$ calculated using m_r, $m_r \pm \sigma_m$ and $m_r \pm 2\sigma_m$ are shown for each sand interval. The wells ranked in order of the lowest salinity groundwater encountered in each well are: Argonaut,

Breaksea Reef, Chama and Copa. The salinities within the Copa well are the highest, with $\overline{TDS}$ in the LTCA ranging between 22.2 g L^{-1} and 30.9 g L^{-1}. The distinctive increase in $\overline{TDS}$ with depth that is apparent at Argonaut (Fig. 3.4a) can also be found in the Breaksea Reef, Chama and Copa wells, although without the same well-defined salinity stratification of the Argonaut data. For example, the Breaksea Reef data reveal elevated salinities in the uppermost sand interval, for which $\overline{TDS}$ is 11.2 g L^{-1}, while the two underlying sand intervals have a $\overline{TDS}$ of 3.8 g L^{-1} and 4.2 g L^{-1}, respectively. Salinities appear to increase with depth thereafter, with the deepest sand interval in the Breaksea Reef well having a $\overline{TDS}$ of 14.7 g L^{-1}. In Argonaut, salinities increase with depth within the LTCA with a $\overline{TDS}$ of 2.2 g L^{-1} calculated for the shallowest sand interval, while the deepest sand interval in the LTCA has a $\overline{TDS}$ of 22.9 g L^{-1}. In the Chama well, salinity in the LTCA also increases with depth, ranging from 13.1 g L^{-1} in the shallowest sand interval to 45.9 g L^{-1} in the deepest sand interval. There were no sand intervals in Copa that had a $\overline{TDS}$ under 22.2 g L^{-1}.

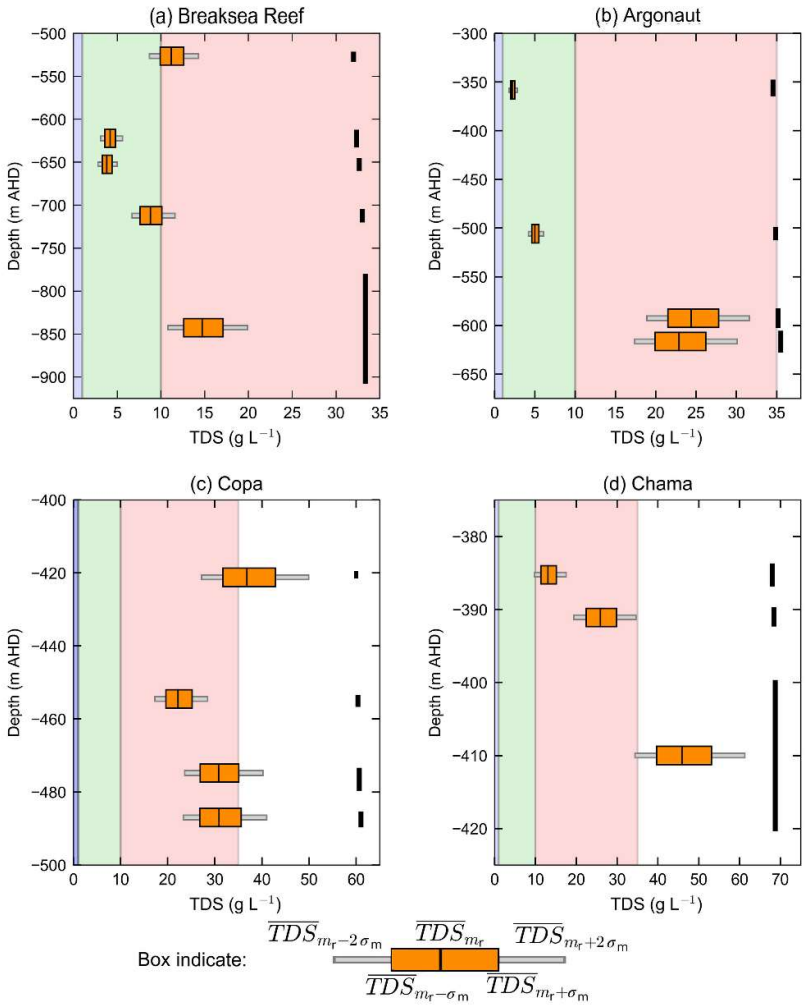

Fig. 3.5. Calculated downhole salinity profiles for the LTCA in the four offshore wells. The red, green, and blue shading indicates, saline, brackish and freshwater, respectively. White background shading indicates that the calculated TDS is above that of typical seawater. The length of the thick black lines on the right-hand side of each plot denotes the thickness of the sand interval captured by the respective box plot. The central line of each orange box shows $\overline{TDS}$ calculated using $m = m_r$, orange box edges show $\overline{TDS}_{m_r \pm \sigma_m}$ which is $\overline{TDS}$ calculated using $m = m_r \pm \sigma_m$, and the outer edges of narrow grey boxes show $\overline{TDS}_{m_r \pm 2\sigma_m}$ which is $\overline{TDS}$ calculated using $m = m_r \pm 2\sigma_m$. Note that scales differ between Fig. 3.5a-d.

3.5.4 Analytical modelling

The interface tip and toe positions calculated using analytical methods for three transects passing through the Breaksea Reef, Argonaut and Copa wells are listed in Table 3.2. Four sets of tip and toe positions were produced for each transect using the Werner and Robinson (2018) solution, in accordance with present-day and pre-development conditions, and using cross sections based on onshore and offshore hydro-stratigraphic data.

Table 3.2. Tip and toe positions calculated using the Werner and Robinson (2018) analytical solution. Positive numbers are offshore while negative numbers are onshore.

Transect	**Cross section from onshore data**		**Cross section from offshore data**		**Distance to well (km)**	**Distance to offshore boundary (km)**
	Tip (km)	**Toe (km)**	**Tip (km)**	**Toe (km)**		
Pre-development conditions						
Breaksea Reef	33.9	9.0	33.9	-3.4	12.3	33.9
Argonaut	32.4	-1.2	32.4	0.5	13.5	32.4
Copa	29.7	18.9	21.2	14.2	33.6	40.0
Present-day conditions						
Breaksea Reef	33.9	-1.2	10.6	-89.9	12.3	33.9
Argonaut	32.4	-14.7	29.7	-6.6	13.5	32.4
Copa	24.1	13.3	15.8	8.8	33.6	40.0

According to Table 3.2, calculated toe positions are shoreward of respective well locations for all simulated cases, and therefore, the analytical solution suggests that seawater is at least partly expected to occur in all wells. There is an underlying presumption here that offshore freshwater-seawater conditions are in equilibrium with present-day or pre-development conditions in onshore aquifers. This is discussed further in later subsections. In the Breaksea Reef transect, the application of the analytical solution to present-day conditions produces interface tips that are 33.9 km and 10.6 km offshore for the onshore and offshore data sets, respectively. The calculated present-day steady-state tip positions for the Argonaut and Copa transects follow a similar pattern, with the interface tip calculated using the offshore data, shoreward of those calculated using the onshore data. That is, tip positions from offshore-based aquifer geometries were shoreward of those obtained from onshore geometries by 2.7 km and 8.3 km for Argonaut and Copa, respectively. The tip positions calculated from the present-day onshore data sets for Breaksea Reef and Argonaut both reach the offshore boundary of the semi-confined aquifer. When the Werner and Robinson (2018) analytical solution was applied to the pre-development data sets for Breaksea Reef and Argonaut, the calculated tip reached the offshore boundary for both the onshore and offshore data sets. The analytical solution suggests that under steady-state conditions, present-day onshore heads are capable of driving freshwater past the Argonaut well for both the onshore and offshore parameter sets. For the transect passing through Breaksea Reef, the onshore parameter set indicates that modern heads are sufficient to drive freshwater seaward of the well location, while the offshore parameter set places the tip ~2 km shoreward of the well.

In the Copa transect, the calculated pre-development tip positions are seaward of their present-day counterparts, as expected given the higher pre-development head. However,

pre-development tip locations are shoreward of the Copa well location (indicating only seawater in the aquifer at the Copa well location) for both the onshore and offshore data sets. Modern heads were also insufficient to drive freshwater to Copa for either parameter set.

3.6 Discussion

3.6.1 Offshore Salinities of the GE

While potable (TDS < 1 g L^{-1}) water was not identified in the offshore wells included in this study, the low calculated salinities ($\overline{TDS}$ 2.2 g L^{-1}) up to 13.5 km offshore suggest that in the south of the GE, potable water may extend a significant distance offshore. These results support the inferences of earlier work (Pollock, 2003; Bush, 2009; Morgan et al., 2015) that there is a potential for OFG in the GE. The downhole salinity profiles within the LTCA in Breaksea Reef and Argonaut are typical of those observed in other OFG bodies (e.g., Groen et al., 2000; Cohen et al., 2010; Post et al., 2013), in which the salinity generally increases with depth, albeit the transition is not necessarily smooth. The sand intervals in Copa return lower resistivity values than the surrounding clay intervals (data not shown). Under constant pore-water salinities, clays typically return lower resistivity values than sands (Waxman and Smits, 1968), and therefore, the clay pore water is potentially fresher than that in the adjacent sand intervals. This may indicate that clays contained entrapped, fresher pore water, as might occur when more permeable sands salinise due to the landward movement of saline groundwater (e.g., due to falling onshore heads). The observation that clays likely contained fresher water than

overlying/underlying sand units may provide useful information on transient interface movements in future investigations of the GE offshore domain.

Using the value of m_r obtained from the LTCA sand layers, preliminary investigations of the possible pore-water salinities in the underlying Sherbrook formation were also undertaken. However, as m_r was established for the LTCA, these values have higher uncertainty. An expanded version of Fig. 3.5 that includes approximate pore-water salinities of the upper Sherbrook Formation is presented in the Appendix 1 (Fig. A1.6). Except for a single sand layer in Chama that has a $\overline{TDS}$ of 11.1 g L^{-1}, the sand layers in the underlying Sherbrook Formation have approximate calculated $\overline{TDS}$ values in the saline range (i.e., $\overline{TDS}$ between 16.7 g L^{-1} and 46.9 g L^{-1}). No clear relationships between salinity and depth are apparent in the $\overline{TDS}$ values for the sand layers of the Sherbrook Formation.

The two separate zones of near-brackish water ($\overline{TDS}$ values of 11.1 g L^{-1} and 13.1 g L^{-1}) in the downhole salinity profile for Chama (Fig. A1.6d) do not conform to the salinity profile expected if these two zones are hydraulically connected and/or maintained through freshwater flow driven by present-day onshore heads. If the two units were hydraulically connected, then buoyancy forces due to density contrasts between fresh and saltwater, would cause the brackish water in the lower zone to migrate upwards. Therefore, it appears that some separation between units of differing hydraulic conductivity is apparent around Chama.

The two southern wells (Breaksea Reef and Argonaut) that contain fresher pore water are both closer to the shoreline and further from any termination of the UTA than the two

northern wells. For example, the more saline Copa well is 2 km from the interpreted northern offshore termination of the UTA. If the LTCA is in contact with the UUA along this zone due to the lack of UTA (aquitard) between the two aquifers (LTCA and UUA) (e.g., Fig. 3.2b), increased groundwater mixing may occur. Similar enhanced mixing due to the incision of submarine paleo-channels through overlying semi-confining units is described by Mulligan et al. (2007). This presumes that the overlying UUA is saline, which is evident from consistently low resistivity values in the downhole resistivity logs. The three paleo-channel features identified in the seismic-line surveys are situated at significant distance (>19 km) from the offshore wells and are therefore unlikely to have a significant impact on the calculated downhole salinities.

The steady-state OFG extents calculated using the Werner and Robinson (2018) analytical solution indicate that present-day heads may be sufficient to drive freshwater past Argonaut for both the onshore and offshore data sets. The calculated tip positions from the Werner and Robinson (2018) solution suggest that the low resistivity-derived salinities observed in Argonaut may be a result of relatively modern freshwater inputs from the onshore semi-confined aquifer. While the tip position predicted along the Breaksea Reef transect using onshore data indicates that freshwater driven by present-day heads is capable of reaching the continental shelf. The present-day tip position calculated using offshore data is between Breaksea Reef and the coastline, suggesting that present-day onshore heads are unlikely to maintain the offshore freshwater, evidenced by low pore-water salinities observed in the resistivity data, in its current location. As the calculated pre-development tip locations for both the onshore and offshore Argonaut and Breaksea Reef data sets occur seaward of the respective well locations, it is possible that pre-development groundwater flows may have assisted in maintaining/forming the

brackish salinities identified from the downhole resistivity data. As groundwater systems are slow to adapt to hydrological changes (Post et al., 2013), it is questionable if the impact of modern changes to the onshore hydrology have reached these offshore well locations. No data set for the Copa transect generated an interface tip that reached the well location. However, this is in agreement with the resistivity-derived salinity data, as the calculated minimum $\overline{TDS}$ for Copa was > 17.5 g L^{-1} (50% of seawater concentration for comparison with the sharp-interface analytical solution).

Both the analytical modelling and the resistivity-derived salinities support previous conceptual models of the offshore GE (e.g., Bush, 2009), in that OFG in the LTCA has both a paleo/pre-development component and an active flow component, generated due to present day onshore conditions. Conceptual diagrams of the three transects modelled using the Werner and Robinson (2018) solution are presented in Fig. 3.6. In all three transects, there is potential for submarine fresh groundwater discharge (SFGD) through the overlying confining unit for several kilometres offshore. However, as no faults were interpreted to extend through the entire overlying unconfined aquifer (i.e., the UUA) this discharge is unlikely to form discrete discharge features on the seafloor. The offshore extent of OFG emplaced under paleo and/or pre-development conditions is likely being reduced due to the landward movement of the saltwater-freshwater interface caused by changes in the hydraulic conditions, and through the diffusion of salt within the UTA.

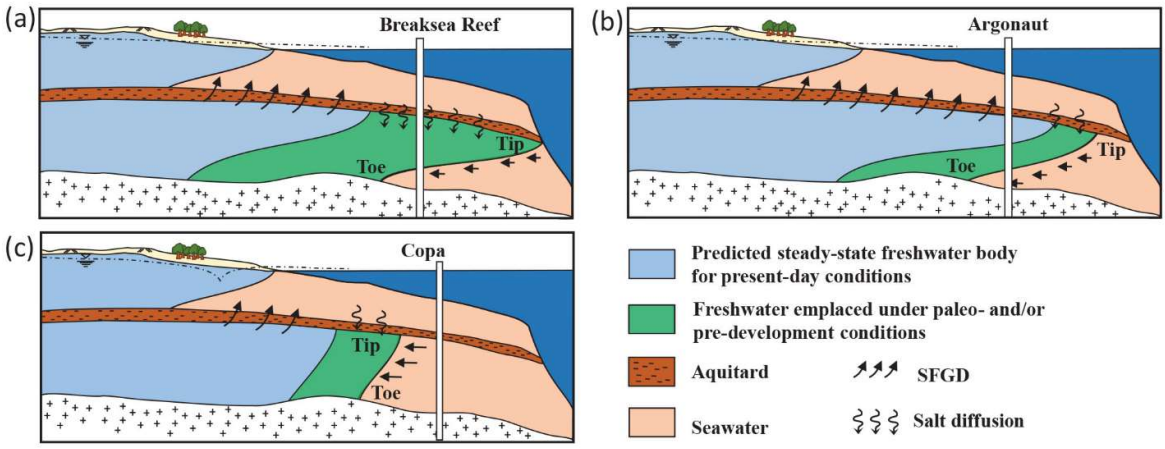

Fig. 3.6. Conceptual representations of the modelled transects, for (a) Breaksea Reef, (b) Argonaut, and (c) Copa. Note, vertical scales vary. The semi-confined aquifer in (a) is ~300 m thick, (b) ~350 m thick and (c) 50 m thick. Modified from (Knight et al., 2018).

The variability between the tip and toe positions calculated using the onshore and offshore data sets are a result of the variations in z_0, H and D. The depth of the overlying seawater is greater in the offshore data sets in the Breaksea Reef and Copa transects, 211 m and 97 m deeper, respectively. Greater seawater depths result in milder offshore hydraulic gradients (and therefore lower freshwater discharge rates) because increased seawater depths impose greater equivalent freshwater heads on the subsea aquifer. However, in the Argonaut transect, a local offshore topographic high causes a shallower seawater depth (i.e., 70 m shallower) for the offshore dataset, yet the calculated tip and toe positions for the transect using offshore data are landward of the tip and toe positions calculated from the transect using onshore data. This suggests that variations in both H and D must also contribute to the landward shift in the tip and toe positions for the Argonaut transect. All transects generated from offshore data have smaller values of H and D than their onshore derived counterparts. A thinning of the confining unit in the

offshore data sets would increase the upwards freshwater leakage through the overlying aquitard in the analytical solution, moving the interface shoreward.

The offshore data sets likely provide a better estimation of the tip position (compared to that obtained using onshore data sets) for the Breaksea Reef and Copa transects, as these data sets capture the thickness of the overlying water column offshore. For the Argonaut transect, the thinner confining unit offshore results in a reduction in the calculated tip position and a reduced estimate of the steady-state freshwater extent. Conversely, when the toe is onshore or close to the shoreline in the GE, it is likely that the onshore data sets provide better estimates of toe positions. This is because the cross sections generated using offshore data may have z_0 values that differ significantly to that identified in the onshore data, resulting in unrealistic calculated toe positions for some offshore transects (e.g., the Breaksea Reef transect that uses offshore data has a toe 89.9 km onshore). The different calculated interface tip positions for the onshore and offshore data sets show that variations in the hydro-stratigraphy make a significant difference to the estimation of subsea interface locations, and that the cross section used to calculate the interface ought to be chosen closest to the expected interface position (e.g., onshore aquifer data for interfaces near the shoreline). In offshore sloping semi-confined aquifers, failure to account for an increase in aquifer depth in the offshore extent has the potential to result in a significant over-estimation of the tip and toe positions if only onshore data are considered in parameterising analytical solutions of the subsea interface.

3.6.2 Data limitations

Previous studies that have applied Archie's law to obtain pore-water salinities either assume a generic value of m for unconsolidated sediment (e.g., Pauw et al., 2017) or adopt a single value from prior regional studies (e.g., Groen et al., 2000). Locally calibrated m values likely produce more reliable estimates of r_f compared to those obtained from generic values of m. Additionally, consideration of the uncertainty in m that accompanies calibrated values allows for an evaluation of the plausible range in offshore groundwater salinity values. In the LTCA, m_r was 1.40 with a σ_m of 0.14. The difference between the calculated value of m_r (1.40) and the standard value of 1.30 for unconsolidated sands (Archie, 1942) is comparable to σ_m. This indicates that the local variability of m may be high and can have a significant impact on the uncertainty of the final salinity estimates. Additional uncertainty is introduced due to m_r being calibrated from onshore petroleum exploration wells where drilling reports indicate that the drilling muds were freshwater based, yet m_r was applied to calculate salinities in offshore wells where drilling reports indicate that saltwater was used in the drilling mud. While deep induction logs were used to minimise the influence of drilling-induced freshening and/or salinisation of both the invaded zone and borehole fluids, the contrasting borehole drilling-fluid salinities in the onshore and offshore wells may have resulted in the calculated offshore salinities being slightly more saline than the true values. The assumption that the values of r_f in the nearby, onshore monitoring wells are the same as those in the onshore petroleum exploration wells where geophysical data are available generates additional uncertainty. The adoption of r_f values from nearby onshore

monitoring wells was necessary as r_f values were unavailable in the onshore petroleum exploration wells that contained the bulk resistivity and porosity data.

The estimates of offshore salinity also incorporate several other possible sources of uncertainty, particularly surrounding the calculation of φ. In the GE, well completion reports note caving of the well walls in sandy zones of the LTCA during drilling. This caving may have caused the calculated porosities to be higher than those observed in the unperturbed LTCA. An overestimation of φ would cause the estimated salinities to be lower than the true values. As both the uncorrected Wyllie time-average equation and the alternative Raymer-Hunt-Gardner equation (Raymer et al., 1980) return unrealistic porosities (i.e., >0.55), the accuracy of the sonic-log derived φ values is questionable. This is despite the more recent Raymer-Hunt-Gardner equation partially correcting for the impact of unconsolidated sediments on sonic velocity data. As both methods originally returned unrealistic porosity estimates, we adopted the Wyllie time-average approach, because this method incorporates a mechanism to scale the sonic-porosity values in unconsolidated sediments, providing that other porosity data such as neutron density-derived porosities are available to estimate correction factors. However, considerable uncertainty is likely to be present due this approach of estimating φ.

The tip and toe positions derived from the analytical model are associated with significant uncertainties. These uncertainties arise primarily as a result of numerous simplifications made in the analytical solution that do not fully reflect, the field conditions. As discussed above, the impact of the flat-lying assumption is tested to some degree by the calculation of a tip and toe position for both onshore (where the aquifer is generally shallower) and offshore parameter sets. The cross sections treat H and D as constant across the transect

despite the hydro-stratigraphic isopachs (Fig. 3.3) showing that *H* and *D* vary spatially across the GE (e.g., near Argonaut the UTA transitions from a thickness of 25-50 m to a thickness of 100-150 m over a distance of ~5 km). Due to uncertainty surrounding the interpreted hydro-stratigraphic unit thickness, discussed below, *H* and *D* in the offshore data sets were obtained from offshore geological well log data. As a result, the spatial variability in *H* and *D* was not captured, and the effect of variability on tip and toe positions remains unclear. In addition to regional variations in *H* and *D*, the transects used to apply the analytical solution omit multiple shore-parallel faults present in the GE. The localised displacement of the hydro-stratigraphic units associated with this faulting appears to generate several zones where the aquitard thins. These zones of localised thinning generate the potential for increased freshwater/saltwater mixing, which if present may cause the analytical solution to over-predict the OFG extent. However, to date, the impact of a varying aquitard thickness on offshore salinities remains unstudied, and the degree to which these fault-based zones of aquitard thinning impact regional salinities is unknown.

The cross-sectional models treat the LTCA vertically as a single homogeneous unit as per previous regional studies (e.g. Love et al., 1993; Morgan et al., 2015). This is contrary to the downhole geological well data indicating the LTCA is comprised of several sandy layers interbedded with clay, which may have significant thickness in places (i.e., up to 85 m). As the Werner and Robinson (2018) analytical solution is only applicable to the upper-most semi-confined aquifer, it is unclear how this layering would affect the calculated interface position. Michael et al. (2016) found that heterogeneity can result in freshwater driven by onshore heads occurring further offshore than expected in equivalent homogeneous aquifers. However, they did not include a semi-confining unit overlying the

homogeneous aquifer, and as a result, their findings apply to a different hydro-stratigraphic arrangement to that adopted by Werner and Robinson (2018).

The offshore stratigraphic interpretations also contain significant uncertainty. The multiple sources of the seismic-line survey data, with variable information surrounding the acquisition parameters, meant that obtaining a minimum vertical resolution was unachievable. As a result, it is likely that the interpreted truncations of the UTA and LTCA do not reflect their true locations, as these units may extend beyond the interpreted end points, albeit at thicknesses below those resolvable from the available seismic data. Confidence in the offshore stratigraphy interpretations is elevated in areas where well ties are possible, particularly around seismic lines that contain multiple well ties. Uncertainty increases rapidly in the offshore direction, as the shore-parallel faulting results in vertical displacement of the seismic horizons, increasing discontinuity in the traced surfaces. Lastly, the seismic exclusion zone imposed between the shoreline and 5 km offshore creates additional uncertainty in the near-shore region. Due to this zone, onshore data were unable to be accurately connected to offshore interpretations.

3.7 Conclusions

Our analyses provide a rare demonstration of the significant uncertainty attached to pore-water salinities calculated using Archie's law (Archie, 1942) due to variations of m. We present a new adaptation of methods commonly used in the petroleum industry for establishing m and its variability, to a coastal hydrogeological investigation. In the GE, σ_m was comparable to the difference between m_r and the m value commonly adopted for

unconsolidated sands. This highlights the importance of establishing the regional variability of m and not merely adopting the mean m.

We produced estimates of offshore salinity in the South Australian portion of the Gambier Embayment (GE) though novel application of both onshore and offshore geophysical well data. Our analyses indicate that low salinity groundwater ($\overline{TDS}$ ~2.2 g L^{-1}) is likely to be present up to 13.5 km offshore in the south of the GE, albeit there is large uncertainty surrounding this distance. In the north of the GE, calculated pore-water salinities are higher. This suggests that extensive OFG is likely restricted to the southern portion of the GE.

There appears to be a possible association between the offshore hydro-stratigraphy and the calculated salinities, with wells closer to terminations in the UTA and LTCA displaying higher salinities. This may occur due to increased vertical freshwater-saltwater mixing in areas where the LTCA becomes connected to overlying seawater. The seismic-survey data suggests that the LTCA around Copa may be disconnected from the onshore system, highlighting the need to view hydro-stratigraphic and salinity data together to prevent unrealistic extrapolations of OFG bodies in areas where hydro-stratigraphic variability precludes the seaward extent of OFG.

Our analytical modelling indicates that while present-day heads are predicted to drive freshwater significant distances offshore, there is conceptual variability that, when tested within the analytical modelling, leads to significant differences in the estimates of OFG extent. When onshore elevations and thicknesses of the aquifer and aquitard are used for present-day conditions, the calculated steady-state tip position occurs seaward of the

Breaksea Reef and Argonaut wells. When elevations and thicknesses that correspond to the offshore well information are used, the calculated interface tip only extends past the well in the Argonaut transect. This indicates that present-day onshore conditions have the potential to explain the occurrence of OFG at Argonaut, while a pre-development OFG component is likely required to explain the calculated salinities at Breaksea Reef. The large discrepancies between calculated tip positions depending on whether onshore or offshore data are used emphasises the need to account for the possible offshore slope of aquifer systems when estimating OFG extents through analytical methods.

Our study presents evidence of a fourth Australian site where OFG is encountered in offshore aquifers. The approach adopted provides a unique example of applying multiple techniques to investigate the potential extent of OFG. Using onshore hydrochemical data, legacy geophysical data and analytical modelling, we were able to approximate offshore salinities, including their uncertainty, and offer hypotheses for OFG origins and influencing factors.

3.8 Acknowledgments

The authors thank Vincent Post and Leanne Morgan for their initial feedback and suggestions, Simon Holford for assistance with the seismic data, and the South Australian Department for Energy and Mining for the provision of the seismic survey and petroleum well data. We also gratefully acknowledge the suggestions of 3 anonymous reviewers. Andrew Knight is supported by an Australian Government Research Training Program scholarship. Adrian Werner is the recipient of an Australian Research Council Future Fellowship (project number FT150100403).

Chapter 4

4. Alongshore freshwater circulation in offshore aquifers

4.1 Abstract

Flow within offshore aquifers is important for the management of fresh groundwater in coastal zones. Alongshore head gradients have been observed in many coastal aquifers; however, this is typically neglected and offshore aquifers are primarily assessed using only cross-sectional representations. This study explores offshore implications of onshore alongshore head gradients, including the alongshore circulation of submarine groundwater, using numerical experimentation of 3D, synthetic onshore-offshore aquifers. Model parameter ranges were guided by those observed in seven real-world cases. Each 3D simulation is compared against three 2D cross-sectional numerical models to identify the potential mismatch between 2D and 3D approaches. The results show that alongshore freshwater circulation (AFWC) increases where the alongshore head gradient is steeper, onshore heads are lower (on average), or the offshore aquitard hydraulic conductivity is less. A maximum AFWC rate of 70.3% was observed across the simulated cases. We conclude that in many situations, freshwater flowing from offshore to onshore aquifers may be recirculated groundwater from the onshore aquifers at a location where the onshore head is higher, rather than relic freshwater, as has been concluded from cross-sectional analysis in previous studies. Additionally, the 3D models show that even though onshore heads indicate active seawater intrusion, alongshore head gradients can protect regions of low head such that recirculated freshwater, instead of seawater, is drawn into onshore wells.

4.2 Introduction

The management of fresh groundwater in coastal regions, which is an important resource for many coastal communities, requires knowledge of both the onshore and offshore components of coastal aquifers (Post et al., 2013; Michael et al., 2017). This is particularly important where offshore groundwater flows onshore, thereby contributing to the water quality in onshore aquifers and of coastal wells (Knight et al., 2018). Offshore freshwater is commonly considered a non-renewable resource, whereby offshore freshwater is mined by onshore extraction. Thus, characterising the extent of offshore freshwater volumes and onshore-offshore aquifer connectivity is critical for predicting the long-term resilience of coastal aquifers to pumping stresses.

Offshore fresh groundwater (OFG) can be generated through both present-day and paleo hydrological processes (Groen et al., 2000). The present-day discharge of freshwater from the onshore portion of confined and semi-confined aquifers (collectively referred to as "semi-confined aquifers" in what follows) into their offshore continuations can generate extensive OFG bodies (Kooi and Groen, 2001; Bakker, 2006; Michael et al., 2016; Werner and Robinson, 2018). Paleo-hydrogeological processes, such as those associated with glacial maxima, are thought to have increased continental shelf exposure and, in some instances, elevated hydraulic heads due to glacial loading (Person et al., 2012). These paleo-processes are thought to have generated extensive freshwater bodies in the semi-confined aquifers of continental shelves (e.g. Cohen et al., 2000). Post-glacial coastline transgression outpaced the landward movement of the freshwater-saltwater interface in many regions (Groen et al., 2000), causing modern OFG extents that are often

in disequilibrium with extents expected from present-day conditions (Groen et al., 2000; Marksamer et al., 2007; Person et al., 2012; Post et al., 2013).

OFG has been studied using both analytical and numerical models. Analytical models adopt the assumption of a pressure equilibrium interface between freshwater and seawater, and provide a rapid approach for estimating steady-state OFG distributions in simplified coastal aquifer systems (Werner and Robinson, 2018). Numerical methods can be applied to a wider range of situations (Yu and Michael, 2019a), including both interface and dispersive mixing zone conditions. However, the latter are limited by the computational effort required for large-scale simulation of density-coupled, dispersive flow and transport.

Analytical solutions include those of Bakker (2006), who formulated analytical solutions to OFG assuming a sharp interface between freshwater and seawater. Four situations were differentiated that depend on whether the interface tip (the top of the interface) is at the offshore limit of the aquifer or not, and whether the interface toe (the bottom of the interface) is onshore or offshore. Bakker (2006) used the solution to examine the extent of freshwater in the Upper Floridian Aquifer (USA), and concluded that present-day conditions are capable of driving freshwater tens of kilometres offshore. Pauw et al. (2017) applied the Bakker (2006) model to several transects of Dutch aquifers and demonstrated how alongshore variations in the hydro-stratigraphy can generate significantly different OFG distributions in the alongshore direction. Werner and Robinson (2018) presented a modification to the Bakker (2006) solutions that allows for a specified salinity in the offshore semi-confining unit overlying the offshore aquifer (where it contains freshwater). The modification by Werner and Robinson (2018) resolves

the issue encountered by Solórzano-Rivas and Werner (2018), who showed that offshore aquitards are more likely to contain freshwater rather than the seawater assumption of Bakker (2006), where aquitards overly fresh offshore aquifers. The solution of Werner and Robinson (2018) was applied to twenty-seven regions across the globe by Knight et al. (2018), who concluded that offshore freshwater is likely influencing onshore salinities in twenty-four of those regions.

Most applications of numerical methods to investigate OFG use 2D cross-sectional representations of offshore conditions. Cross-sectional models of dispersive flow and transport are significantly less computationally expensive relative to 3D models, which are often only practical using relative coarse grid discretisation. This limits the simulation of local-scale dispersive processes that might otherwise require fine grid resolution. Cross-sectional numerical models have been used to investigate the emplacement of OFG under glacial conditions (e.g., Person et al., 2003; Marksamer et al., 2007; Person et al., 2012), the effect of pumping both onshore and offshore on OFG extent and longevity (e.g., Amir et al., 2013; Morgan et al., 2018; Paldor et al., 2019; Yu and Michael, 2019a, 2019b) and the effect of geological heterogeneity on offshore flow paths (e.g., Michael et al., 2016). However, 2D approaches require the assumption that the system is unchanging in the alongshore direction, whereas alongshore head gradients are likely widespread, as evidenced several studies (e.g., Nativ and Weisbrod, 1994; de Melo et al., 2001; Kalaris et al., 2002; Zulfic et al., 2008; Morgan et al., 2016).

OFG has been investigated through more realistic 3D numerical modelling in only a small number of cases. For example, Cohen et al. (2010) and Siegel et al. (2014) explored the role of glacial loading and sea-level fluctuations on OFG development. Both studies

incorporated a time-variable sea level and applied onshore boundary conditions that accounted for a significant increase in hydraulic head due to the accumulation of considerable overlying ice mass. The model domain used by Cohen et al. (2010) extends several hundreds of kilometres in the alongshore direction, while the model domain used by Siegel et al. (2014) is 50 km in the alongshore direction. Both studies concluded that elevated glacial-driven recharge during glacial maxima can generate OFG extents that vary across the model domains in the alongshore direction. Mulligan et al. (2007) used a simplified 3D numerical model to investigate the impact that paleo-channels that incise through the offshore confining unit have on offshore freshwater-saltwater exchange. They found that increased freshwater-saltwater mixing can occur around submarine paleo-channels. Mulligan et al. (2007) also identified that paleo-channels can generate localised lateral flow towards the paleo-channel in the offshore semi-confined aquifer, increase the offshore freshwater flux at the coastline and reduce the predicted OFG extent. Investigations into the longevity of the New Jersey (USA) water supply by McAuley et al. (2001) and Pope (2006) provide rare examples of regional-scale 3D numerical models that explore OFG distributions due to both present-day and pre-development conditions. Both studies identified an offshore freshwater-saltwater interface and estimate an approximate freshwater resource lifespan of several hundred years under several extraction scenarios.

In several locations globally, significant alongshore hydraulic gradients (AHGs) have been identified at the regional scale (e.g., Nativ and Weisbrod, 1994; de Melo et al., 2001; Kalaris et al., 2002; Zulfic et al., 2008; Morgan et al., 2016), either due to natural forces (e.g., varying recharge or topographic influences) or human impacts (e.g., groundwater abstraction). In these regions, it is unlikely that the negligible transverse flow assumption

required to apply 2D analytical and/or numerical models is valid. Despite this, 2D cross-sectional approaches have been applied to OFG investigations in at least two of these areas (e.g., Amir et al., 2013; Morgan et al., 2018; Paldor et al., 2019). Knight et al. (2018) hypothesised that in some regions AHGs may result in alongshore freshwater circulation (AFWC) (i.e. where freshwater passes into the offshore portion of the semi-confined aquifer in places of highest onshore head before circulating within the offshore aquifer and subsequently flowing back onshore at another location). However, the occurrence and magnitude of any freshwater recirculation remains unstudied. Additionally, the validity of using cross-sectional models to investigate OFG in regions with an AHG is unknown.

This study seeks to explore the potential for AFWC to occur as a result of an AHG. We aim to identify if, and under what conditions, AFWC can occur. Using 3D numerical modelling, freshwater fluxes at the coastline are explored to determine potential AFWC percentages for a range of conditions. We compare the modelled freshwater-saltwater interface from several 2D and 3D numerical models of simplified coastal aquifer systems to investigate potential deviations between the different approaches. This study is the first published investigation of the 'negligible transverse flow' assumption that is often made in offshore aquifers investigations that use 2D cross-section models.

4.3 Methods

Hydrogeological parameters from seven regions were collated from existing literature to guide the development and parameterisation of the synthetic 3D numerical models used in this study. A conceptualisation of the simplified model domain is shown in Fig. 4.1a, with

the regional parameters presented in the Appendix 2 Table A2.1. The parameters of interest to this study are the aquifer hydraulic conductivity (K_a) (L T^{-1}), the aquitard hydraulic conductivity (K_v) (L T^{-1}), depth below sea level to the top of the aquitard (H_s), the thicknesses of the aquifer (H)and aquitard (H_l), the maximum and minimum onshore heads (h_{max} and h_{min}, respectively), the transverse distance between h_{max} and h_{min} (Δy), and the onshore and offshore lengths of the semi-confined aquifer (L_c and L_s, respectively). 2D and 3D models are compared using 2D models at the front face, middle and back face of 3D models, as illustrated in Fig. 4.1b.

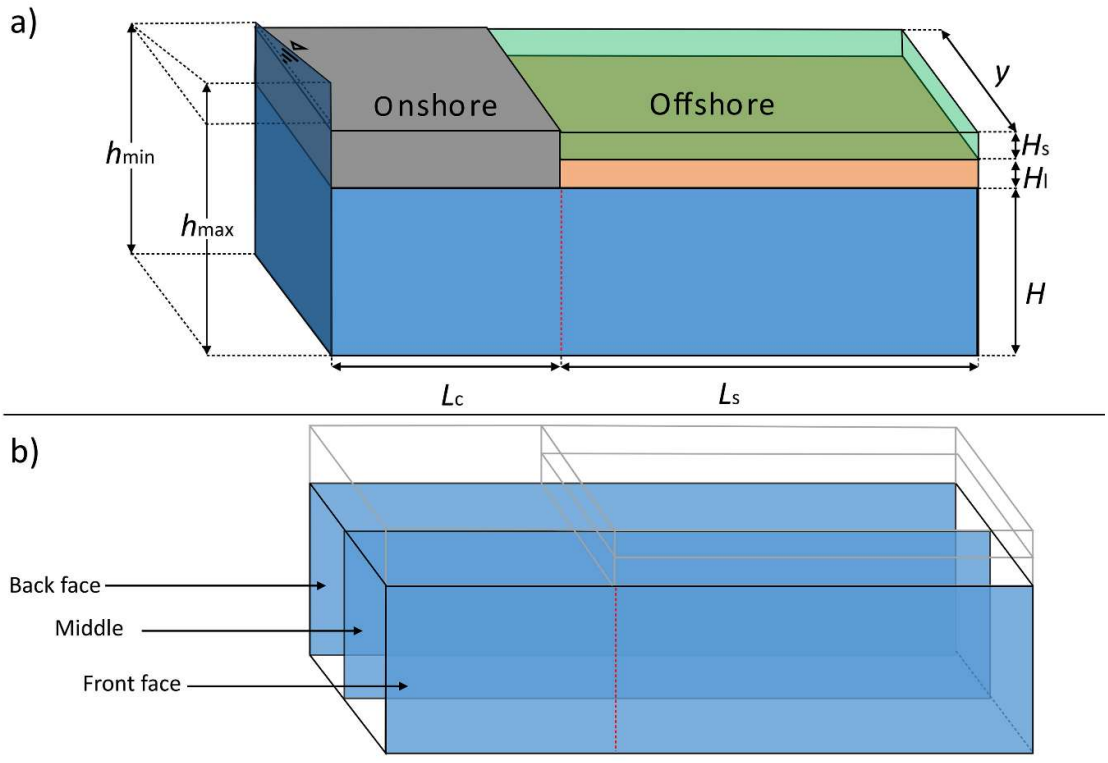

Fig. 4.1. (a) A conceptual diagram of a simplified onshore-offshore coastal aquifer adopted in evaluated freshwater circulation caused by an AHG. The no flow zone and semi-confining unit are marked by grey and tan shading, respectively. The implied overlying seawater column is represented by light green shading. The coastline is

indicated by the vertical red dashed line. A linear distribution of head, parallel to the shoreline, is applied at the onshore boundary. (b) Positions of 2D cross sections: Front face, middle and back face. Heads at the onshore boundary are h_{max}, h_{mid} and h_{min} at the front face, middle and back face, respectively.

Twelve parameter combinations were selected to explore AFWC using variable-density numerical models. Numerical simulations were undertaken using SEAWAT (Langevin et al., 2007). In all simulations, Δy was fixed at 15 km while H and H_l were 40 m and 10 m respectively. Δy varies in the real-world cases between 4.4 km and 83 km (see Table A2.1). The alongshore width selected represents a balance between computational load and the need to simulate regional-scale situations. The model domain extends 5 km onshore while the modelled offshore domain varied between simulations. To ensure that the model domain was sufficient to prevent the interface from reaching the offshore boundary and introducing potential boundary effects, the Werner and Robinson (2018) analytical solution was used to calculate an OFG extent for each parameter combination. The offshore boundary was set to 10 km seaward of the maximum offshore freshwater extent calculated for each parameter set using the sharp-interface analytical model. The offshore distance of the aquifer is inconsequential as long as the offshore domain includes the freshwater extent, because flows within the seawater part of the aquifer are small relative to rates of freshwater flow.

The parameters of the twelve synthetic models, presented in Table 4.1, are within the upper and lower limits of the recorded real-world values. The vertical leakance (c) of the aquitard in the synthetic models spans the range of c values observed in the real-world cases despite the thickness of the synthetic model aquitard being equal to the thinnest

recorded real-world case (i.e., 10 m; Adelaide, Zulfic et al., 2008). Here, $c = \frac{H_l}{K_v}$ (Bakker, 2006). Typical ranges in aquitard conductance were represented by modifying K_v to avoid simulating thick aquitards and thereby reducing the numerical burden; an important goal in 3D simulation. The AHG in synthetic models ranged between 0.4 m km^{-1} and 1.8 m km^{-1}, while the AHGs of the real world regions ranged between 0.05 m km^{-1} and 2 m km^{-1}. The twelve simulations are herein referred to as s1 to s12 according to their case descriptor in Table 4.1.

Table 4.1. Parameters applied to simplified numerical models. Values consistent with those listed in s1 are shown with a hyphen (-). 0 m (sea level) is taken as the datum for *h* values.

Case	K_a (m/d)	H_s (m)	H (m)	h_{mid} (m)	h_{max} (m)	h_{min} (m)	L_c (km)	H_l (m)	K_v (m/d)	L_s (km)	$\Delta h/\Delta y$ (m km^{-1})
s1	10	30	40	5	11	-1	5	10	2.5E^{-5}	44	0.8
s2	-	-	-	-	-	-	-	-	1.0E^{-5}	68	-
s3	-	-	-	-	-	-	-	-	1.0E^{-4}	26	-
s4	-	-	-	-	-	-	-	-	1.0E^{-3}	13	-
s5	-	-	-	0	6	-6	-	-	-	37	-
s6	-	-	-	2.5	8.5	-3.5	-	-	-	44	-
s7	-	-	-	10	16	4	-	-	-	50	-
s8	-	-	-	20	26	14	-	-	-	55	-
s9	-	-	-	-	6.5	3.5	-	-	-	38	0.2
s10	-	-	-	-	8	2	-	-	-	41	0.4
s11	-	-	-	-	14	-4	-	-	-	48	1.2
s12	-	-	-	-	17	-7	-	-	-	50	1.8

A grid sensitivity study was undertaken to evaluate the impact of grid discretization and dispersivity on the results. Due to resource constraints, grid sensitivity was undertaken using 2D cross-sectional models (rather than in the 3D). Seven different horizontal cell widths (Δx) (i.e., 5 m, 10 m, 25 m, 50 m, 75 m, 100 m and 125 m) were tested on the s4

transect (see Table 4.1) that had an onshore head of h_{max} and a longitudinal dispersivity (α_L) of 25 m. Four sets of dispersivity values were also tested using the s4 transect with a cell size of 5 m, namely α_L values of 1 m, 5 m, 10 m and 25 m. Horizontal and vertical transverse dispersivity (α_T and α_V respectively) values were set at $\alpha L/10$. The 50% isochlors of each simulation were compared to identify: (1) the slope of the freshwater-saltwater interface calculated using $\text{Slope} = H/x_{\text{tip50\%}} - x_{\text{toe50\%}}$, where $x_{tip50\%}$ and $x_{toe50\%}$ are x_{tip} and x_{toe} of the 50% isochlor, respectively; (2) displacement in the position of the mixing zone.

In the twelve synthetic models included in Table 4.1, the offshore cells have a fixed width and length of 125 m. In the onshore domain, between the onshore boundary and 2.5 km from the coastline, the length (perpendicular to the coastline) of the onshore cells decreases from 375 m near the boundary to 125 m. The change in cell size between neighbouring cells does not exceed 50%. Aquitard and aquifer layers have a fixed thickness of 1 m and 2 m, respectively. The cell sizes adopted in this study are finer than those adopted in other studies of a similar scale, e.g 50-500m (Mulligan et al., 2007), 2 km (Siegal et al., 2014). A longitudinal dispersivity (α_L) of 25 m was adopted in the aquifer, while α_T and α_V values were set at 2.5 m. These values are not inconsistent with parameters of similar studies (Mulligan et al., 2007; Amir et al., 2013; Siegel et al., 2014). A α_L of 0.5 m with α_T and α_V of 0.05 m were applied in the aquitard where flow is assumed to be dominantly vertical. The molecular diffusion coefficient was 10^{-9} m^2 s^{-1}. Dispersion parameters and the cell size represent a balance between computation load, stability of the numerical method, and accuracy. Significant testing of the 2D model was undertaken for the grid resolution and dispersion parameters, with the results of this

testing provided in the following section. The design of the 3D models involved a grid Péclet number (Pe_x, where $Pe_x = \Delta x/\alpha_L$) in the aquifer that exceeds the critical value of 2 suggested by Zheng and Bennett (2002) to minimise numerical oscillations. However, decreasing the cell size to reduce Pe_x would have resulted in excessive computational loads.

The ocean was represented using a specified saltwater hydraulic head set to 0 m for both the vertical offshore boundary and the top cells of the aquitard in the offshore region. Transport conditions for these cells were set to allow saltwater (35 g L^{-1}) inflows and ambient concentration outflows. This approach assumes that freshwater outflows do not result in significant local freshening of the ocean. The landward vertical face of the model domain was a specified-head boundary. Heads at the front face (see Fig. 4.1b) of the onshore boundary were set as h_{max}, with heads decreasing linearly to h_{min} at the back face (see Fig. 4.1b) of the onshore boundary. The onshore boundary had freshwater (0 g L^{-1}) inflows and ambient concentration outflows. The onshore portion of the semi-confining unit, the lower boundary, and the front and the back faces of the model domain were set as no flow conditions. Three 2D models were also generated for each parameter set (see Fig. 4.1b). The 2D models replicated the conditions modelled at the front face, middle row and back face of each 3D model, which differed according to the head at the inland boundary (h_{max}, h_{mid} and h_{min}, respectively).

The parameter combinations of the twelve synthetic models were selected to investigate the behaviour of AFWC for variations in three different processes. The parameters of the first simulation (s1) are a central base case, from which parameters were increased and decreased to produce offshore freshwater extents that were both larger and small than s1.

The first set of simulations (s1-s4) investigate how changes in K_v impact AFWC. Simulations s5-s8 in addition to s1 investigate how the onshore heads influence AFWC. The third group of simulation (s1 and s9-s12) investigate how the AHG alters AFWC. In these simulations, h_{mid} remains fixed with the onshore boundary heads in either direction alongshore changing by the specified gradient ($\Delta h/\Delta y$).

All numerical simulations were run to steady state that was assessed according to the total mass within the model domain. The 5%, 50% and 95% seawater concentration isochlors were extracted from the top and bottom layers of the semi-confined aquifer to capture the position of the tip (x_{tip}) and toe (x_{toe}) of the freshwater-saltwater interface. These values were used in the comparisons between the 2D and 3D approaches.

The horizontal fluxes and fluid salinity across the coastline were evaluated to calculate AFWC. That is, freshwater fluxes were calculated in each cell at the shoreline using:

$$Q_f = Q(1 - \frac{C}{C_s}) \quad (1)$$

Where Q_f is the freshwater flux [$L^3\ T^{-1}$], Q is the total flux across the shoreline in each model cell [$L^3\ T^{-1}$], C is the salinity within each model cell [$M\ L^{-3}$], and C_s is the salinity of seawater [$M\ L^{-3}$]. AFWC was calculated as sum of Q_f crossing the shoreline in the onshore direction for the entire model divided by the sum of Q_f in the offshore direction.

4.4 Results

4.4.1 Grid dependency

$x_{tip50\%}$ and $x_{toe50\%}$ for each of the grid-dependency simulations and sensitivity analysis of dispersivity are shown in Fig 4.2. In the grid-dependency simulations (Fig. 4.2a), the largest change in $x_{tip50\%}$ for a meter increase in Δx is present between the Δx=5 m and Δx=10 m simulations. There is a continued offshore shift in $x_{tip50\%}$ as Δx increases, though to a lesser degree. This suggests that $x_{tip50\%}$ has a higher sensitivity to changes Δx at low values of Δx. $x_{toe50\%}$ shows a slightly non-monotonic behaviour. For the lower values of Δx (i.e., Δx=5 m to Δx=25 m), $x_{toe50\%}$ moves shoreward as Δx increases. However, between Δx=25 m and Δx=125 m $x_{toe50\%}$ shifts offshore as Δx is increased. The slope of the interface decreases from 17.8% in the Δx=5 m simulation to ~8% in the Δx=25 m simulation, thereafter the slope of the interface remains constant. This suggests that both $x_{tip50\%}$ and $x_{toe50\%}$ move offshore at the same rate for a given increase in Δx after the Δx=25 m simulation.

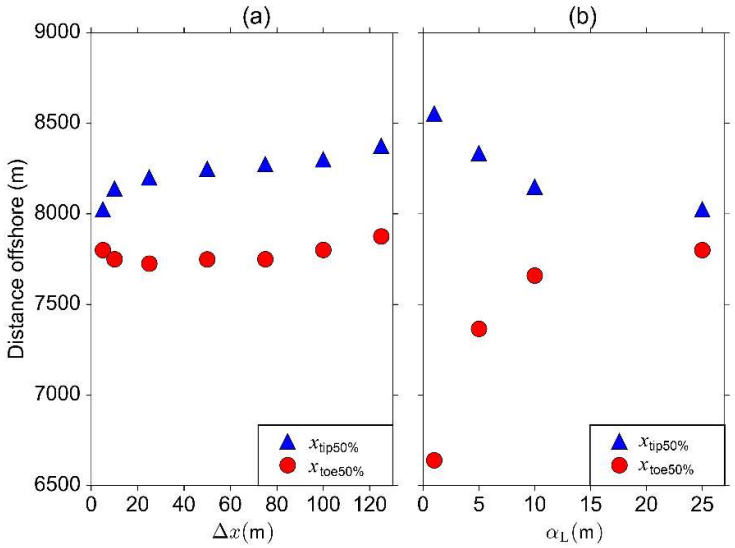

Fig. 4.2. The modelled position of $x_{tip50\%}$ and $x_{toe50\%}$ for (a) the grid-dependency tests and (b) the α_L sensitivity analysis.

The data corresponding to the simulations investigating the sensitivity to changes in α_L (shown in Fig. 4.2b) indicate that for the ranges of α_L and Δx tested, both $x_{tip50\%}$ and $x_{toe50\%}$ are more sensitive to the changes in α_L than the changes in Δx. For the α_L simulations (that use Δx=5 m), $x_{tip50\%}$ shows greater sensitivity to increases in α_L at low values of α_L. In all simulations that investigate sensitivity to α_L, $x_{tip50\%}$ moves shoreward as α_L increases. $x_{toe50\%}$ appears to be more sensitive to increases in α_L than $x_{tip50\%}$, especially at low α_L values. In all simulation tested, $x_{toe50\%}$ shifts offshore as α_L increases. The slope of the interface increases from 2.1% for α_L=1 m to 17.8% for α_L=25 m. This change in slope is caused by the movement of both $x_{tip50\%}$ and $x_{toe50\%}$, with $x_{tip50\%}$ 6.2% (530 m) further offshore in the α_L=1 m simulation than in the α_L=25 m simulation, while x_{toe} is 17.5% (1160 m) further onshore in the α_L=1 m simulation than in the α_L=25 m simulation.

4.4.2 Calculated alongshore freshwater circulation

Simulations were undertaken using Intel i7 3.6 GHz processors with the model run times for the 3D simulations ranging from 27 days to 35+ days. Model run time was strongly dependent on the length of the offshore domain modelled, with s4 having the shortest required run time. A visualisation of the salinity distribution within the semi-confined aquifer for s4 is presented in Fig. 4.3. This figure shows how the change in onshore head along the onshore boundary from h_{max} (front face) to h_{min} (back face) results in an OFG extent that correspondingly reduces across the model domain.

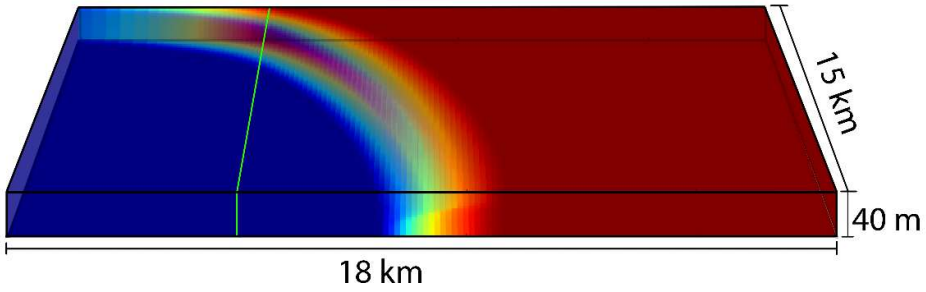

Fig. 4.3. A visualisation of the freshwater-saltwater distribution in the semi-confined aquifer for s4. Blue and red colour floods represent freshwater and saltwater, respectively. The freshwater-saltwater interface is indicated by rainbow colour flood. The coastline is marked by the green line. The vertical to horizontal ratio is ~1:450.

The percentage of AFWC for each simulation are presented in Fig. 4.4. The simulations investigating the impact of K_v on AFWC (Fig. 4.4a) indicate that as K_v increases the percentage of AFWC decreases from 19.2% to 1.7%. This trend appears to be non-linear as the change between s2 and s3 (K_v=1.0E^{-5} m d^{-1} and K_v=1.0E^{-4} m d^{-1}, respectively) results in the calculated AFWC decreasing by 17.5%, while the change between s3 and s4

(K_v=1.0E^{-4} m d^{-1} and K_v=1.0E^{-3} m d^{-1}, respectively) only results in a 0.9% decline in AFWC.

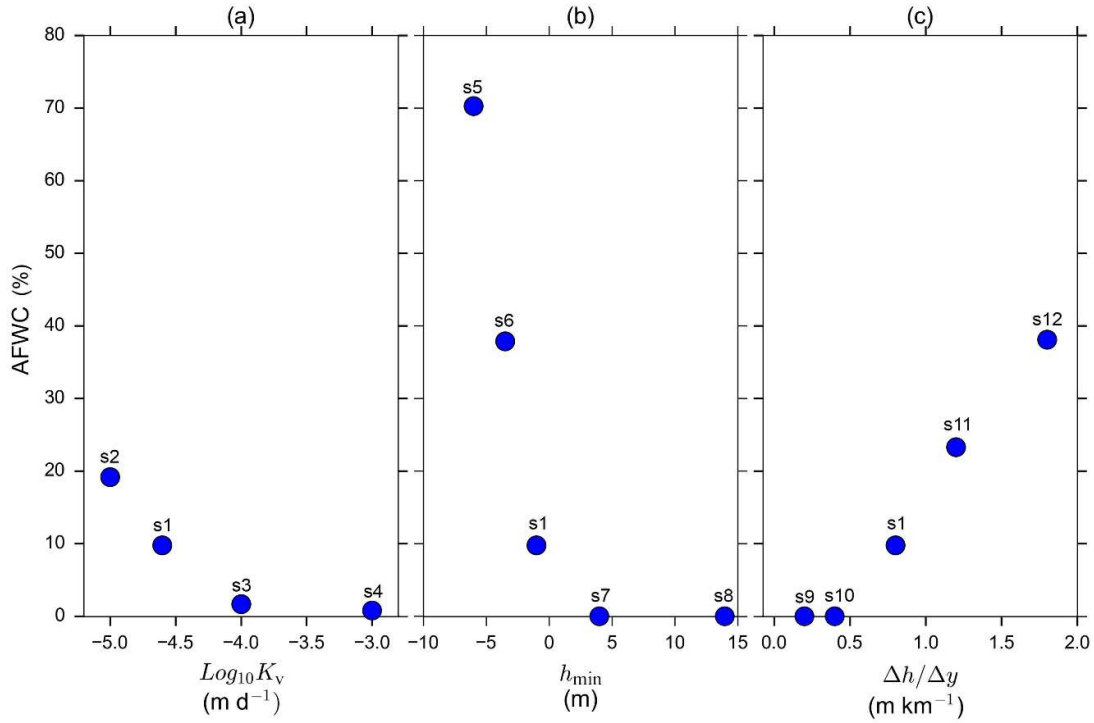

Fig. 4.4. The percentage of calculated AFWC for each simulation. The simulations are divided into their respecting investigation groups. Panel (a) shows the simulations investigating the role of K_v on AFWC, (b) shows the simulations investigating the effect of the onshore head relative to sea level, while (c) show the response of AFWC due to varying the AHG. s1 is repeated in all panels.

The group of simulations that investigate the impact of the onshore head (relative to sea level) on AFWC are shown in Fig. 4.4b. The percentage of AFWC decreases rapidly from 70.3% to 0% as h_{min} increases towards the minimum head required to prevent the onset of active SWI, (i.e., 1 m). This threshold value was calculated using $h_f = \delta(H_s + H_l)$, where h_f is the equivalent freshwater head imposed by the sea, δ is the dimensionless difference between the density of freshwater (ρ_f, M L^{-3}) and the density of saltwater (ρ_f, M L^{-3}) as

calculated by $\delta = \frac{(\rho_s - \rho_f)}{\rho_f}$ (Werner, 2017a). Active SWI is predicted when $h_f >$ the onshore head. For simulations s7 and s8, h_{min} is $> h_f$ and no AFWC occurs. In the systems modelled, a 1 m decline in the onshore heads relative to sea level results in approximately a 10% increase in AFWC.

The relationships between AFWC and the AHG are shown in Fig. 4.4c. In this set of simulations, no notable AFWC is predicted in s9 and s10 as h_{min} remains $> h_f$. In simulation s10, h_{min} at the base of the aquifer is lower than the equivalent freshwater head of seawater at the base of the aquifer (h_{fbase}), where $h_{fbase} = \delta(H_s + H_l + H)$, as a result there is a slight onshore freshwater flux at the coastline in this section of the aquifer. However, the total volume of AFWC in s10 is negligible (0.01%). In simulations s1, s11 and s12 $h_{min} < h_f$. In these three simulations, the percentage of AFWC increases approximately linearly as the AHG increases. An increase in the AHG of 1 m km^{-1} causes a 28% increase in AFWC.

The flow vectors for simulations s1 and s5-s8 are shown in Fig. 4.5. Flow vectors for the remaining simulations are presented in Appendix 2 Fig. A2.1 and Fig. A2.2. The data presented in Fig. 4.5 suggest that the transverse flow of freshwater within the onshore domain is a major control on the onshore salinities. This trend is common across all simulations where part of the onshore domain has a head lower than h_f. For the simulations shown in Fig. 4.5, the component of transverse flow in the offshore domain decreases as the head at the onshore boundary increase. This matches the observed reduction in AFWC as the onshore heads increase (Fig. 4.4). In s7 there is still notable transverse freshwater flow in the offshore domain despite h_{min} being $> h_f$. There is only a minor transverse offshore flow component in s8. In simulations s1-s4 shown in Fig. A2.1,

the transverse flow component reduces as K_v increases. All of the simulations that investigate the impact of the AHG (s1, s9-s12) had notable transverse flow in the offshore aquifer (Fig. A2.2). In these simulations the proportion of transverse offshore flow increased as the AHG increased. Interestingly, the location of the freshwater-saltwater interface in these five simulations shows little variation despite h_{max} ranging from 6.5 m to 17 m.

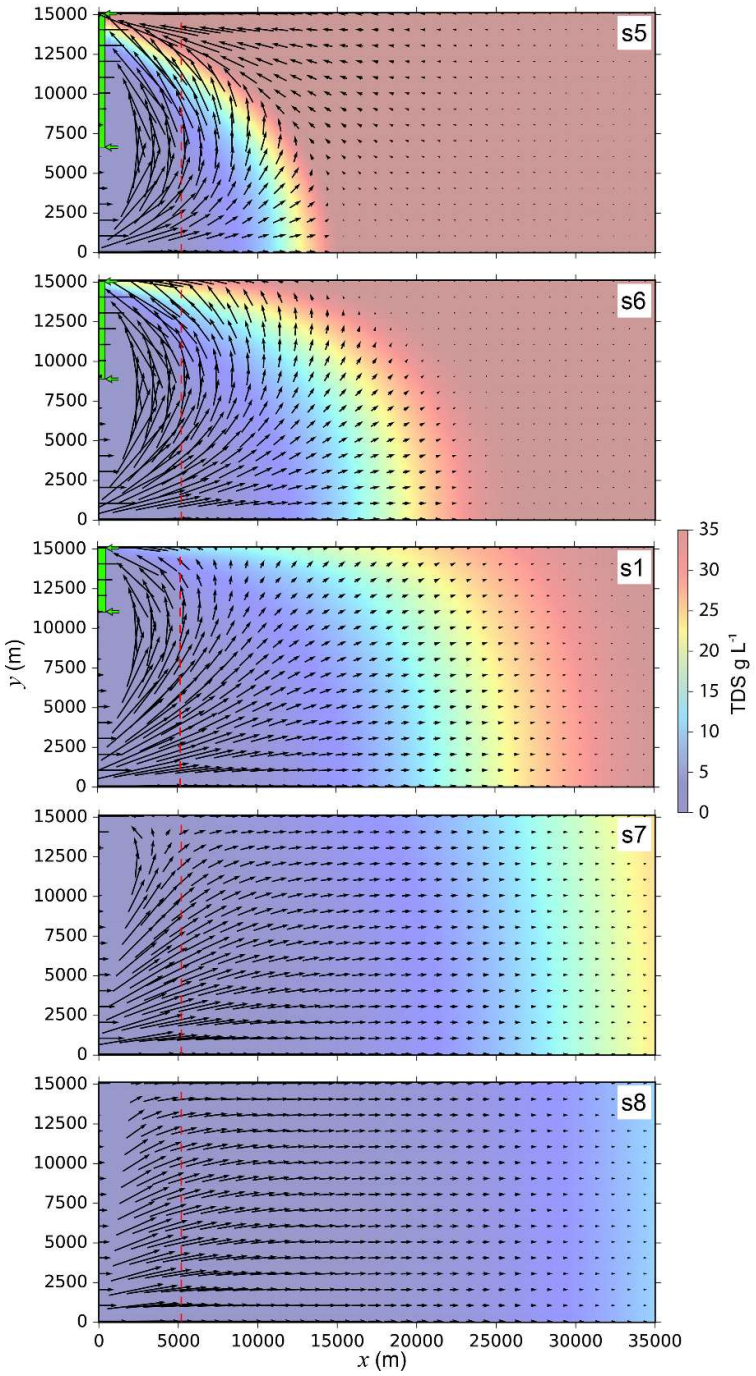

Fig. 4.5. Plan view plots of the upper layer of the semi-confined aquifer for simulations s1 and s5-s8. Colour shading indicates salinity, with dark blue and red being freshwater and saltwater, respectively. The dashed red line indicates the shoreline. The green arrows and the green shading along the onshore boundary mark the zone where active SWI is expected. Plots are ranked in order of increasing h_{min}. Black arrows indicate flow

direction, with vectors of every 8th row and column shown. The offshore boundary is located > 10 km to the right of the image in all cases. The offshore lengths of each simulation are given in Table 4.1.

Fluid flow through the coastline for simulation s5 is shown in Fig. 4.6. The data in Fig. 4.6a show that the zone of maximum onshore flow does not necessarily coincide with the zone of maximum onshore freshwater flow shown in Fig. 4.6b. This disconnect is due to the total flux cross the coastline (shown in Fig. 4.6a) incorporating both freshwater and saltwater components. There appears to be slightly higher rates of AFWC in the lower portions of the semi-confined aquifer than the upper portions. Conversely, there appear to be slightly higher rates of freshwater discharging to the offshore region in the upper portions of the semi-confined aquifer. Plots of the freshwater component of flow across the coastline for all simulations are presented in Fig. A2.3 to Fig A2.5.

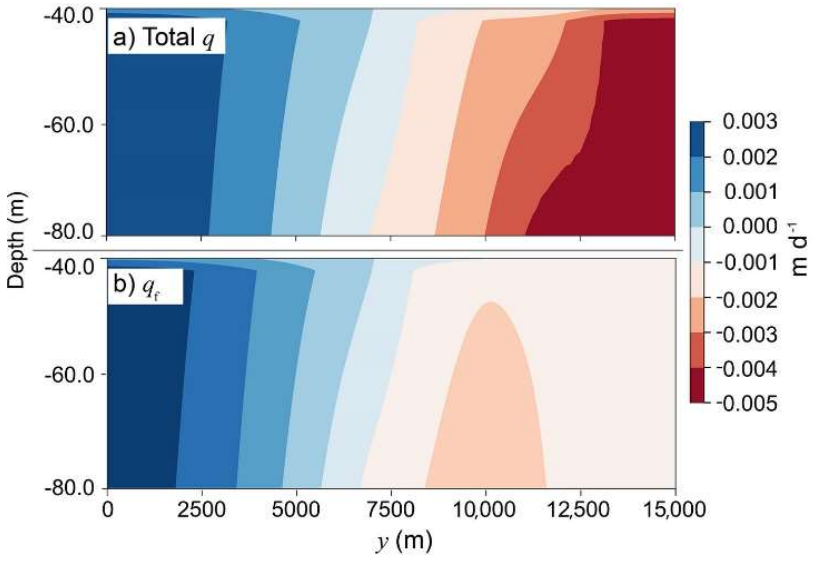

Fig. 4.6. a) A vertical slice along the coastline looking onshore (from the seaward side) of s5, showing combined freshwater and saltwater flow (q, m d^{-1}) where $q = Q / A$, where A

is the cross-sectional area of the cell. On the x-axis, y =0 m marks the front face (i.e., the h_{max} end) of the model while 15,000 m marks the back face (i.e., the h_{min} end). Blue shades represent water discharging to the offshore aquifer and red shades indicate flow to the onshore domain from offshore. b) The freshwater component of flow (q_f, m d^{-1}), where $q_f = Q_f / A$, across the coastline. Blue shades indicate freshwater discharging offshore, while red shades show freshwater fluxes moving to the onshore domain from offshore.

4.4.3 Comparison of the 2D and 3D simulations

Fig. 4.7 displays the difference between $x_{tip50\%}$ for the front face, middle row, and back face of each 3D model and their 2D equivalents. The data shown in Fig. 4.7a indicate that the difference between the $x_{tip50\%}$ in the 2D and 3D simulations generally decrease as K_v increases. The 2D simulations over predict the offshore extent at the front face (h_{max}) and under predict the OFG extent at the back face (h_{min}) for low values of K_v. $x_{tip50\%}$ at the back face shows non-monotonic behaviour. Initially the difference between the 2D and 3D simulations increases as K_v increases. Yet as K_v continues to increase past K_v=2.5E^{-5} m d^{-1} the difference in $x_{tip50\%}$ between the 2D and 3D simulations starts to decrease. There is minimal deviation between the $x_{tip50\%}$ in the 2D and 3D simulations for the middle row comparisons.

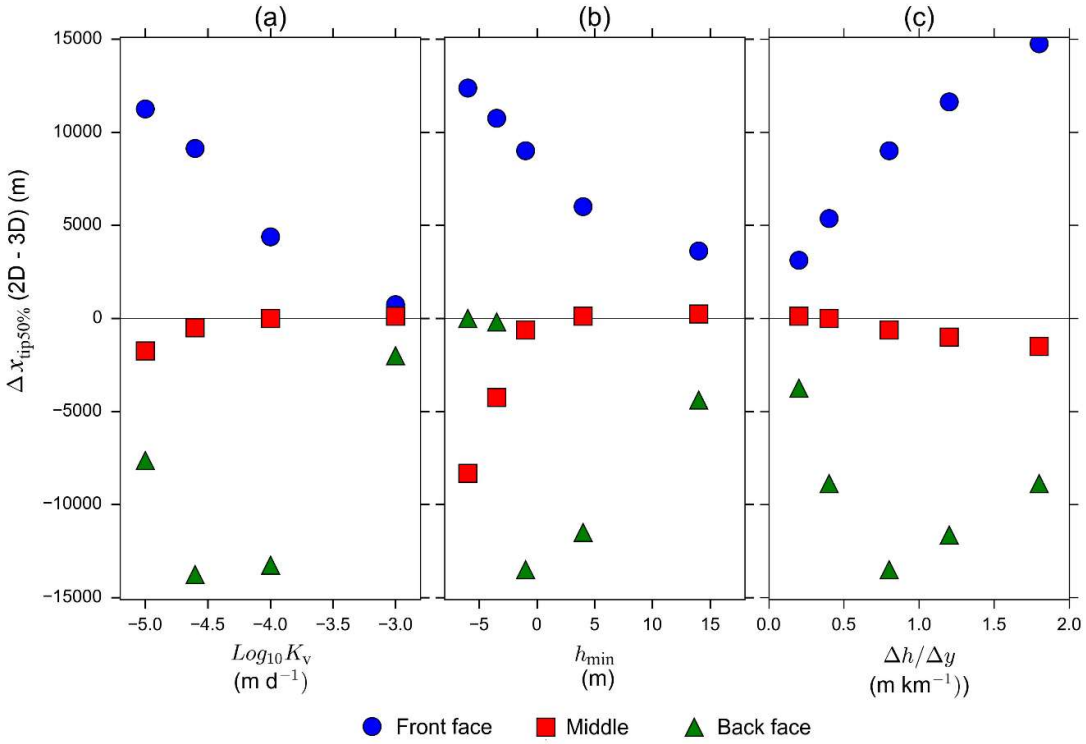

Fig. 4.7. Comparisons of the position of the $x_{tip50\%}$ for the 3D simulations front face, back face and middle row and their respective 2D equivalent models for each simulation. Panel (a) shows the simulations investigating the effect of K_v, (b) shows the simulations exploring the effect of the onshore head relative to sea level, and (c) displays the difference due to variations in the AHG. Simulation s1 is repeated in all panels.

The data shown in Fig. 4.7b show that the difference between the tip position in the 2D and 3D simulations at the front face (h_{max} boundary) decreases as the onshore heads increase. In the back-face data set, the freshwater-saltwater interface has been modelled to reach the onshore boundary in both the 2D and 3D simulations in the first two data points (i.e., s5 and s6). As such, these two data points return a minimal difference between $x_{tip50\%}$ of the 2D and 3D simulations. While h_{min} is also less than sea level in the third back-face data point shown in Fig. 4.7b (s1), $x_{tip50\%}$ at the back-face of the 3D simulations

remains offshore due to the transverse movement of freshwater both onshore and offshore. This results in a major difference between OFG extents predicted by the 2D and 3D models. In the simulations where $h_{min} > h_f$, the difference at the back face between the 2D and 3D simulations decreases as h_{min} increases. When viewing the data for the middle row, there is initially a large difference between the $x_{tip50\%}$ in the 2D and 3D models. However, after $h_{min} > h_f$, the difference between $x_{tip50\%}$ of the 2D and 3D models for the middle row becomes negligible once more.

Fig. 4.7c displays the comparison data for simulation where the AHG was varied. The difference between $x_{tip50\%}$ for the 2D and 3D simulations at the front face increases steadily as the AHG increases. Two distinct trends are apparent in the data showing the back-face comparisons. These appear to be controlled by the presence of active SWI in the model domain. Active SWI is not predicted at the back face for the simulations with an AHG of 0.2 m km^{-1} and 0.4 m km^{-1}. In these first two simulations, the difference between the 2D and 3D model predictions increases as the slope increases, with the 2D models under predicting the extent of OFG at the back face. However once $h_{min} < h_f$, the difference between the 2D and 3D models progressively decreases as the AHG increases, though the 2D simulation still under-predict the OFG extent at the back face in all AHG simulations. For the data comparing the 2D and 3D data for the middle section of the model domain, there appears to be minimal difference in the calculated OFG extent. Under higher AHGs, the 2D simulations appear to slightly under-predict the OFG extent in the middle cross section of the model.

4.5 Discussion

4.5.1 Grid sensitivity

In the 2D grid sensitivity simulations, the cell size of 125 m and α_L of 25 m, which was used in the 3D models, generates an interface that is further offshore than in the models with a finer grid discretisation and a smaller α_L. However, the shoreward shift in the interface due to the adopted α_L value is mitigated by the seaward shift in the calculated interface due to the increase in cell size. When the effects of both the increased Δx and larger α_L are combined, there is only a 2.1% difference in x_{tip} between the fine discretisation (Δx=5 m and α_L= 1 m) and coarse discretisation (Δx=125 m and α_L= 25 m) simulations. At the toe, the increased Δx and larger α_L both cause a seaward shift in $x_{toe,}$ when compared to x_{toe} of the simulation with a fine discretisation. As a result, x_{toe} in the coarse discretisation model is ~17% further offshore than in its finer discretised counterpart. These data suggest that the impact of the selected discretisation is likely greater at the base of the aquifer.

The trends observed our dispersion simulations are similar to those identified by Solórzano-Rivas et al. (2019) in their investigation into the effects of dispersion on offshore freshwater-saltwater interfaces. Solórzano-Rivas et al. (2019) identify that an increase in α_L from 1 m to 20 m results in a shoreward shift in x_{tip} and an offshore shift in x_{toe} of similar a magnitude (a dimensionless sensitivity (S) of 0.29-0.32) to those observed in our simulations (i.e., S= 0.29). S is calculated using $S = \frac{\Delta x_{tip} \alpha_L}{x_{tip} \Delta \alpha_L}$ (Werner and Robinson, 2017).

Due to resource constraints it was not feasible to assess the impacts of the selected discretisation using 3D simulations. While the effect of the selected model parameters on the 3D simulations is challenging to predict, it is likely that the cell discretisation and α_L adopted in the 3D simulations would result in an over estimation of the OFG extent, particularly at the toe, when compared to a finer discretised model. However, as there is no notable change in the freshwater fluxes at the coastline in the 2D grid dependency simulations, it is unlikely that the increase offshore extent has a significant impact on the calculated AFWC.

4.5.2 Calculated alongshore freshwater circulation

AFWC occurs in all the cases modelled where $h_{min} < h_f$. All three of the hydrogeological processes explored were able to generate AFWC to some degree over the range of conditions modelled. The simulations that investigate the effect of K_v on AFWC show that for a relatively thin semi-confining unit (i.e., H_l =10 m) with a low K_v (1E^{-5} m d^{-1}) up to 19% of the freshwater discharged into the offshore domain may return onshore. However, the proportion of AFWC rapidly decreases as K_v increases. When comparing the c of semi-confining units modelled against the real-world cases presented in Table A2.1, two of the seven regions have c values of the same order of magnitude as the s2, three have values of c comparable to s3, while the last two have a value of c that falls between s3 and s4.

The results also suggest that AFWC is highly sensitive to the magnitude of the onshore heads relative to sea level. Lowering the onshore heads has two effects on the model. Firstly, by reducing the head along the onshore boundary, the percentage of the model

domain subjected to active SWI conditions (i.e., onshore heads < 1 m) increases. Simulations s6 and s12 both have a similar percentage of the onshore boundary < 1 m (39% and 36%, respectively), and share AFWC rates of 38%. This suggests that the proportion of the onshore boundary with heads < h_f may form a strong control on the AFWC percentages. To test this, one additional simulation (herein referred to as s13) was undertaken with a $\Delta h/\Delta y$ of 0.4 m km^{-1}, and h_{mid}=0.525 m, all other parameters were consistent with s1. These parameters generate a model with the proportion of the onshore boundary with heads < h_f comparable to s5. The calculated percentage of AFWC in s13 was similar to s5 (63.9% and 70.3%, respectively). This supports the notion that AFWC in the model domain is strongly controlled by the proportion of the onshore boundary under active SWI conditions. Secondly, lowering the onshore heads reduces Q_f in the offshore direction, resulting in a landward movement of the freshwater-saltwater interface. When viewing Fig. 4.5, it appears that transverse flow in the offshore semi-confined aquifer is greatest close to the shoreline. The reduced OFG extent due to a lower offshore Q_f means a larger proportion of the OFG body falls in this nearshore zone. This, in part, may explain the higher observed AFWC percentages observed in the simulations with lower onshore heads relative to sea level.

The apparent relationship between the AFWC and the proportion of the onshore boundary with heads < 1 m is also visible when viewing the response of AFWC to changes in the AGH. It is interesting to note that although h_{min} in s12 is lower than in s5 (-7 m and -6 m, respectively) the percentage of AFWC in s5 (70.3%) is almost double the percentage of AFWC measured in s12 (38.1%). This is despite the maximum seaward Q_f in s12 being four time greater than in s5, while the maximum landward Q_f in s12 is three time greater than in s5. When plotting the percentage of AFWC against the percentage of the onshore

boundary < h_f for simulations s5-s12, a clear linear relationship becomes apparent. These data are shown in Fig. 4.8. The line of best fit though these data returns a relationship of AFWC% $= 1.07x - 2$ where x is the percent of the onshore boundary < h_f. This relationship has a R^2 of 0.97. The data of the simulations that investigated changes in K_v (shown in Fig. 4.8) indicate that K_v may change the relationship between the percentage of the onshore boundary < h_f and the degree of AFWC. However, further investigations into the relationship between K_v, AFWC and the proportion of the onshore boundary < h_f are beyond the scope of this study.

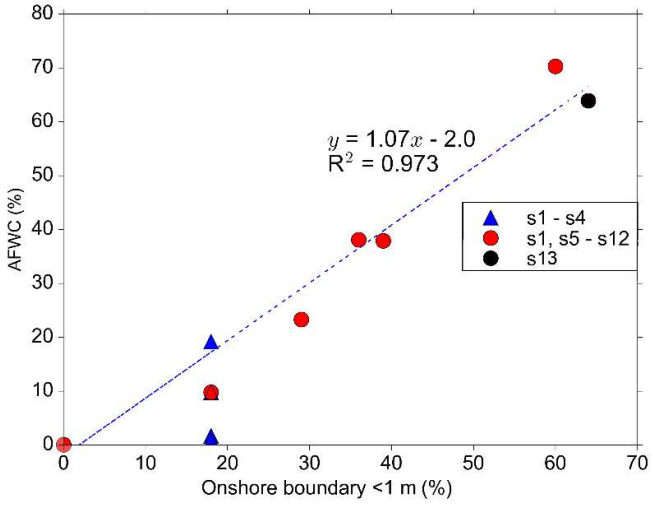

Fig. 4.8. The relationship between the proportion of the onshore boundary with a head < 1 m and the degree of AFWC. Red dots show the data from simulations s1, s5-s12, blue triangles show the data from simulations s1-s4, while the black dot shows the data from the additional simulation (s13). The line of best fit is calculated using only the data from s1 and s5-s13.

The results of this study indicate that AFWC may play a key role in maintaining onshore water qualities in some coastal aquifers. Fig. 4.9 shows an illustration of the potential role

that AFWC may play in maintaining onshore freshwater under steady-state conditions. In the illustration of s5 shown in Fig. 4.9, AFWC shifts the freshwater-saltwater interface towards h_{min} (i.e., the 15,000 m end). Similar behaviour is visible in all simulations with $h_{min} < 1$ m. These findings are significant as they indicate that a reduction in h_{max} may have major downstream implications both onshore and offshore. In some regions, lowering h_{max} would likely reduce transverse freshwater flow in both the onshore and offshore domains, causing the freshwater-saltwater interface to shift towards h_{max}. This would result in an increased zone of salinization in the onshore region that would otherwise remain fresh under steady-state conditions.

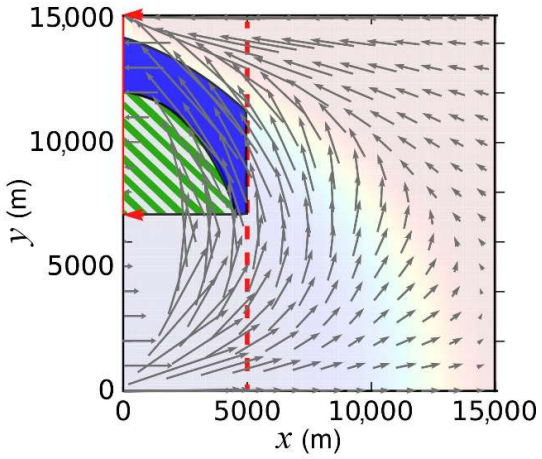

Fig. 4.9. An illustration of the regions in the onshore aquifer supported by alongshore freshwater flow where saltwater would otherwise be expected. The green stripe pattern shows the zone where alongshore onshore flow prevents salinization. Solid blue fill marks the zone where AFWC inhibits salinization. Red arrows mark the zone where onshore boundary heads predict active SWI. Faint blue and red shading indicate freshwater and saltwater, respectively.

AFWC has potential implications on the estimation of coastal chemical and nutrient budgets. The data indicate that in regions with both a high c and moderate proportion of the onshore domain under active SWI conditions, ignoring AFWC could result in the overestimation of terrestrially derived nutrient input into the ocean by up to 70%. This suggests that it is vital that AFWC is considered when developing regional scale coastal nutrient budgets. Additionally, AWRC may have implications for coastal contaminant fate models, as the data of this study indicate that there is potential for terrestrially originating contaminants to re-enter the onshore environment from the coastal boundary.

4.5.3 Comparison of 2D and 3D simulations

The data suggest that the negligible transverse assumption required to apply 2D models may only add low uncertainty to the predicted OFG extent in systems with a low AHG, a low c (i.e., a high K_v and/or a small H_l) and high onshore heads relative h_f across the model domain. At the h_{max} end, it is likely that using a 2D model will result in an overestimation of the OFG extent generated from active freshwater discharge. Conversely, simply assuming that OFG is unable to persist under steady-state conditions in a region where the onshore head is lower than the h_f may result in a significant underestimation of the OFG extent.

When looking at the 2D to 3D comparison data from the simulations included in this study, in the majority of cases, the 2D transect taken at h_{mid} approximated the OFG of the 3D simulation data through the middle row. This may indicate that adopting h_{mid} as the head in first pass 2D investigations could provide a rough estimate of the average OFG in the region. However, as the simulations in this model were simplified representations that

were run to an approximate steady state, this observation may not hold true in transient cases where local pumping effects can generate non-uniform hydraulic gradients. This investigation is unable to rule out the potential of estimating AFWC percentages from 2D transect models. However, when viewing the data generated in this study such a possibility appears unlikely.

The findings of this investigation suggest that the calculated OFG extents due to present day hydrogeological configurations in five of the 27 regions explored in Chapter 2 may shift if 3D numerical approaches were applied. While eight of the regions had an AHG, three of these regions display characteristics that are not conducive to notable AFWC. In the Gambier Embayment there is a very low AHG, in the Perth Basin both h_{max} and h_{min} are insufficient to prevent active SWI, while in Eckernförde Bay, the relatively high K_v ($1.2x10^{-3}$ m/day) would limit AFWC due to higher vertical leakance through the overlying aquitard. In Adelaide, Aveiro, Canterbury, Palmahim, and Southeast Georgia, AFWC may be present to some degree. However, a detailed hydrogeological characterisation of each of these regions would be required to assess the magnitude of any potential AFWC.

4.6 Conclusion

The present study determined that significant amounts of AFWC (up to 70 %) can occur in coastal semi-confined aquifer systems. The twelve 3D numerical simulations included in this study showed that AFWC is predicted under a range of realistic conditions. We were able to conclude that when part of the onshore domain has a head < h_f, there is

potential for significant AFWC. The proportion of AFWC is increased as the hydraulic conductivity of the overlying confining unit decreases.

This investigation indicates that the percent of AFWC in a region may be strongly related to the proportion of the onshore boundary with heads < h_f. The data suggest that similar percentages of AFWC would be expected in two systems with different AHGs yet a comparable proportion of the onshore boundary with heads < h_f. This suggests that while the AHG controls the magnitude of freshwater flow across the coastline, it does not have a strong control on the proportion of freshwater returning onshore due to AFWC. A detailed analysis of the relationship between AFWC and the proportion of the onshore boundary with heads < h_f for varying K_a to K_v ratios would provide a valuable addition to the body of work included in this study.

Through comparing the 3D model results to equivalent 2D cross-section simulations, we are able to conclude that in the majority of cases when AHG are present, 2D approaches are likely to over predict the OFG extent at the location of h_{max}, and under predict the OFG at the location of h_{min}. While the model results indicate that the OFG extents predicted at h_{mid} using 2D approaches have minimal deviation from the extents predicted using 3D models, it is unclear if this observation hold true in transient cases where non-uniform onshore head gradients between h_{max} and h_{min} are expected.

The significant proportions of AFWC observed in our simulations suggest that accounting for AFWC may improve coastal nutrient budget estimations for some regions. Additionally, the potential for AFWC prevent or reduce the degree of salinization predicted in an onshore aquifer under steady-state conditions may be of value to onshore

water managers. This body of work highlights the importance of considering the down-stream implications when establishing new zones of extraction in semi-confined coastal aquifers.

Chapter 5

5. Conclusions

5.1 Summary of findings

The potential use of OFG as a strategic resource to assist onshore freshwater supply necessitates a firm understanding of both the formation mechanisms and present-day extents of OFG, and the relationship OFG has with onshore forcings. The three studies contained in this thesis investigate: 1) the present-day use of OFG in coastal regions through onshore extractions; 2) the application of legacy petroleum exploration data to identifying new OFG bodies; 3) the influence of alongshore head gradients in onshore aquifers on OFG. This chapter outlines the main findings of the three previous chapters.

In Chapter 2, data from twenty-seven regions from across the world were assessed using both analytical models and groundwater observation data to determine the potential present-day onshore influence of OFG. From the freshwater-saltwater extent identified in observation data and insights gained from analytical modelling, seven different conceptual models incorporating both present-day and pre-development conditions were generated. They illustrate for the first time how OFG generated from paleo- or pre-development conditions can delay the onset of SWI in the onshore portion of coastal aquifers, assisting in the persistence of freshwater supply from onshore coastal wells. Through analytical modelling it was determined that under present-day conditions active SWI will eventually impact onshore pumping wells at fourteen of the twenty-seven sites, while passive SWI is expected onshore in an additional ten regions. In these twenty-four

regions, the onshore movement of OFG is likely delaying the onset of SWI within the onshore domain. Using the available data, it was concluded that onshore extraction regimes are by and large mining OFG. As such, where OFG is connected to onshore aquifers it should primarily be considered as an existing freshwater input rather than a new potential resource.

Chapter 3 combined geophysical data, hydraulic information and a first-order mathematical analysis to provide a leading example of evaluating OFG extent using multiple techniques. The investigation involved a novel application of Archie's law to constrain offshore groundwater salinities in the Gambier Embayment, South Australia. This study is the first to demonstrate the significant uncertainty due to rock matrix properties present when applying Archie's law to infer OFG. Despite this, the data suggest that in the south of the study area, pore-water with TDS of 2.2 g L^{-1} is found up to 13.2 km offshore. The salinities inferred from downhole geophysical data could be explained by a regional hydro-stratigraphic model that was generated from seismic data and the results from analytical modelling. This work provides a rare example of a comprehensive investigation using legacy petroleum exploration data and identified a fourth Australian OFG body evidenced by offshore data.

Chapter 4 used numerical simulations of simplified coastal aquifers to explore the behaviour of OFG in regions with an along-shore head gradient (AHG). Numerical simulations involved twelve 3D models and 36 2D models. Simulations investigated the response of OFG in systems with an AHG to changes in K_v, the onshore head relative to sea level, and the steepness of the AHG. Each 3D simulation was compared to three 2D simulations to test the discrepancy between 2D and 3D approaches. This investigation

showed for the first time that significant volumes (up to 70%) of the freshwater discharging from the onshore aquifer to its offshore extent may in-fact return onshore through alongshore circulation. The proportion of AFWC is greater in systems with a steep AHG, low onshore heads relative to sea level, and an offshore aquitard with a low K_v. It was also identified that when AHGs are present, 2D approaches have the tendency to overpredict the steady-state OFG extent at h_{max} and under predict the OFG extent at h_{min}. Through this investigation it was discovered that the onshore movement of OFG can persist under steady-state conditions in some regions, and that not all onshore movement of OFG represents the mining of relic OFG.

5.2 Future work

The three investigations contained in this thesis simplified the aquifer to be flat lying. An offshore slope in the semi-confined aquifer would, in most cases, result in an overlying saltwater column that also increases in depth with distance offshore. A changing seawater column thickness would increase h_f acting on the top of the semi-confined aquifer, thereby changing the calculated OFG extents. In the investigations presented in Chapter 2 and Chapter 3, the flat-lying simplification was required to apply the available analytical model. An absence of work that investigates the effect of offshore slope on OFG distribution increased the uncertainty surrounding the results of these two studies, and in all applications of the available offshore analytical models. The analytical modelling presented in Chapter 3 of this thesis demonstrated that an increase in h_f with distance offshore can result in a reduction in the expected extent of OFG under steady-state conditions. However, this conclusion was drawn from the application an analytical solution to paired conceptual models that represented conditions at the shoreline and

conditions several kilometres offshore in the study area. As such, a detailed investigation into the effect that an offshore slope has on OFG behaviour remains beneficial. Future work in this area would reduce the uncertainty involved with OFG extents calculated through the application of currently available analytical models.

The investigation into AFWC undertaken in Chapter 4 identified several avenues of potential future work. Future work could extend upon the work presented in this thesis through: (1) investigating how an offshore slope in the semi-confined aquifer effects AFWC and the predicted OFG extent; (2) exploring the potential relationships between K_v, AFWC and the proportion of the onshore boundary < h_f, as the results of Chapter 4 work indicate that these three factors may have a strong control on AFWC; (3) the investigation of AFWC under transient condition such as those generated due to an increase in groundwater extractions and/or the inclusion of groundwater age as a potential tracer.

The estimation of OFG extent through numerical simulations would benefit from work investigating how zones of higher K_v in the offshore region (e.g., paleo-channels and breaks in the semi-confining unit) change regional offshore flow paths. While Mulligan et al. (2007) explored fluid fluxes along paleo-channel margins, an investigation into the impact that zones of higher K_v have on regional flow, for both offshore and onshore head gradients at the coastline, would allow for a marked improvement in the estimation of OFG extents and resource longevity. Additionally, though the implications of aquifer heterogeneity and the connectivity of flow paths have been studied by Michael et al (2016) and Yu and Michael (2019a, 2019b), these investigations were limited to 2D sections. Investigating the alongshore flow component in systems with an alongshore

hydraulic gradient would be highly beneficial. Such work would build upon the findings of Chapter 4 of this thesis, which indicated that notable alongshore flow is likely present offshore in many coastal groundwater systems.

1 References

Amir, N., Kafri, U., Herut, B., Shalev, E., 2013. Numerical simulation of submarine groundwater flow in the coastal aquifer at the Palmahim area, the Mediterranean Coast of Israel. Water Resour. Manag. 27 (11), 4005–4020. https://doi.org/10.1007/s11269-013-0392-2.

Anomohanran, O., 2015. Hydrogeophysical and hydrogeological investigations of groundwater resources in Delta Central, Nigeria. J. Taibah Univ. Sci. 9 (1), 57–68. https://doi.org/10.1016/j.jtusci.2014.06.003.

Archie, G.E., 1942. The electrical resistivity log as an aid in determining some reservoir characteristics. J. Pet. Technol. 5, 1‑8. https://doi.org/10.2118/942054-G.

Bakken, T.H., Ruden, F., Mangset, L.E., 2012. Submarine groundwater: a new concept for the supply of drinking water. Water Resour. Manag. 26, 1015–1026. https://doi.org/10.1007/s11269-011-9806-1.

Bakker, M., 2006. Analytic solutions for interface flow in combined confined and semi-confined, coastal aquifers. Adv. Water. Resour. 29, 417–425. https://doi.org/10.1016/j.advwatres.2005.05.009.

Bakker, M., Miller, A.D., Morgan, L.K., Werner, A.D., 2017. Evaluation of analytic solutions for steady interface flow where the aquifer extends below the sea. J. Hydrol. 551, 660–664. https://doi.org/10.1016/j.jhydrol.2017.04.009.

Barlow, P.M., 2003. Ground water in freshwater-saltwater environments of the Atlantic coast (Vol. 1262). Geological Survey (USGS). US Geol. Surv. Circ., 1262 (2003), p. 113.

Beebe, C.R., Ferguson, G., Gleeson, T., Morgan, L.K., Werner, A.D., 2006. Application of an analytical solution as a screening tool for sea water intrusion. Groundwater 54 (5), 709–718. https://doi.org/10.1111/gwat.12411.

Boult, P.J., Hibburt, J.E., 2002. The petroleum geology of South Australia. Vol. 1: Otway Basin. 2nd edn. South Australia Department of Primary Industries and Resources. Petroleum Geology of South Australia Series, 1. ISBN 073-0-841472.

Bratton, J.F., 2010. The three scales of submarine groundwater flow and discharge across passive continental margins. J. Geol. 118, 565‑575. https://doi.org/10.1086/655114.

Bresciani, E., Batelaan, O., Banks, E.W., Barnett, S.R., Batlle-Aguilar, J., Cook, P.G., Costar, A., Cranswick, R.H., Doherty, J., Green, G., Kozuskanich, J., Partington, D.,Pool, M., Post, V.E.A., Simmons, C.T., Smerdon, B.D., Smith, S.D., Turnadge, C.,Villeneuve, S., Werner, A.D., White, N., Xie, Y., 2015. Assessment of Adelaide Plains Groundwater Resources: Summary Report. Goyder Institute for Water Research Technical Report Series No. 15/31. Goyder Institute for Water Research, Adelaide, South Australia. ISSN 1839-2725.

Buapeng, S., Wattayakorn, G., 2008. Groundwater Situation in Bangkok and Its Vicinity. Paper presented at Hydrological changes and management fromheadwater to the ocean, At Kyoto Garden Palace, Kyoto, Japan, 1–3 October, 2008. http://dx.doi.org/10.13140/2.1.1734.7528.

Bush, A.L., 2009. Physical and chemical hydrogeology of the Otway Basin, southeast Australia (Doctoral dissertation). School of Earth Sciences, The University of Melbourne.

Caraivan, G., Dinu, I., Fulga, C., Radu, V., 2010. Possiblility of extending the drinking water supply for the Constanta harbour. Geo-Eco-Marina 16, 75–84.

Chitea, F., Georgescu, P., Ioane, D., 2011. Geophysical detection of marine intrusions in Black Sea coastal areas (Romania) using VES and ERT data. Geo-Eco-Marina 17, 95–102.

Clarke, J.D.A., Lewis, S.J., Fontaine, K., Kilgour, P.L., Stewart, G., 2015. Regional Hydrogeological Characterisation of the Otway Basin, Victoria and South Australia: Technical report for the National Collaboration Framework Regional Hydrogeology Project. Record 2015/12. Geoscience Australia, Canberra. DOI: 10.11636/Record.2015.012.

Cohen, D., Person, M., Wang, P., Gable, C.W., Hutchinson, D., Marksamer, A., Dugan, B., Kooi, H., Groen, K., Lizarralde, D., 2010. Origin and extent of fresh paleowaters on the Atlantic continental shelf, USA. Ground Water 48, 143– 158. https://doi.org/10.1111/j.1745-6584.2009.00627.x.

Danskin, W.R., 2012. Gaining the necessary geologic, hydrologic and geochemical understanding for additional brackish groundwater development, coastal San Diego, California, United States. In: Proceedings of the 22nd Salt Water Intrusion Meeting (SWIM), Buzios, Brazil, June 17-22, 2012.

de Melo, M.C., da Silva, M.M., Edmunds, W.M., 1999. Hydrochemistry and flow modelling of the Aveiro multilayer Cretaceous aquifer. Phys. Chem. Earth (B) 24 (4), 331–336. https://doi.org/10.1016/S1464-1909(99)00009-X.

de Melo, M.C., Paquete, P.C., Da Silva, M.M., 2001. Evolution of the Aveiro Cretaceous aquifer (NW Portugal) during the Late Pleistocene and present day: evidence from chemical and isotopic data. In: Edmunds, W.M., Milne, C.J. (Eds.) Palaeowaters in Coastal Europe: Evolution of Groundwater Since the Late Pleistocene. Geological Society, London, Special Publications 189 (1). pp.139- 154. ISBN 1-86239-086-X.

Delinom, R.M., 2008. Groundwater management issues in the Greater Jakarta area, Indonesia. In: Tanaka. T., (Ed.) Proceedings of international workshop on integrated watershed management for sustainable water use in a humid tropical region. TERC Bull., University of Tsukuba 8 (2). pp. 40-54.

Department of Environment and Water (DEW), 2019. Online groundwater data from Water Connect, as part of DEW, Government of South Australia.<https://www.waterconnect.sa.gov.au/Systems/GD/Pages/default.aspx>(cited 27.04.19).

Department of Environment, Water and Natural Resources, 2013. North Adelaide Plains PWA, T1 aquifer, Groundwater Level and Salinity Status Report. Department of Environment, Water and Natural Resources, Government of South Australia. ISBN 978-1-922174-44-4.

Department of Environment, Water and Natural Resources, 2015. Southern Basins PWA Uley South lens, Groundwater level and salinity status report. Department of Environment, Water and Natural Resources, Government of South Australia. ISBN 978-1-925369-81-6.

DePaul, V.T., Rosman, R., 2015. Water-level conditions in the confined aquifers of the New Jersey Coastal Plain, 2008. US Geological Survey Scientific Investigations Report 2013–5232. US Department of the Interior, US Geological Survey. http://dx.doi. org/10.3133/sir20135232.

Dodson, W.J., 2009. Groundwater recharge from the Gascoyne River, Western Australia. Department of Water Hydrogeological record series HG 32. Department of Water, Government of Western Australia. ISBN 978-1-921508- 60-8.

Edmunds, W.M., Buckley, D.K., Darling, W.G., Milne, C.J., Smedley, P.L., Williams, A. T., 2001. Palaeowaters in the aquifers of the coastal regions of southern and eastern England. In: Edmunds, W.M., Milne, C.J. (Eds.) Palaeowaters in Coastal Europe: Evolution of Groundwater Since the Late Pleistocene. Geological Society, London, Special Publications 189 (1). pp. 71-92. ISBN 1-86239-086-X.

Essaid, H.I., 1990. A multilayered sharp interface model of coupled freshwater and saltwater flow in coastal systems: model development and application. Water Resour. Res. 26 (7), 1431–1454. https://doi.org/10.1029/WR026i007p01431.

Essink, G.H.O., 2001. Improving fresh groundwater supply - problems and solutions. Ocean Coast. Manag., 44 (5-6), 429-449. https://doi.org/10.1016/S0964-5691(01)00057-6.

Ferguson, G., Gleeson, T., 2012. Vulnerability of coastal aquifers to groundwater use and climate change. Nat. Clim. Change 2 (5), 342–345. https://doi.org/10.1038/nclimate1413.

Foyle, A.M., Henry, V.J., Alexander, C.R., 2002.Mapping the threat of seawater intrusion in a regional coastal aquifer-aquitard system in the southeastern United States. Environ. Geol. 43 (1), 151–159. https://doi.org/10.1007/s00254-002-0636-6.

Francés, A.P., Ramalho, E.C., Fernandes, J., Groen, M., Hugman, R., Khalil, M.A., De Plaen, J., Santos, F.A.M., 2015. Contributions of hydrogeophysics to the hydrogeological conceptual model of the Albufeira-Ribeira de Quarteira coastal aquifer in Algarve, Portugal. Hydrogeo. J. 23 (7), 1553–1572. https://doi.org/10.1007/s10040-015-1282-x.

Freeman, B., Boult, P.J., Yielding, G., Menpes, S., 2010. Using empirical geological rules to reduce structural uncertainty in seismic interpretation of faults. J. Struct. Geol. 32 (11), 1668‑1676. https://doi.org/10.1016/j.jsg.2009.11.001.

Fulthorpe, C.S., Hoyanagi, K., Blum, P., 2011. IODP Expedition 317: exploring the record of sea-level change off New Zealand. Sci. Drill. 12, 4–14. https://doi.org/10.2204/iodp.sd.12.01.2011.

Glover, Paul, 2009. What is the cementation exponent? A new interpretation. Leading Edge 28 (1), 82‑85. https://doi.org/10.1190/1.3064150.

Glover, P., 2016. Petrophysics MSc. Course Notes. University of Leeds. (accessed 02/05/2018).<http://homepages.see.leeds.ac.uk/~earpwjg/PG_EN/CD%20Contents/GGL-66565%20Petrophysics%20English/Chapter%2016.PDF>.

Goldman, M., Levi, E., Kafri, U., Tezkan, B., Yogeshwar, P., Herut, B., Tibor, G., 2010. Delineating fresh groundwater aquifer within sub-seafloor sediments offshore Israel using a short offset marine TDEM system. In: Proceedings of SWIM 21: 21st Salt Water Intrusion Meeting, Azores, Portugal. pp. 69-72. ISBN 978-972-97711-5-6.

Groen, J., Velstra, J., Meesters, A., 2000. Salinization processes inpaleowaters in coastal sediments of Suriname: evidence from d 37 Cl analysis and diffusion modelling. J. Hydrol. 234, 1–20. https://doi.org/10.1016/S0022-1694(00)00235-3.

Haider, K., Engesgaard, P., Sonnenborg, T.O., Kirkegaard, C., 2015. Numerical modeling of salinity distribution and submarine groundwater discharge to a coastal lagoon in Denmark based on airborne electromagnetic data. Hydrogeol. J. 23, 217–233. https://doi.org/10.1007/s10040-014-1195-0.

Harvey, C.F., 2002. Groundwater flow in the Ganges Delta. Science 296 (5573), 1563-1563. https://doi.org/10.1126/science.296.5573.1563a.

Hathaway, J.C., Poag, C.W., Valent, P.C., Miller, R.E., Schultz, D.M., Manhe, F.T., Kohout, F.A., Bothner, M.H., Sangi, D.A., 1979. United-States geological survey core drilling on the Atlantic shelf. Sci. 206 (4418), 515–527. https://doi.org/10.1126/science.206.4418.515.

Hennig, A., Otto, C., 2005. A hydrodynamic characterisation of the offshore Vlaming Sub-basin. Research Program, 1.2. Technologies for Assessing Sites for CO2 Storage. Report No. RPT05-0223. CO2CRC, Canberra.

Holford, S., Tuitt, A., Hillis, R., Green, P., Stoker, M., Duddy, I., Sandiford, M., Tassone, D., 2014. Cenozoic deformation in the Otway Basin, southern Australian margin: implications for the origin and nature of post-breakup compression at rifted margins. Basin Res. 26 (1), 10‐37. https://doi.org/10.1111/bre.12035.

Hugman, R., Stigter, T.Y., Monteiro, J.P., Costa, L., Nunes, L.M., 2015. Modeling the spatial and temporal distribution of coastal groundwater discharge for different water use scenarios under epistemic uncertainty: case study in South Portugal. Environ. Earth Sci. 73 (6), 2657–2669. https://doi.org/10.1007/s12665-014-3709-4.

Hutchinson, C.B., 1990. Analysis of ground-water flow in the A-sand aquifer at Paramaribo, Suriname, South America. US Geological Survey, Water-Resources Investigations Report 90-4036. Department of the Interior, US Geological Survey.

Ivkovic, K.M., Marshall, S.K., Morgan, L.K., Werner, A.D., Carey, H., Cook, S., Sundaram, B., Norman, R., Wallace, L., Caruana, L., Dixon-Jain, P., Simon, D., 2012. A National Scale Vulnerability Assessment of Seawater Intrusion: Summary Report, Waterlines Report Series 85. National Water Commission, Canberra. ISBN 978-1-922136-00-8.

Jiao, J.J., Shi, L., Kuang, X., Lee, C.M., Yim, W.-S., Yang, S., 2015. Reconstructed chloride concentration profiles below the seabed in Hong Kong (China) and their implications for offshore groundwater resources. Hydrogeol. J. 23, 277–286. https://doi.org/10.1007/s10040-014-1201-6.

Jorgensen, D.G., 1996. The ratio method of estimating water resistivity and TDS from resistivity logs. Groundwater 34 (3), 519‐522. https://doi.org/10.1111/j.1745-6584.1996.tb02033.x.

Kaleris, V., Lagas, G., Marczinek, S., Piotrowski, J., 2002. Modelling submarine groundwater discharge: an example from the western Baltic Sea. J. Hydrol. 265, 76–99. https://doi.org/10.1016/S0022-1694(02)00093-8.

Kinnaman, S.L., Dixon, J.F., 2009. Potentiometric Surface of the Upper Floridan Aquifer in the St. Johns River Water Management District and vicinity, Florida, May 2009. US Geological Survey Scientific Investigations Map 3091. US Department of the Interior, US Geological Survey.

Knight, A.C., Werner, A.D., Morgan, L.K., 2018. The onshore influence of offshore fresh groundwater. J. Hydrol. 561, 724‐736. https://doi.org/10.1016/j.jhydrol.2018.03.028.

Knowling, M.J., Werner, A.D., Herckenrath, D., 2015. Quantifying climate and pumping contributions to aquifer depletion using a highly parameterised groundwater model: Uley South Basin (South Australia). J. Hydrol. 523, 515–530. https://doi.org/10.1016/j.jhydrol.2015.01.08.1.

Kooi, H., Groen, J., 2001. Offshore continuation of coastal groundwater systems; predictions using sharp-interface approximations and variable-density flow modelling. J. Hydrol. 246, 19–35. https://doi.org/10.1016/S0022-1694(01)00354-7.

Koussis, A.D., Mazi, K., Destouni, G., 2012. Analytical single-potential, sharp interface solutions for regional seawater intrusion in sloping unconfined coastal aquifers,

with pumping and recharge. J. Hydrol. 416–417, 1–11. https://doi.org/10.1016/j.jhydrol.2011.11.012.

Krantz, D.E., Manheim, F., Bratton, J.F., Phelan, D.J., 2004. Hydrogeologic setting and ground water flow beneath a section of Indian River Bay, Delaware. Groundwater 42 (7), 1035–1051. https://doi.org/10.1111/j.1745-6584.2004.tb02642.x.

Laattoe, T., Werner, A.D., Simmons, C.T., 2013. Seawater intrusion under current sea-level rise: Processes accompanying coastline transgression, Chapter 14. In: Wetzelhuetter, C. (Ed.), Groundwater in the Coastal Zones of Asia-Pacific. Coastal Research Library. Springer, pp. 295–313. ISBN 978-94-007-5647-2.

Lamontagne, S., Le Gal La Salle, C., Hancock, G.J., Webster, I.T., Simmons, C.T., Love, A.J., James-Smith, J., Smith, A.J., Kampf, J., Fallowfield, H.J., 2008. Radium and radon radioisotopes in regional groundwater, intertidal groundwater, and seawater in the Adelaide Coastal Waters Study area: implications for the evaluation of submarine groundwater discharge. Mar. Chem. 109, 318–336. https://doi.org/10.1016/j.marchem.2007.08.010.

Love, A.J., Herczeg, A.L., Armstrong, D., Stadter, F., Mazor, E., 1993. Groundwater flow regime within the Gambier Embayment of the Otway Basin, Australia: evidence from hydraulics and hydrochemistry. J. Hydrol. 143 (3‐4), 297‐338. https://doi.org/10.1016/0022-1694(93)90197-H.

Lubis, R.F., Sakura, Y., Delinom, R., 2008. Groundwater recharge and discharge processes in the Jakarta groundwater basin, Indonesia. Hydrogeol. J. 16 (5), 927–938. https://doi.org/10.1007/s10040-008-0278-1.

Lundegard, P.D., Trevena, A.S., 1990. Sandstone diagenesis in the Pattani Basin (Gulf of Thailand): history of water-rock interaction and comparison with the Gulf of Mexico. Appl. Geochem. 5 (5–6), 669–685. https://doi.org/10.1016/0883-2927(90)90064-C.

Maathuis, H., Wak, W., Adi, S., 2000. Hydrogeology of the Coastal basins of Jakarta, Indonesia. In: Sililo, O., (Ed.) Groundwater: Past Achievements and Future Challenges: Proceedings of the XXX IAH congress on groundwater, Cape Town, South Africa, 26 November- 1 December 2000. pp. 209–213. ISBN 90-5809-159-7.

Marksamer, A.J., Person, M.A., Day-Lewis, F.D., Lane, J.W. Jr., Cohen, D., Dugan, B., Kooi, H., Willett, M., 2007. Integrating geophysical, hydrochemical and

hydrologic data to understand the freshwater resources on Nantucket Island, Massachusetts. In: Hyndman D.W., Day-Lewis F.D., Singha K., (Eds.) Surface hydrology: data integration for properties and processes. Geophysical Monograph Series 171. Washington, DC: American Geophysical Union. pp.143-159. http://dx.doi.org/10.1029/171GM12.

Masterson, J.P., Barlow, P.M., 1994. Effects of simulated ground-water pumping and recharge on ground-water flow in Cape Cod, Martha's Vineyard, and Nantucket Island Basins, Massachusetts. US Geological Survey Open File Report 94-316. US Department of the Interior, US Geological Survey.

McAuley, S.D., Barringer, J.L., Paulachok, G.N., Clark, J.S., Zapecza, O.S., 2001. Groundwater flow and quality in the Atlantic City 800 Foot Sand, New Jersey. New Jersey Geological Survey Report 41. New Jersey Geological Survey.

Meisler, H., Leahy, P.P., Knobel, L.L., 1984. Effect of eustatic sea-level changes on saltwater-freshwater in the Northern Atlantic Coastal Plain. US Geological Survey Water Supply Paper 2255. Reston, Virginia, US Geological Survey.

Meyer, F.W., 1989. Hydrogeology, ground-water movement, and subsurface storage in the Floridan aquifer system in southern Florida. US Geological Survey Professional Paper 1403-G. US Department of the Interior, US Geological Survey.

Michael, H.A., Scott, K.C., Koneshloo, M., Yu, X., Khan, M.R., Li, K., 2016. Geologic influence on groundwater salinity drives large seawater circulation through the continental shelf. Geophys. Res. Lett. 43 (20). https://doi.org/10.1002/2016GL070863.

Michael, H.A., Post, V.E.A., Wilson, A.M., Werner, A.D., 2017. Science, society, and the coastal groundwater squeeze. Water Resour. Res. 53, 210–2617. https://doi.org/10.1002/2017WR020851.

Morgan, L.K., Werner, A.D., 2015. A national inventory of seawater intrusion vulnerability for Australia. J. Hydrol. Reg. Stud. 4, 686–698. https://doi.org/10.1016/j.ejrh.2015.10.005.

Morgan, L.K., Werner, A.D., Morris, M.J., Teubner, M.D., 2013. Application of a rapidassessment method for seawater intrusion vulnerability: Willunga Basin, South Australia. In: Wetzelhuetter, C. (Ed.), Groundwater in the Coastal Zones of Asia-Pacific. Springer Netherlands, Dordrecht, pp. 205–225. ISBN 978-94-007-5648-9.

Morgan, L.K., Harrington, N., Werner, A.D., Hutson, J.L., Woods, J., Knowling, M.J., 2015. South East Regional Water Balance Project – Phase 2. Development of a Regional Groundwater Flow Model. Goyder Institute for Water Research Technical Report Series No. 15/38. Goyder Institute for Water Research, South Australia. ISSN 1839-2725.

Morgan, L.K., Werner, A.D., Patterson, A., 2016. First-order analysis of offshore groundwater in the Perth Basin, Western Australia, using analytic and numerical modelling. In: Werner, A.D. (Ed.) Proceedings of the 24th Salt Water Intrusion Meeting and the 4th Asia-Pacific Coastal Aquifer Management Meeting, 4-8 July, 2016, Cairns, Australia. pp. 90. ISBN 1-876346-64-7.

Morgan, L.K., Werner, A.D., Patterson, A.E., 2018. ‘A conceptual study of offshore fresh groundwater behaviour in the Perth Basin (Australia): modern salinity trends in a prehistoric context. J. Hydrol. Reg. Stud. 19, 318‑334. https://doi.org/10.1016/j.ejrh.2018.10.002.

Morrissey, S., Clark, J., Bennet, M., Richardson, E., Stute, M., 2010. Groundwater reorganization in the Floridan Aquifer following Holocene sea-level rise. Nat. Geosci. 3, 683–687. https://doi.org/10.1038/NGEO956.

Nativ, R., Weisbrod, N., 1994. Hydraulic connections among subaquifers of the Coastal Plain Aquifer, Israel. Ground Water 32 (6), 997–1007. https://doi.org/10.1111/j.1745-6584.1994.tb00939.x.

NCEI, 2017. Bathymetric Data Viewer, version 2.8.6. National Centers for Environmental Information, Viewed March 20 2017, https://maps.ngdc.noaa.gov/viewers/bathymetry.

Onodera, S.I., Saito, M., Sawano, M., Hosono, T., Taniguchi, M., Shimada, J., Umezawa, Y., Lubis, R.F., Buapeng, S., Delinom, R., 2009. Erratum to ‘‘Effects of intensive urbanization on the intrusion of shallow groundwater into deep groundwater: examples from Bangkok and Jakarta”. Sci. Total. Environ. 407 (9), 3209–3217. https://doi.org/10.1016/j.scitotenv.2009.01.050.

Oteri, A.U., 1988. Electric log interpretation for the evaluation of salt water intrusion in the eastern Niger Delta. Hydrological Sci. J. 33, 19–30. https://doi.org/10.1080/02626668809491219.

Oteri, A.U., Atolagbe, F.P., 2003. Saltwater Intrusion into Coastal Aquifers in Nigeria. Paper presented at The Second International Conference on Saltwater Intrusion

and Coastal Aquifers—Monitoring, Modeling, and Management. Mérida, Yucatán, México, March 30–April 2, 2003.

Paldor, A., Shalev, E., Katz, O., Aharonov, E., 2019. Dynamics of saltwater intrusion and submarine groundwater discharge in confined coastal aquifers: a case study in northern Israel. Hydrogeo. J., 1-15. https://doi.org/10.1007/s10040-019-01958-5.

Pauw, P.S., Groen, J., Groen, M.M.A., van der Made, K.J., Stuyfzand, P.J., Post, V.E.A., 2017. Groundwater salinity patterns along the coast of the Western Netherlands and the application of cone penetration tests. J. Hydrol. 551, 756–767. https://doi.org/10.1016/j.jhydrol.2017.04.021.

Person, M., Marksamer, A., Dugan, B., Sauer, P.E., Brown, K., Bish, D., Licht, K.J., Willett, M., 2012. Use of a vertical d18O profile to constrain hydraulic properties and recharge rates across a glacio-lacustrine unit, Nantucket Island, Massachusetts, USA. Hydrogeol. J. 20, 325–336. https://doi.org/10.1007/s10040-011-0795-1.

Pollock, R.M., 2003. Sequence Stratigraphy of the Paleocene to Miocene Gambier Subbasin, Southern Australia (Doctoral dissertation). University of Adelaide, School of Earth and Environmental Sciences, National Centre for Petroleum Geology and Geophysics and Discipline of Geology and Geophysics.

Pope, D.A., 2006. Simulation of proposed increases in ground-water withdrawals from the Atlantic City 800-foot sand, New Jersey Coastal Plain. Scientific Investigations Report 2006-5114, US Department of the Interior, US Geological Survey.

Post, V.E.A., 2005. Fresh and saline groundwater interaction in coastal aquifers: Is our technology ready for the problems ahead? Hydrogeol. J. 13, 120–123. https://doi.org/10.1007/s10040-004-0417-2.

Post, V.E.A., Werner, A.D., 2017. Coastal aquifers: Scientific advances in the face of global environmental challenges. J. Hydrol. 551, 1–3. https://doi.org/10.1016/j.jydrol.2017.04.046.

Post, V.E.A., Groen, J., Kooi, H., Person, M., Ge, S., Edmunds, W.M., 2013. Offshore fresh groundwater reserves as a global phenomenon. Nat. 504, 71–78. https://doi.org/10.1038/nature12858.

Raymer, L.L., Hunt, E.R., Gardner, J.S., 1980. An improved sonic transit time-to-porosity transform: Society of Professional Well Log Analysts 21st Annual Logging Symposium Transactions, paper P, unpaginated. Doc. I.D. SPWLA-1980-P.

Ryder, A., 2008. Groundwater trends in the Albany Hinterland sub-region.Department of Agriculture, Government of Western Australia. ISSN 1447-4980.

Sanford, W.E., Buapeng, S., 1996. Assessment of a groundwater flow model of the Bangkok Basin, Thailand, using carbon-14-based ages and paleohydrology. Hydrogeol. J. 4 (4), 26–40. https://doi.org/10.1007/s100400050083.

Schaeffer, J., 2008. Scaling Point Based Aquifer Data for Developing Regional Groundwater Models: application to the Gippsland Groundwater System (Ph.D. Thesis). Engineering, Civil and Environmental Engineering, The University of Melbourne, Australia.

Schafer, D., Johnson, S., Kern, A., 2008. Hydrogeology of the Leederville aquifer in the western Busselton–Capel Groundwater Area. Department of Water, Hydrogeological Record Series, HG31. Department of Water, Government of Western Australia. ISSN 1834-9188.

Scott, M., Wilson, N., 2012. Seawater intrusion network review. Environment Canterbury Technical Report 12/35. Environment Canterbury. ISBN 978-1-927210-26-0.

Shen, S.L., Xu, Y.S., 2011. Numerical evaluation of land subsidence induced by groundwater pumping in Shanghai. Can. Geotech. J. 48 (9), 1378–1392. https://doi.org/10.1139/T11-049.

Siegel, J., Person, M., Dugan, B., Cohen, D., Lizarralde, D., Gable, C., 2014. Influence of late Pleistocene glaciations on the hydrogeology of the continental shelf offshore Massachusetts, USA. Geochem. Geophys. Geosyst. 15, 4651–4670.https://doi.org/10.1002/2014GC005569.

Smith, P.C., Rogers, P.A., Lindsay, J.M., White, M.R., Kwitko, G., 2012. Gambier basin. In: Drexel, J.F., Preiss, W.V. (Eds.), The Geology of South Australia. 2, The Phanerozoic. South Australia. Geological Survey. Bulletin, pp. 195–198.

Solórzano-Rivas, S.C., Werner, A.D., 2018. On the representation of subsea aquitards in models of offshore fresh groundwater. Adv. Water. Resour. 112, 283–294. https://doi.org/10.1016/j.advwatres.2017.11.025.

Soulet, G., Delaygue, G., Vallet-Coulomb, C., Böttcher, M.E., Sonzogni, C., Lericolais,G., Bard, E., 2010. Glacial hydrologic conditions in the Black Sea

reconstructed using geochemical pore water profiles. Earth Planet. Sci. Lett. 296 (1), 57–66.https://doi.org/10.1016/j.epsl.2010.04.045.

Spechler, R.M., 1994. Saltwater intrusion and quality of water in the Floridan aquifer system, northeastern Florida. Water-Resources Investigations Report 92 (4174). US Department of the Interior, US Geological Survey.

Stewart, S., 2006. McLaren Vale Prescribed Wells Area Groundwater Monitoring Status Report. DWLBC Report 2006/04. Department of Water, Land and Biodiversity Conservation, Government of South Australia. ISBN 1-921218-07-x.

US Army Corps of Engineers, 1998. Water resource assessment of Suriname. Viewed Feburary 12, 2017, http://suriname.wedd.de/docs/Suriname%20Water%20Resources%20Assessment.pdf.

Varma, S., Michael, K., 2012. Impact of multi-purpose aquifer utilisation on a variable-density groundwater flow system in the Gippsland Basin, Australia. Hydrogeol. J. 20 (1), 119–134. https://doi.org/10.1007/s10040-011-0800-8.

Voronin. L.M., Spitz, F.J., McAuley, S.D., 1996. Evaluation of saltwater intrusion and travel time in the Atlantic City 800-foot sand, Cape May County, New Jersey, 1992, by use of a coupled-model approach and flow-path analysis. Water-Resources Investigations Report 95-4280, US Department of the Interior, US Geological Survey.

Waxman, M.H., Smits, L.J.M., 1968. Electrical conductivities in oil-bearing shaly sands. Soc. Pet. Eng. J. 8 (2), 107–122. https://doi.org/10.2118/1863-A.

Werner, A.D., 2017a. On the classification of seawater intrusion. J. Hydrol. 551, 619–631. https://doi.org/10.1016/j.jhydrol.2016.12.012.

Werner, A.D., 2017b. Correction factor to account for dispersion in sharp-interface models of terrestrial freshwater lenses and active seawater intrusion. Adv. Water Resour.102, 45–52. https://doi.org/10.1016/j.advwatres.2017.02.001.

Werner, A.D., Gallagher, M.R., 2006. Characterisation of sea-water intrusion in the Pioneer Valley, Australia using hydrochemistry and three-dimensional numerical modelling. Hydrogeo. J. 14 (8), 1452-1469. https://doi.org/10.1007/s10040-006-0059-7.

Werner, A.D., Robinson, N.I., 2018. Revisiting analytical solutions for steady interface flow in subsea aquifers: aquitard salinity effects. Adv. Water Resour. 116, 117–126. https://doi.org/10.1016/j.advwatres.2018.01.002.

Werner, A.D., Bakker, M., Post, V.E.A., Vandenbhoede, A., Lu, C., Ataie-Ashtiani, B., Simmons, C.T., Barry, D.A., 2013a. Seawater intrusion processes, investigation and management: recent advances and future challenges. Adv. Water. Resour. 51, 3–26. https://doi.org/10.1016/j.advwatres.2012.03.004.

Werner, A.D., Zhang, Q., Xue, L., Smerdon, B.D., Li, X., Zhu, X., Yu, L., Li, L., 2013b. An initial inventory and indexation of groundwater mega-depletion cases. Water Resour. Manag. 27 (2), 507–533. https://doi.org/10.1007/s11269-012-0199-6.

Wyllie, M.R.J., Gregory, A.R., Gardner, L.W., Gardner, G.H.F., 1958. An experimental investigation of factors affecting elastic wave velocities in porous media. Geophysics 23 (3), 459–493. https://doi.org/10.1190/1.1438493.

Yokoyama, Y., Lambeck, K., De Deckker, P., Johnston, P., Fifield, L.K., 2000. Timing of the Last Glacial Maximum from observed sea-level minima. Nature 406 (6797), 713–716. https://doi.org/10.1038/35021035.

Yu, X., Michael, H.A., 2019a. Offshore pumping impacts onshore groundwater resources and land subsidence. Geophysical Research Letters 46 (5), 2553-2562. https://doi.org/10.1029/2019GL081910.

Yu, X., Michael, H.A., 2019b. Mechanisms, configuration typology, and vulnerability of pumping-induced seawater intrusion in heterogeneous aquifers. Adv. Water Res., 128, 117-128. https://doi.org/10.1016/j.advwatres.2019.04.013

Zheng, C., Bennett, G.D., 2002. Applied Contaminant Transport Modeling. Wiley-Interscience, New York, p. 656.

Zulfic, H., Osei-Bonsu, K., Barnett, S.R., 2008. Adelaide Metropolitan Area Groundwater Modelling Project. DWLBC Report 2008/05. Department of Water, Land and Biodiversity Conservation, Government of South Australia. ISBN 978-1-921218-86-6.

Appendix 1

Table A1.1. Summary of available well data, including lithological descriptions of sand layers within each bore log, available geophysical data, and regional parameters obtained from analysis of each well. Gamma and bulk resistivity data were available for all wells. m AHD is metres Australian Height Datum, where 0 m AHD is approximately mean sea level.

Well	Depth (m AHD)	Lithological description	Sonic log	Bulk density	r_f obtained from a local well or calculated	Well used in parameter estimation		
						c_p	φ_r	m_r
Onshore wells								
Lake Eliza	345-360	Medium to very coarse quartz sand, clear - milky trace pyrite	Yes	No	Local well	No	Yes	Yes
McNamara	230-245	Fine to very coarse quartz sand, clear - milky trace pyrite and mica	Yes	No	Local well	No	Yes	Yes
Kent Grove	185-195	Quartz sand, clear - milky trace pyrite, minor ferric staining	Yes	No	Local well	No	Yes	Yes
Douglas Point	335-355	Med-coarse quartz sand, subangular to sub-rounded, ferric staining	Yes	No	Local well	No	Yes	Yes
Northumberland	370-390	Medium to coarse grey quartz sand, subangular	Yes	No	Local well	No	Yes	Yes

		to sub-rounded, trace mica						
Offshore wells								
Breaksea Reef	524-530, 615-630, 648-657, 707-717, 783-905	Medium to coarse sand, clear to translucent, well rounded, very clean at shallower depths	Yes	Yes	Calculated	Yes	Yes	No
Argonaut	350-362, 501-510, 585-600, 608-625	Medium to pebbly quartz sand, clear, fairly well rounded, (calcareous around 500 m)	Yes	No	Calculated	No	Yes	No
Chama	384-386.5, 390-392, 400-420	medium to coarse sand, clear to milky, subangular to sub-rounded, trace glauconite, trace pyrite	Yes	Yes	Calculated	Yes	Yes	No
Copa	421-422, 456-454, 486-489	Medium to coarse quartz grains sub-rounded to rounded, white to milky white	No	No	Calculated	No	No	No

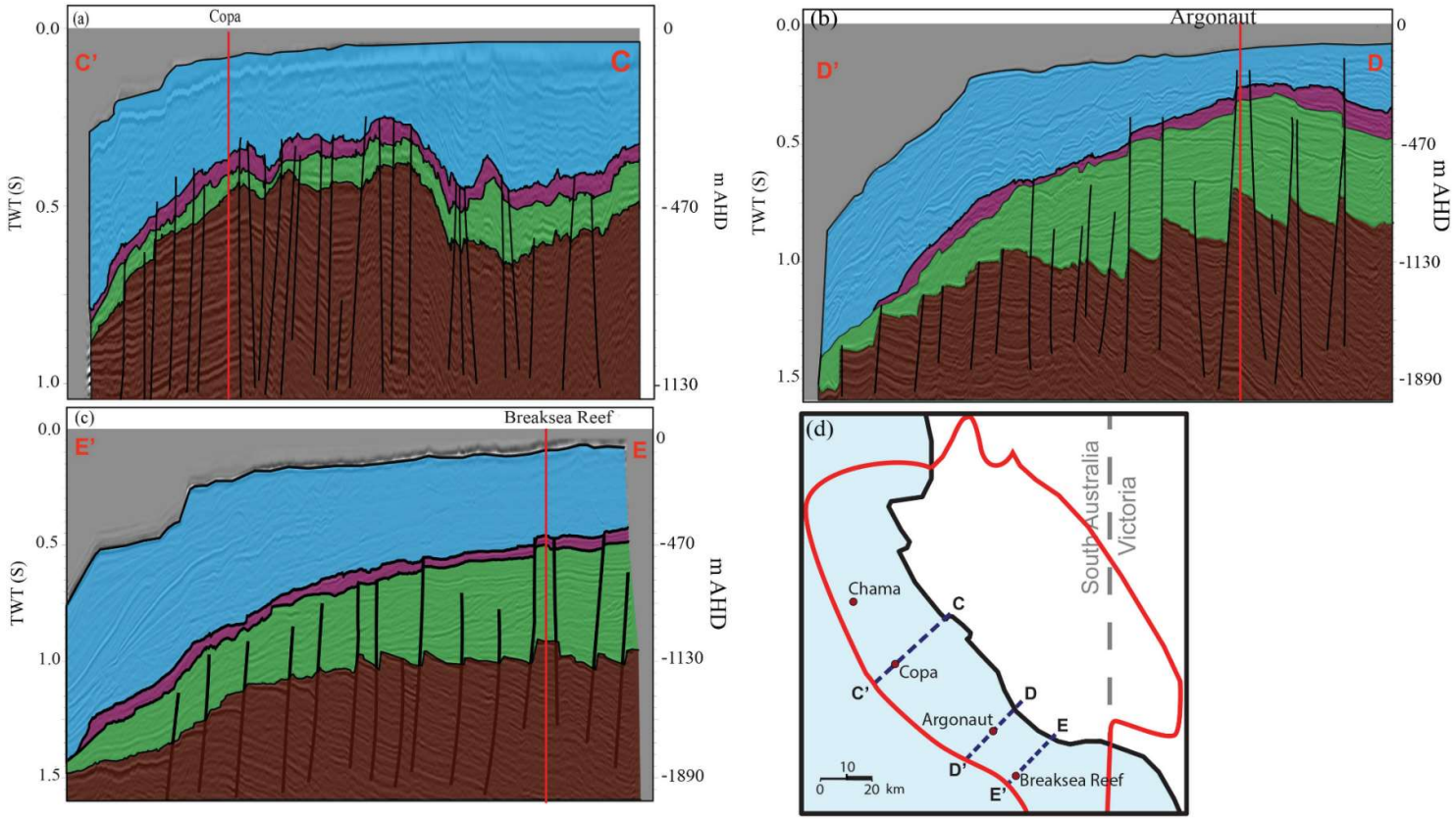

Fig. A1.1. Seismic-survey lines passing through: (a) Copa, (b) Argonaut and (c) Breaksea Reef. Faults are shown by the solid black lines. Blue, purple, and green shading indicates the UUA, UTA, and LTCA units, respectively. (d) Inset map showing seismic line locations. Well locations are marked by the solid red lines.

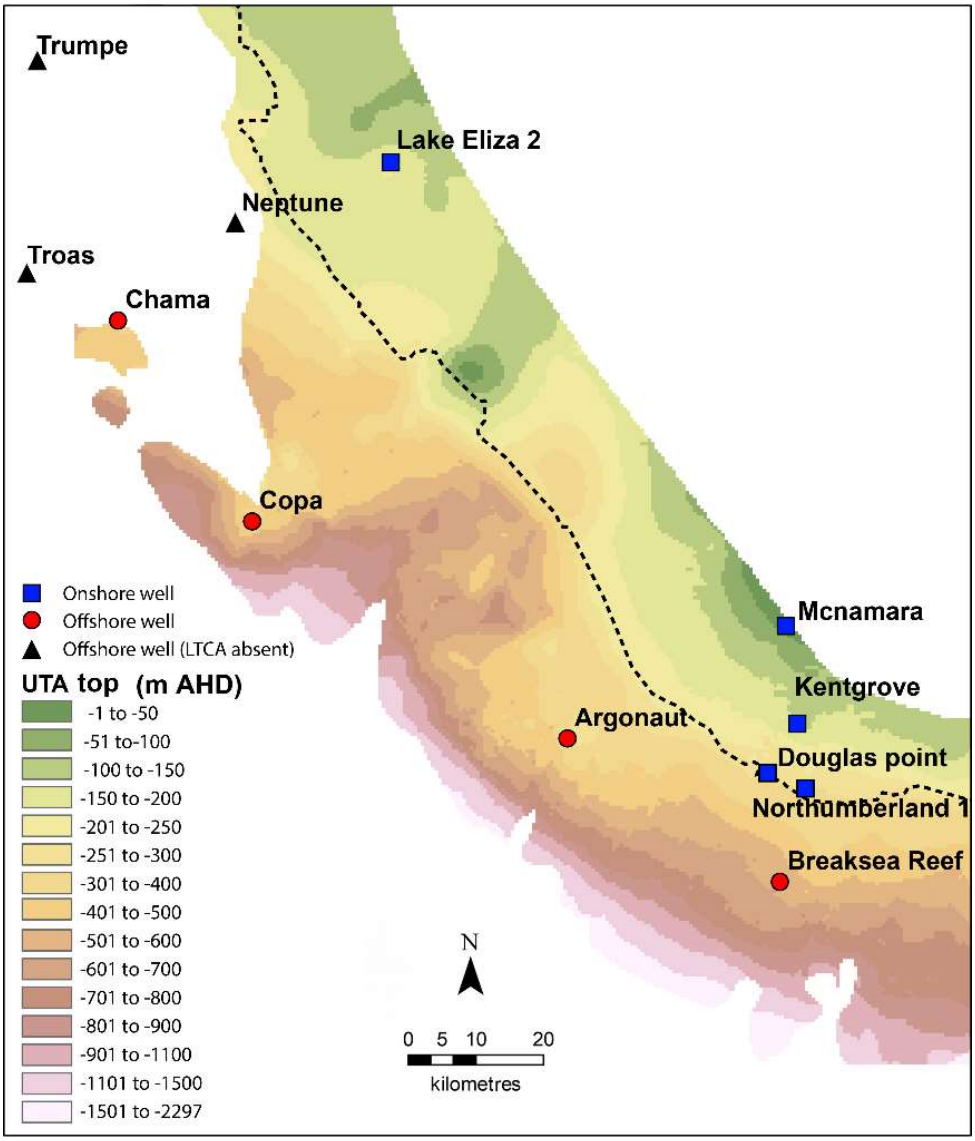

Fig. A1.2. Depth to the top of the Upper Tertiary Aquitard (UTA). The blue squares and red dots indicate onshore and offshore wells, respectively. Black triangles indicate offshore wells where the UTA and LTCA are absent in lithological logs.

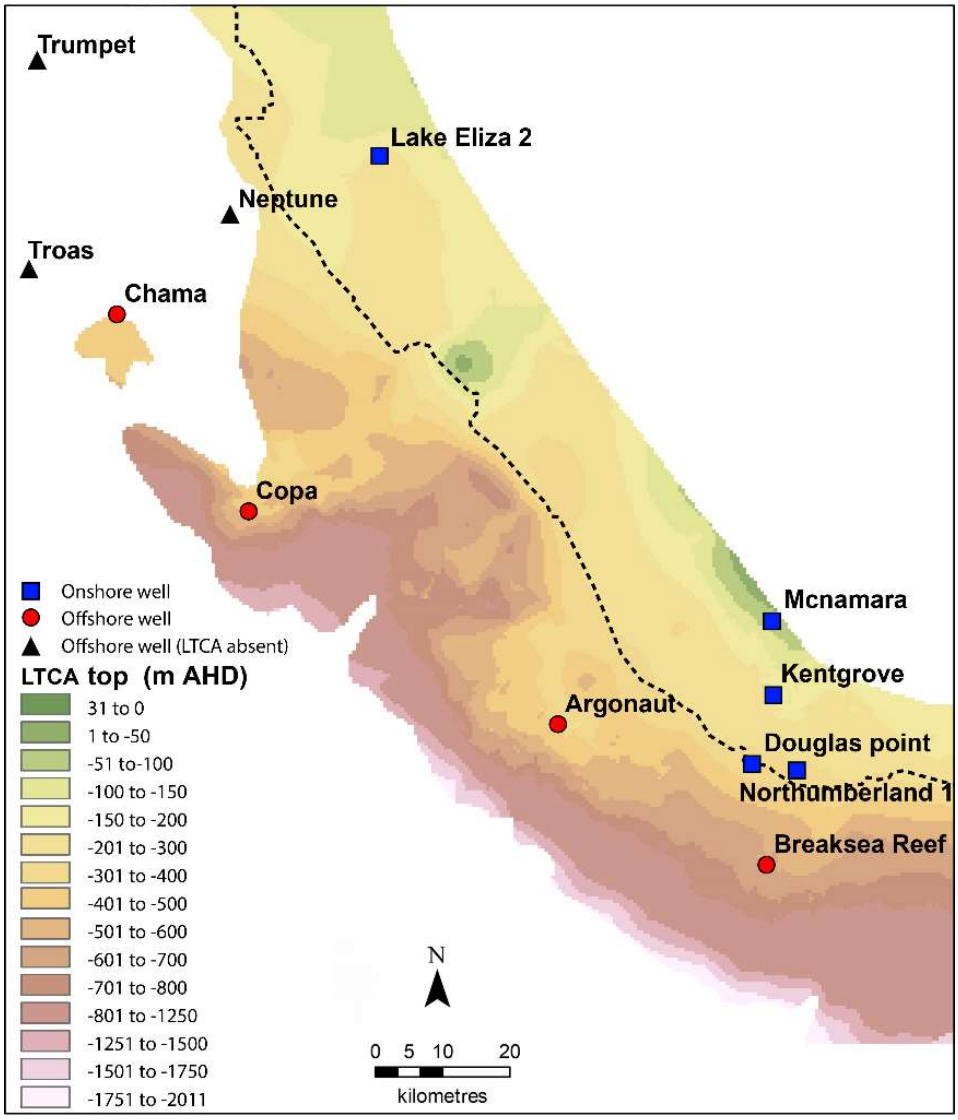

Fig. A1.3. Depth to the top of the Lower Tertiary Confined Aquifer (LTCA). The blue squares and red dots indicate onshore and offshore wells, respectively. Black triangles indicate offshore wells where the UTA and LTCA are absent in lithological logs.

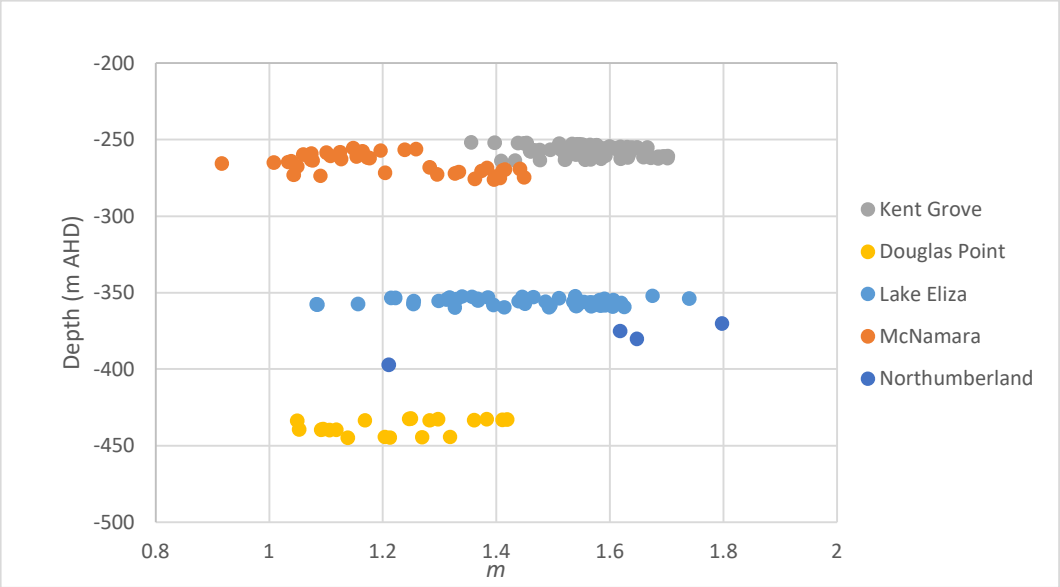

Fig. A1.4. Calculated cementation exponent (m) values versus depth for onshore well data. Data are restricted to the upper sand layer of the LTCA in each well. Depths are presented as metres below sea level (m AHD).

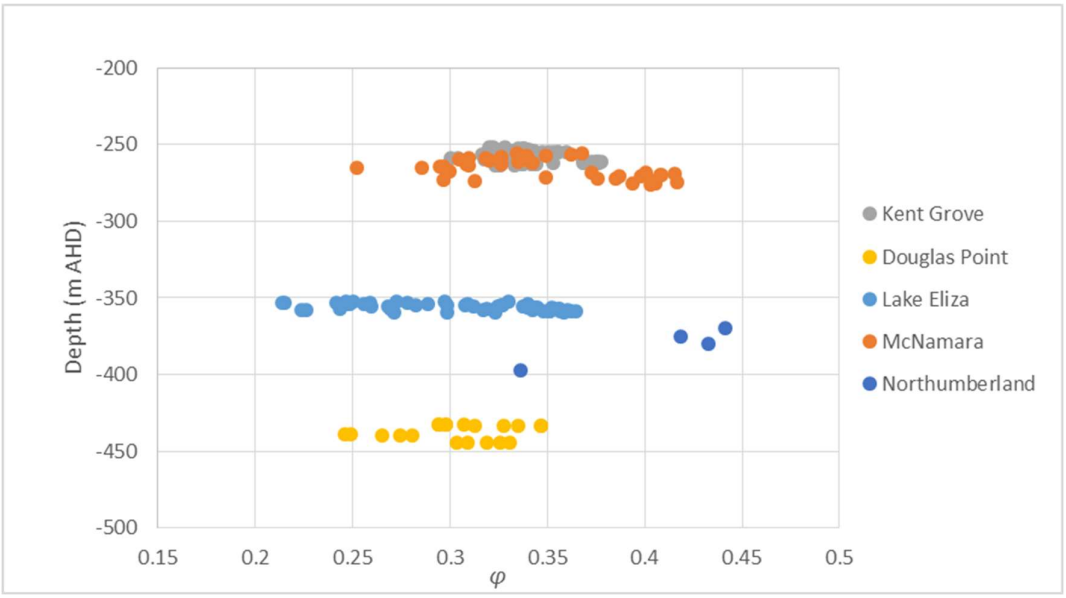

Fig. A1.5. Calculated total porosity (φ) versus depth (m AHD) for onshore well data. Data are restricted to the upper sand layer of the LTCA in each well.

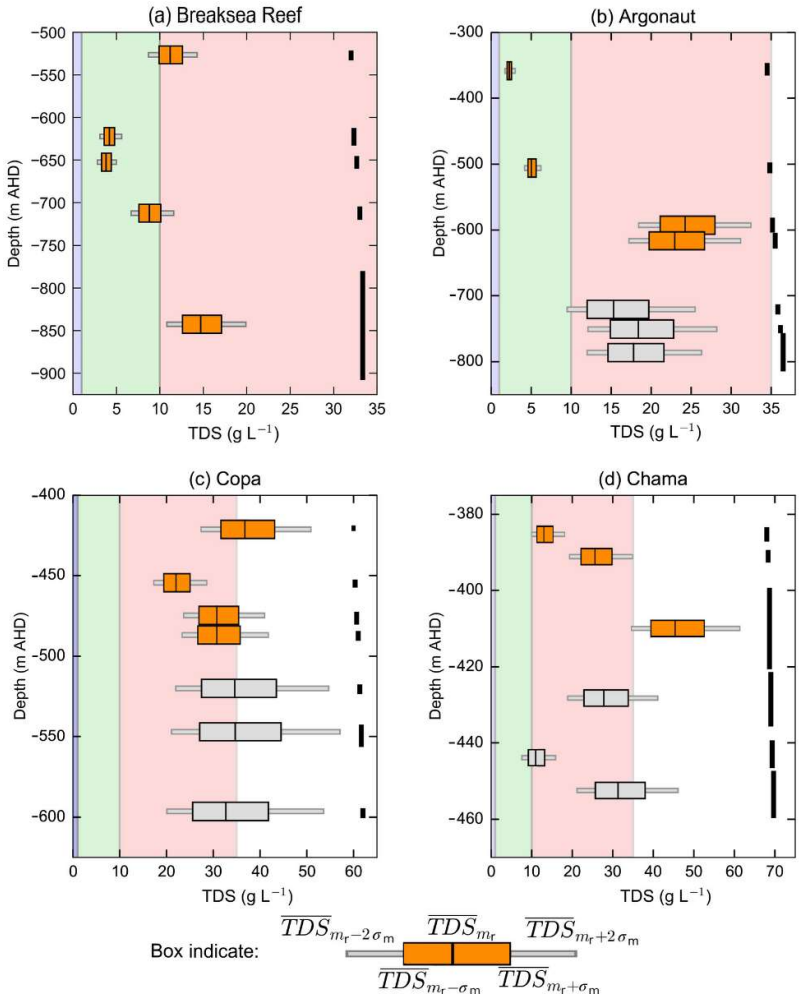

Fig. A1.6. Calculated downhole salinity profiles for the four offshore wells. The red, green, and blue shading indicates, saline (10 g L^{-1} to 35 g L^{-1}), brackish (1 g L^{-1} to 10 g L^{-1}) and freshwater (< 1 g L^{-1}), respectively. White background shading indicates that the calculated TDS is above that of typical seawater (> 35 g L^{-1}). The length of the thick black lines on the right-hand side of each plot denotes the thickness of the sand interval captured by the respective box plot. The central line of each orange box shows $\overline{TDS}$ calculated using $m = m_r$, large box edges show $\overline{TDS}_{m_r \pm \sigma_m}$, which is $\overline{TDS}$ calculated using $m = m_r \pm \sigma_m$, and the outer edges of narrow grey boxes show $\overline{TDS}_{m_r \pm 2\sigma_m}$, which is $\overline{TDS}$ calculated using $m = m_r \pm 2\sigma_m$. Note that scales differ between sub-figures. Orange boxes indicate that the sand layer was within the LTCA, while grey boxes indicate sand layers within the Sherbrook Formation.

Appendix 2

Table A2.1. Parameters obtained from regional studies

Region	K_a **(m/d)**	H_s **(m)**	H **(m)**	h_{mid} **(m)**	h_{max} **(m)**	h_{min} **(m)**	L_c **(km)**	H_l **(m)**	K_v **(m/d)**	L_s **(km)**	Δy ***(km)***	$\Delta h/\Delta y$ **(m/km)**
Gambier Embayment (Australia)	10	360	400	17.05	18.9	15	5	40	1E-4	25	83	0.05
Palmahim (Israel)	10	120	40	3.5	5.5	1.5	3	30	$1E^{-5}$	15	14	0.3
Southeast Georgia (U.S.A)	15	214	36	1.5	12.1	-9	3	30	$3E^{-4}$	40	29.5	0.7
Adelaide (Australia)	2.5	100	80	-7.5	5	-20	5	10	$5E^{-4}$	50	2	1.3
Eckernförde Bay (Germany)	45	13	150	6	9	4	5	38	$1.2E^{-3}$	6	4.4	1.3
Aveiro (Portugal)	1	130	200	28	50	5	1	80	$1E^{-4}$	40	31.4	1.4
Perth Basin (Australia)	2	1650	1500	-20	0	-40	4.5	100	$1E^{-5}$	70	19.6	2

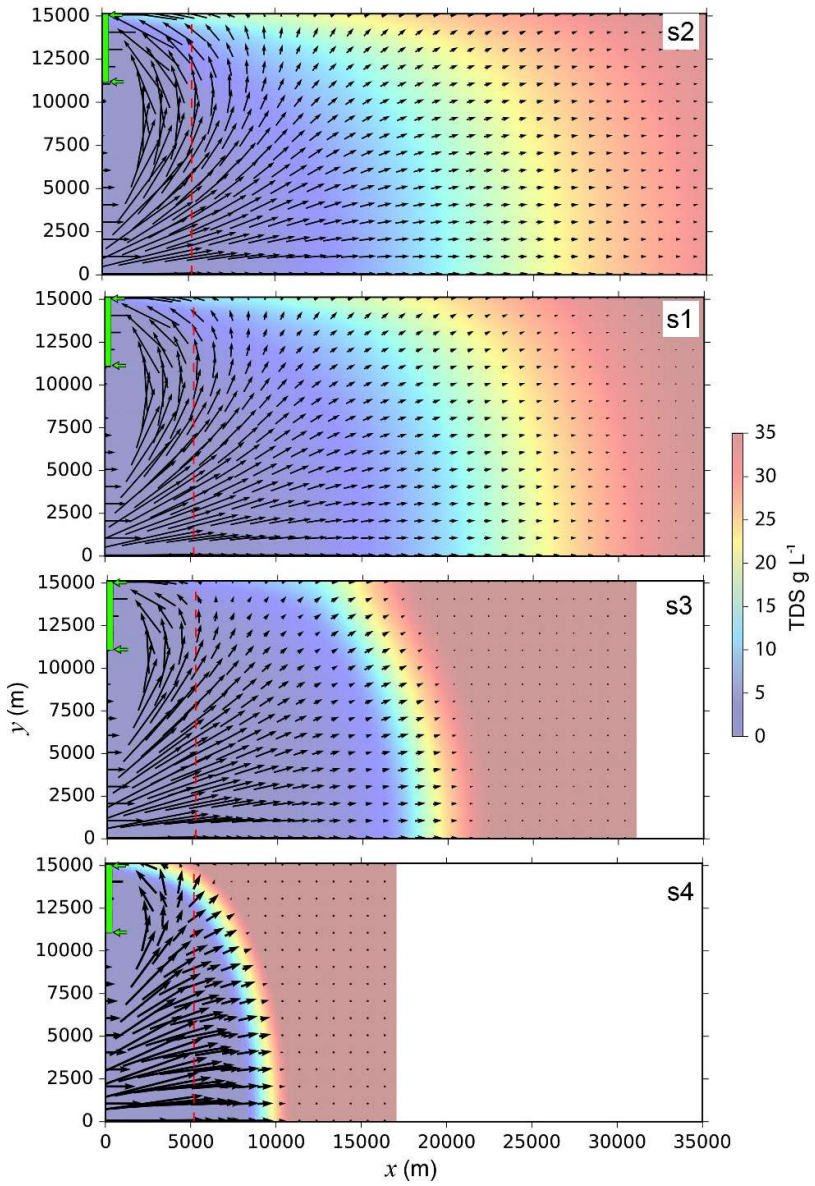

Fig. A2.1. Plan view plots of the upper layer of the semi-confined aquifer for simulations s1- s4. Colour shading indicates salinity, with dark blue and red being freshwater and saltwater, respectively. The dashed red line indicates the shoreline. The green arrows and the green shading along the onshore boundary mark the zone where active SWI is expected. Plots are ranker in order of increasing K_v. Arrows indicate flow direction with vectors of every 8th row and column shown. The offshore boundary is located > 10 km to the right of the image in s1 and s2. The offshore lengths of each simulation are given in Table 1. The white zones in s3 and s4 indicates that the model domain does incorporate the area.

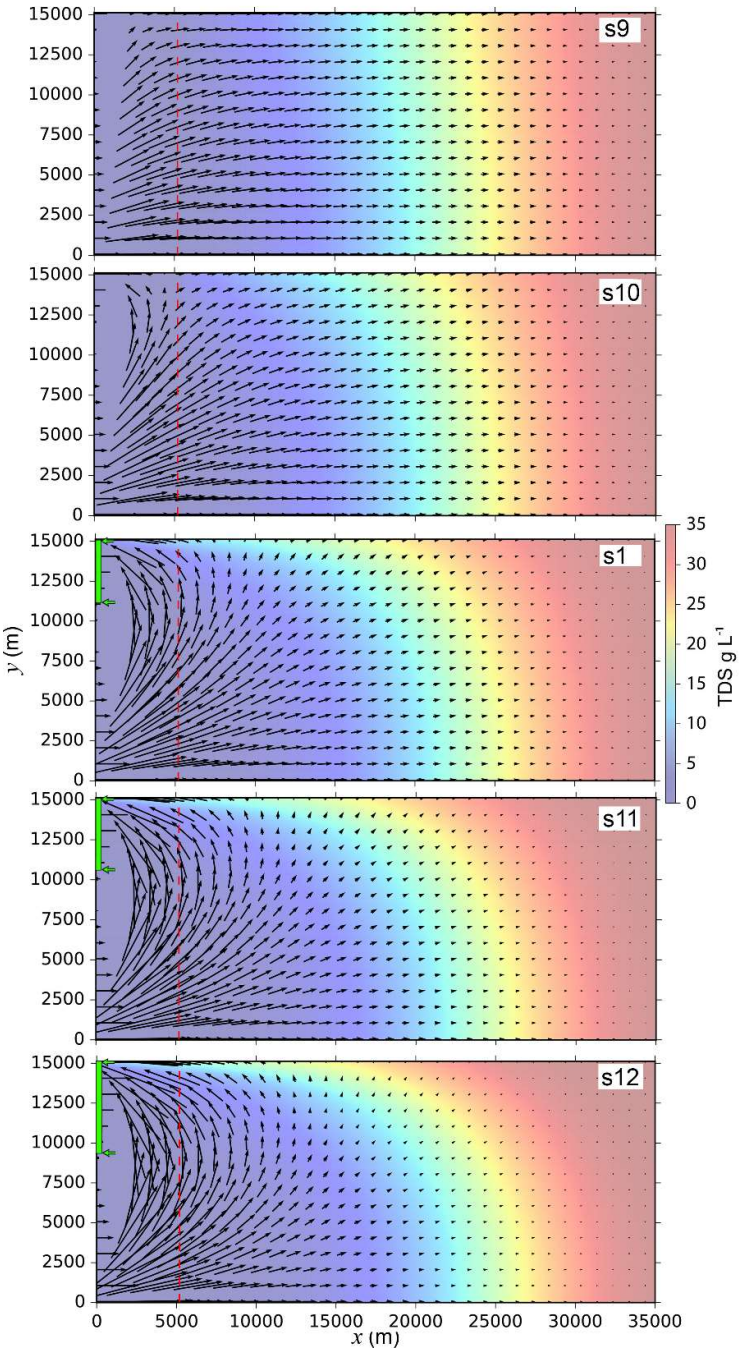

Fig. A2.2. Plan view plots of the upper layer of the semi-confined aquifer for simulations s1- s4. Colour shading indicates salinity, with dark blue and red being freshwater and saltwater, respectively. The dashed red line indicates the shoreline. The green arrows and the green shading along the onshore boundary mark the zone where active SWI is expected. Plots are ranker in order of increasing AHG. Arrows indicate flow direction with vectors of every 8th row and column shown. The offshore boundary is located > 10

km to the right of the image in all plots. The offshore lengths of each simulation are given in Table 1.

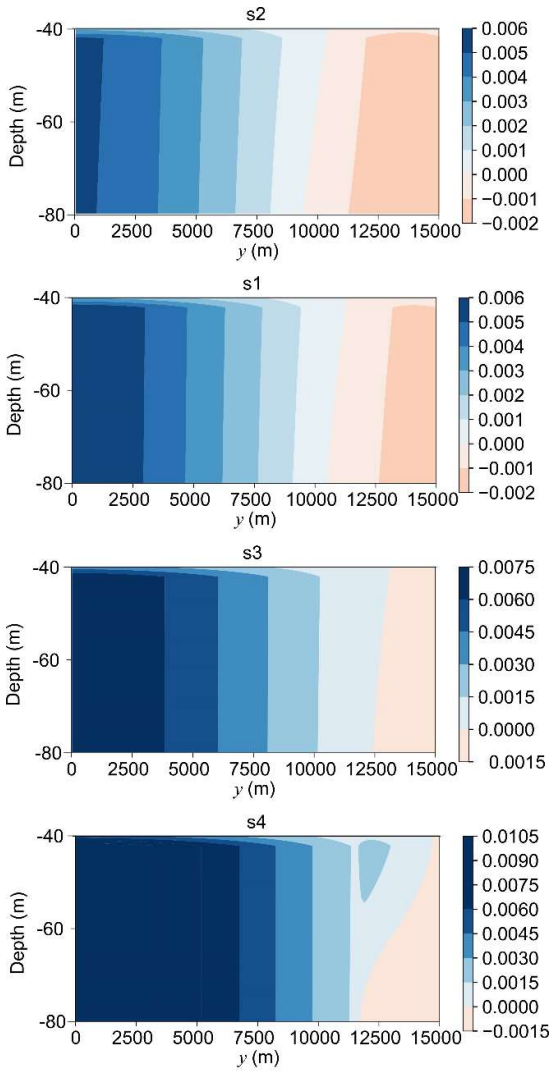

Fig. A2.3. A vertical slice along the coastline looking onshore (from the seaward side), showing q_f where $q_f = Q_f / A$, where A is the cross-sectional area of the cell. On the x-axis, 0 m marks the high head end of the model (i.e., the front face) while 15,000 m marks the low head end (i.e., the back face). Blue shades indicate freshwater discharge to the offshore aquifer and red shades indicate freshwater flow to the onshore domain. Simulations are ranked in order of increasing K_v.

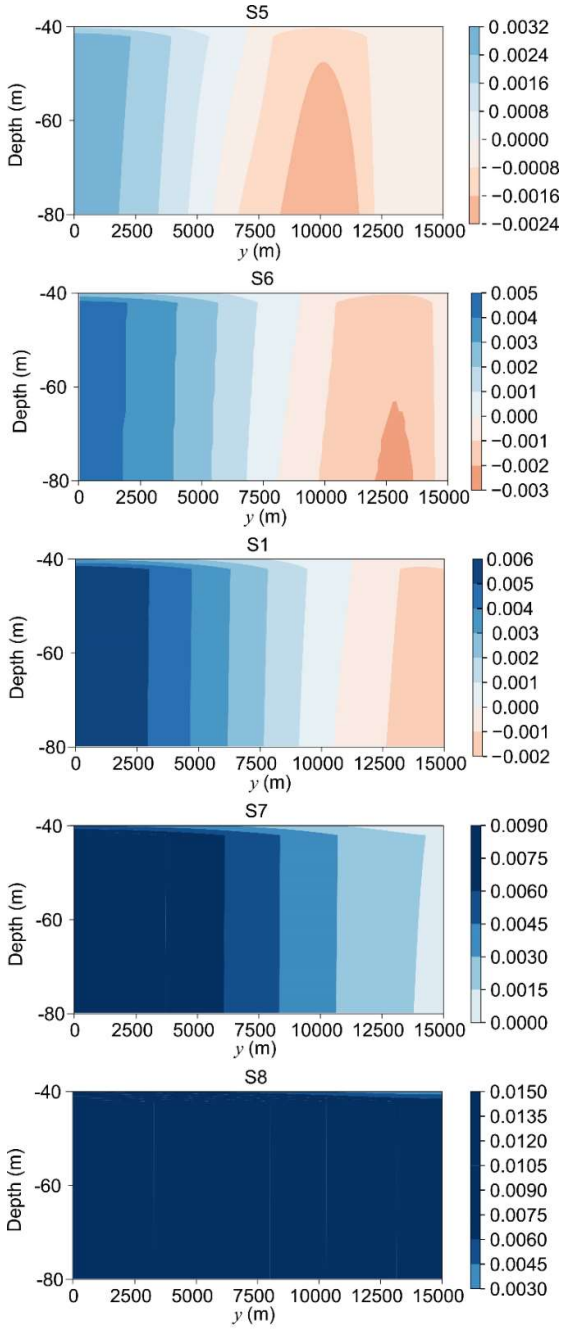

Fig. A2.4. A vertical slice across the coastline looking towards the onshore boundary of the q_f where $q_f = Q_f / A$, where A is the cross-sectional area of the cell. On the x-axis 0 m marks the high head end of the model while 15,000 m marks the low head end. Blue and red shades indicate offshore freshwater flow and onshore freshwater flow, respectively. Plots are ranked in order of increasing h_{min}.

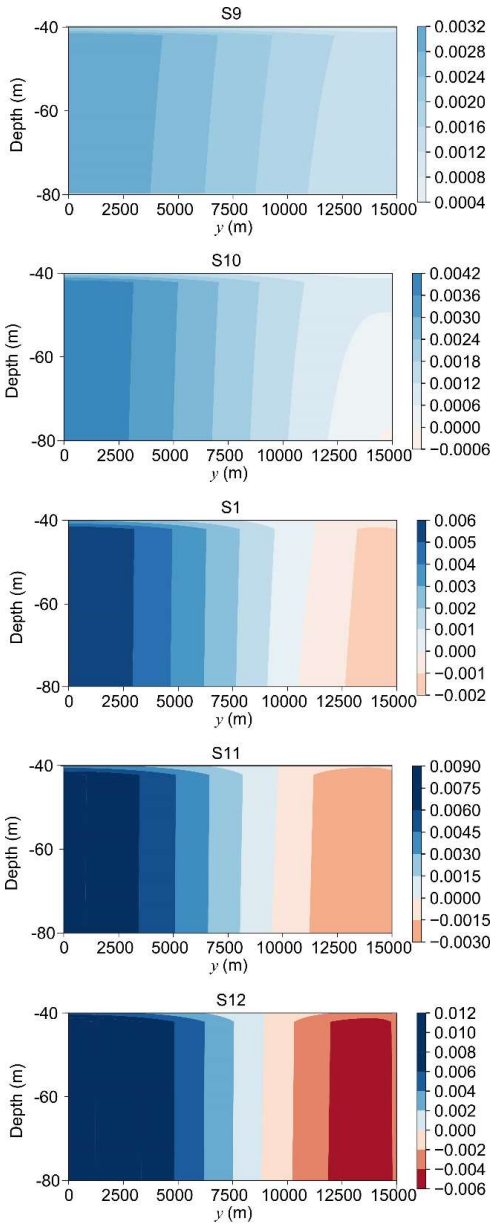

Fig. S5. A vertical slice across the coastline looking towards the onshore boundary of the q_f where $q_f = Q_f / A$, where A is the cross-sectional area of the cell. On the x-axis 0 m marks the high head end of the model while 15,000 m marks the low head end. Blue and red shades indicate offshore freshwater flow and onshore freshwater flow, respectively. Simulation are ranked in order of increasing AHG.